

การวิเคราะห์คุณลักษณะและการผสมเข้ากันได้ของพอลิเมอร์ผสมสามส่วนประกอบ
ซึ่งมีผลึกเหลวหน้าหนักโมเลกุลต่ำอยู่ด้วย



นางสาว ศิริรัตน์ วัชรวิชานันท์

สถาบันวิทยบริการ
จุฬาลงกรณ์มหาวิทยาลัย
วิทยานิพนธ์นี้เป็นส่วนหนึ่งของการศึกษาตามหลักสูตรปริญญาวิศวกรรมศาสตรดุษฎีบัณฑิต


สาขาวิชาวิศวกรรมเคมี ภาควิชาวิศวกรรมเคมี
คณะวิศวกรรมศาสตร์ จุฬาลงกรณ์มหาวิทยาลัย
ปีการศึกษา 2546

ISBN 974-17-4855-8

ลิขสิทธิ์ของจุฬาลงกรณ์มหาวิทยาลัย

CHARACTERIZATION AND MISCIBILITY ANALYSIS
OF TERNARY BLENDS CONTAINING LOW MOLAR MASS
LIQUID CRYSTAL

Miss Sirirat Wacharawichanant



A Thesis Submitted in Partial Fulfillment of the Requirements
for the Degree of Doctor of Engineering in Chemical Engineering
Department of Chemical Engineering
Faculty of Engineering
Chulalongkorn University
Academic Year 2003
ISBN 974-17-4855-8

Thesis Title CHARACTERIZATION AND MISCIBILITY ANALYSIS OF TERNARY
 BLEND S CONTAINING LOW MOLAR MASS LIQUID CRYSTAL
By Siriat Wacharawichanant
Field of study Chemical Engineering
Thesis Advisor Assistant Professor M.L.Supakanok Thongyai, Ph.D.
Thesis Co-advisor Siriporn Tanodekaew, Ph.D.

Accepted by the Faculty of Engineering, Chulalongkorn University in Partial
Fulfillment of the Requirements for the Doctor's Degree

.....Dean of Faculty of Engineering
(Professor Direk Lavansiri, Ph.D.)

THESIS COMMITTEE

.....Chairman
(Professor Piyasan prasertdam, Dr.Ing.)

.....Thesis Advisor
(Assistant Professor M.L.Supakanok Thongyai, Ph.D.)

.....Thesis Co-advisor
(Siriporn Tanodekaew, Ph.D.)

.....Member
(Assistant Professor Siriporn Damrongsakkul, Ph.D.)

.....Member
(Assistant Professor Seeroong Prichanont, Ph.D.)

.....Member
(Saran Poshyachinda, Ph.D.)

ศิริรัตน์ วัชรวิชานันท์ : การวิเคราะห์คุณลักษณะและการผสมเข้ากันได้ของพอลิเมอร์ผสม
สามส่วนประกอบซึ่งมีผลึกเหลวหน้าหนักโมเลกุลต่ำอยู่ด้วย (CHARACTERIZATION AND
MISCIBILITY ANALYSIS OF TERNARY BLENDS CONTAINING LOW MOLAR
MASS LIQUID CRYSTAL) อ.ที่ปรึกษา : ผศ.ดร.มล. สุกกนก ทองใหญ่, อ.ที่ปรึกษาร่วม :
ดร.สิริพร โตนดแก้ว, 110 หน้า. ISBN 974-17-4855-8

ผลของการเคลื่อนที่ของโมเลกุลที่เกิดผ่านชั้นแรกการแยกเฟสแบบสไปนูดิสคอมโพสิชัน
ในพอลิเมอร์ผสมระหว่างสไควอินอะครีโลไนไตรโคพอลิเมอร์ประกอบด้วย 25 เปอร์เซ็นต์โดย
น้ำหนักของอะครีโลไนไตรและพอลิเมทิลเมทาครีเลต (20/80 เปอร์เซ็นต์โดยน้ำหนัก) หลังจาก
การเติมสารผลึกเหลวหน้าหนักโมเลกุลต่ำสองชนิด(CBC33 และ CBC53) และสารหล่อลื่นสองชนิด
(GMS และ Zinc Stearate) โดยใช้เครื่องวัดการกระเจิงแสง ตัวอย่างถูกวัดค่าสัมประสิทธิ์การแพร่
ปรากฏ (D_{app}) ได้จากการทดลองการแยกเฟสของพอลิเมอร์ผสม ชั้นแรกของการแยกเฟสทำการ
ทดลองโดยใช้เครื่องวัดการกระเจิงแสงจากกระบวนการแพร่และประมาณค่าจากทฤษฎีเส้นตรง
ของคาน์และฮิลลาร์ด ผลของสารผลึกเหลวหน้าหนักโมเลกุลต่ำทำให้การเคลื่อนที่ของโมเลกุลของ
พอลิเมอร์ผสมเพิ่มขึ้น สารผลึกเหลวหน้าหนักโมเลกุลต่ำทำให้ค่าสัมประสิทธิ์การแพร่ปรากฏของ
คาน์และฮิลลาร์ดเพิ่มขึ้นหลังจากการเติมที่ความเข้มข้น 0.2 เปอร์เซ็นต์โดยน้ำหนัก สารหล่อลื่น
(GMS และ Zinc Stearate) สามารถเพิ่มการเคลื่อนที่ของโมเลกุลของพอลิเมอร์ผสมแต่น้อยกว่าและ
เพิ่มน้อยกว่าเมื่อความเข้มข้นสูงขึ้น ในอีกทางหนึ่งเมื่อความเข้มข้นสารผลึกเหลวเพิ่มขึ้นก็ทำให้
การเคลื่อนที่ของโมเลกุลสูงตามไปด้วย ในทุกระบบค่าอนุพันธ์อันดับสองของพลังงานอิสระจะ
เท่ากับศูนย์ที่อุณหภูมิเดียวกัน การเพิ่มขึ้นของการเคลื่อนที่ของโมเลกุลดูเหมือนว่าเกิดจากการ
เปลี่ยนแปลงทางจลนศาสตร์มากกว่าทางเทอร์โมไดนามิกส์

ภาควิชา.....วิศวกรรมเคมี.....ลายมือชื่อนิสิต.....
สาขาวิชา.....วิศวกรรมเคมี.....ลายมือชื่ออาจารย์ที่ปรึกษา.....
ปีการศึกษา.....2546.....ลายมือชื่ออาจารย์ที่ปรึกษาร่วม.....

4271822521 : MAJOR CHEMICAL ENGINEERING

KEY WORD: LOW MOLAR MASS LIQUID CRYSTAL / SPINODAL

DECOMPOSITION / POLYMER BLEND / LIGHT SCATTERING

SIRIRAT WACHARAWICHANANT: CHARACTERIZATION AND
MISCIBILITY ANALYSIS OF TERNARY BLENDS CONTAINING LOW
MOLAR MASS LIQUID CRYSTAL. THESIS ADVISOR: ASSISTANT
PROFESSOR ML. SUPAKANOK THONGYAI, Ph.D., THESIS CO-
ADVISOR: SIRIPORN TANODEKAEW, Ph.D., 110 pp. ISBN 974-17-4855-8.

The effects on molecular motion observed through early stage phase separation via spinodal decomposition, in melt mixed poly(styrene-co-acrylonitrile) (SAN) containing 25% by weight of acrylonitrile (AN) and poly(methyl methacrylate) (PMMA) (20/80 %wt) blends after adding two low molar mass liquid crystals (CBC33 and CBC53) and two lubricants (GMS and Zinc stearate) were investigated using light scattering techniques. The samples were assessed in terms of the apparent diffusion coefficient (D_{app}) obtained from observation of phase separation in the blends. The early stages of phase separation as observed by light scattering were dominated by diffusion processes and approximately conformed to the Cahn-Hilliard linearised theory. The major effect of liquid crystal (LC) was to increase the molecular mobility of the blends. The LC generally increased the Cahn-Hilliard apparent diffusion coefficient, D_{app} , of the blend when added with concentrations as low as 0.2 %wt. GMS and zinc stearate can also improve the mobility of the blend but to a lesser extent and the effect does not increase at higher concentration. On the other hand, the more LC added, the higher the mobility. In all systems the second derivative of the Gibbs free energy becomes zero at the same temperature. The improved mobility seem therefore to arise from changes in dynamics rather than thermodynamic effects

Department Chemical Engineering student's signature.....
Field of study Chemical Engineering Advisor's signature.....
Academic year 2003 Co-advisor's signature.....

Acknowledgement

The author would like to express her sincere gratitude to Assistant Professor M.L. Supakanok Thongyai, who supervised and encouraged throughout this course, to Dr. Siriporn Tanodekaew for her kindly advice and invaluable discussion. The author also gratefully acknowledges Professor Julia Higgins and Dr. Nigel Clarke for the collaboration and useful discussion.

I am also grateful to Professor Dr. Piyasan Praserttham, Dr.Saran Poshyachinda, Assistant Professor Dr. Siriporn Damrongsakkul and Assistant Professor Dr. Seeroong Prichanont for serving as the chairman and the member of the thesis committee, respectively, whose comments were constructively and especially helpful.

The financial support from Thailand Graduate Institute of Science and Technology (TGIST) and The Thailand Research Fund (TRF) is gratefully acknowledgement.

Sincere thanks are made to the Department of Chemical Engineering, and King Mongkut's Institute of Technology North Bangkok for their assistance about twin screw extruder machine.

Also thanks to Bayer Polymer Co., Ltd. for providing SAN and Thai Petrochemical Industries Public Ltd. who supported PMMA used in this study.

Sincere thanks to all my friends and all members of polymer engineering research laboratory for their assistance.

Finally I would like to dedicate this thesis to my parents and my families, who generous supported and encouraged me through the year spent on this study.

Contents

	Page
ABSTRACT (IN THAI).....	iv
ABSTRACT (IN ENGLISH).....	v
ACKNOWLEDGEMENT.....	vi
CONTENTS.....	vii
LIST OF TABLES.....	x
LIST OF FIGURES.....	xi
NOMENCLATURE.....	xvi
CHAPTER 1	
INTRODUCTION.....	1
1.1 Literature Review of Liquid Crystal and Polymer Blends.....	2
1.2 Literature Review of Miscible Polymer Blends.....	5
1.3 Objectives.....	5
1.4 Organization of Thesis.....	6
CHAPTER 2	
MISCIBILITY AND THERMODYNAMICS OF POLYMER BLENDS.....	7
2.1 Principles for Polymer-Polymer Miscibility.....	7
2.2 Mechanism of Phase Separation.....	10
2.2.1 Nucleation and Growth.....	14
2.2.2 Spinodal Decomposition.....	15
2.3 Thermodynamic Theories.....	16
2.3.1 The Flory-Huggins Theory.....	16
2.3.2 The Flory Equation of State Theory.....	18
2.4 Blending Techniques.....	21
2.4.1 Mechanical Blending.....	21
2.4.2 Solution Blending.....	21
2.4.3 In-situ Polymerization.....	22
2.5 Determination of Miscibility.....	22
2.5.1 Glass Transition Temperature Study	22
2.5.2 Scattering study.....	23
2.5.3 Morphology study.....	23
2.6 Conclusions.....	24
CHAPTER 3	
KINETICS OF PHASE SEPARATION IN POLYMER BLENDS.....	26
3.1 Spinodal Decomposition.....	28
3.1.1 Cahn-Hilliard Linearised Theory.....	29
3.2 Conclusions.....	34
CHAPTER 4	
LIQUID CRYSTALS & LUBRICANTS.....	36

Contents (continued)

	Page
4.1 Liquid Crystals.....	36
4.1.1 Classification of Liquid crystals.....	36
4.1.2 Types of Liquid Crystals.....	37
4.1.2.1 Rod-Like Liquid Crystals.....	37
4.1.2.2 Discotic Liquid Crystals.....	37
4.1.2.3 Lyotropic Liquid Crystals.....	38
4.1.3 Phase Structures of Liquid Crystals.....	38
4.1.3.1 Nematic Structure.....	38
4.1.3.2 Smectic Structure.....	40
4.1.3.3 Cholesteric or Chiral Structure.....	42
4.1.4 Mesophasic Transition Temperatures.....	42
4.1.5 Polymer Liquid Crystals.....	43
4.2 Lubricants.....	44
4.2.1 The Mechanism of Lubricant Action.....	44
4.2.1.1 Internal Lubricants.....	44
4.2.1.2 External Lubricants.....	45
 CHAPTER 5	
MATERIALS AND EXPERIMENTAL TECHNIQUES.....	46
5.1 Material Characteristics.....	46
5.2 Equipment and Methods.....	50
5.2.1. Small Angle Light Scattering (SALS).....	50
5.2.2 Twin screw extrusion.....	51
5.2.3 Differential Scanning Calorimeter (DSC).....	52
5.2.4 Scanning Electron Microscopy (SEM).....	54
 CHAPTER 6	
MISCIBILITY, KINETICS AND MORPHOLOGY OF PHASE SEPARATION	56
6.1 Glass Transition Temperature (T _g) Study	57
6.2 Phase Behavior.....	58
6.2.1 Cloud Point Determination.....	58
6.2.2 Spinodal Determination.....	62
6.3 Effects of Liquid Crystals and Lubricants on Kinetics of Phase Separation.....	69
6.3.1 The Cahn-Hilliard Growth Rate (R(q)).....	69
6.3.1.1 Concentration Effects of Liquid Crystals and Lubricants.....	70
6.3.1.2 Molecular Structure Effects of Liquid Crystals.....	71
6.3.1.3 Molecular Structure Effects of Lubricants.....	72
6.3.1.4 Comparison of Effects of Liquid Crystals and Lubricants...	73

Contents (continued)

	Page
6.3.2 The maximum scattering wave number (q_m).....	74
6.3.3 The maximum growth rate ($R(q_m)$).....	75
6.3.3.1 Concentration Effects of Liquid Crystals and Lubricants.....	75
6.3.3.2 Comparison of Effects of Liquid Crystals and Lubricants.....	78
6.3.4 The apparent diffusion coefficient (D_{app}).....	79
6.3.4.1 Concentration Effects of Liquid Crystals and Lubricants.....	80
6.3.4.2 Comparison of Effects of Liquid Crystals and Lubricants.....	82
6.4 Morphology.....	85
6.4.1 Scanning Electron Microscopy Results.....	85
6.5 Conclusions.....	93
CHAPTER 7	
CONCLUSIONS AND RECOMMENDATIONS.....	94
7.1 Conclusions.....	94
7.2 Recommendations for further works	95
REFERENCES.....	99
VITAE.....	109

สถาบันวิทยบริการ
จุฬาลงกรณ์มหาวิทยาลัย

List of Tables

	Page
4.1 Properties of low molar mass thermotropic liquid crystals.....	49
6.1 T_g of SAN/PMMA (20/80) blends after adding 1.0 wt% of Zinc Stearate, GMS, CBC33 and CBC53.....	58
6.2 Spinodal temperatures of SAN/PMMA (20/80) blends after adding 1.0 wt% of Zinc Stearate, GMS, CBC33 and CBC53 at different q ranges.....	67
6.3 Spinodal temperatures of SAN/PMMA (20/80) blends before and after addition of 0.2, 0.4, 1.0 wt% of CBC33, CBC53, GMS and Zinc Stearate.	68



 สถาบันวิทยบริการ
 จุฬาลงกรณ์มหาวิทยาลัย

List of Figures

	Page
2.1 Plots of Gibbs free energy of mixing as a function of composition for a binary mixture exhibiting three types of mixing behaviour; immiscibility (A), complete miscibility (B), partial miscibility (C).....	8
2.2 (a) The corresponding LCST-type phase diagram for a binary mixture, (b) The corresponding UCST-type phase diagram for a binary mixture.....	9
2.3 Presents a schematic representation of various types of phase diagrams for polymer mixtures.....	10
2.4 Illustration of the corresponding miscibility limits in temperature and composition.....	12
2.5 Schematic illustration of the free energy -concentration diagrams: (a) unstable region, (b) metastable.....	13
2.6 Schematic illustration of a phase separation by the nucleation and growth mechanism: (a) one-dimensional evolution of concentration profiles, (b) two-dimensional pictures of the phase structure.....	14
2.7 Schematic illustration of a phase separation by the spinodal decomposition mechanism: (a) one-dimensional evolution of concentration profiles, (b) two-dimensional pictures of the phase structure.....	15
2.8 Approximate ranges of experimental techniques to study blend morphology of: (1) interatomic; (2) molecular, spherulites; (3) filler aggregates, compatibilised blends; (4) reinforcements, noncompatible blends; (5) voids.	24
3.1 Schematic diagrams show the concentration fluctuation in the early (a), intermediate (b) and late stage of spinodal decomposition(c) [Hashimoto 1993]. $\Delta\phi=\phi_{Ai}-\phi_{AO}$ is the amplitude of fluctuation, Λ is the wavelength of concentration fluctuation.....	28
4.1 Discotic liquid crystal phases.....	37
4.2 Nematic structure.....	39
4.3 Typical rod-like liquid crystal forming molecule. (a) Schematic and (b) Example. R denotes an end group, O a ring structure, and B a bridging group.....	40
4.4 Smectic structure.....	41

List of Figures (continued)

		Page
4.5	A cholesteric structure.....	42
4.6	Phase transition of Liquid Crystal.....	43
5.1	The chemical structure of poly(methyl methacrylate) (PMMA).....	46
5.2	The chemical structure of styrene-co-acrylonitrile (SAN)	48
5.3	Structure of CBC33.....	48
5.4	Structure of CBC53.....	49
5.5	Structure of glycerol monostearate (GMS)	49
5.6	Structure of zinc stearate.....	49
5.7	A light scattering equipment.....	50
5.8	Illustration of a plasticating extruder.....	52
5.9	A schematic diagram of differential scanning calorimeter.....	53
5.10	A photographic illustration of SEM model JSM-6400.....	54
6.1	A plot of intensity against temperature for SAN/PMMA (40/60) blend at 217 °C and the heating rate of 1.0 °C /min.....	59
6.2	The observed cloud point temperatures at different heating rate.....	60
6.3	Phase diagram of SAN/PMMA determined by light scattering technique. The cloud points were obtained from zero heating rate method. (a)-(b) \overline{M}_w of PMMA is 72575, \overline{M}_w of SAN is 149926, (c) \overline{M}_w of PMMA is 167000, \overline{M}_w of SAN is 82000, (d) \overline{M}_w of PMMA is 178000, \overline{M}_w of SAN is 83000.....	61
6.4	A plot of $\ln(\text{Intensity})$ against time for SAN/PMMA (20/80) blends, obtained from a temperature jump experiment at 217 oC. As seen in this Fig., the delay time is approximately 1700 s.....	63
6.5	Plots of $R(q)/q^2$ against q^2 for SAN/PMMA (20/80) obtained from different temperatures.....	64
6.6	Plots of D_{app} against temperatures for SAN/PMMA (20/80), Spinodal temperatures, T_s can be obtained by extrapolating the apparent diffusion coefficients to the x-axis when the D_{app} became zero.....	65

List of Figures (continued)

		Page
6.7	Plots of D_{app} against temperatures for SAN/PMMA (20/80) at different q ranges, T_s can be obtained by extrapolating the apparent diffusion coefficients to the x-axis when the D_{app} became zero.....	66
6.8	Plots of D_{app} against temperatures for SAN/PMMA (20/80) after adding 1.0 wt% CBC53 at different q ranges, T_s can be obtained by extrapolating the apparent diffusion coefficients to the x-axis when the D_{app} became zero	66
6.9	Plots of D_{app} against temperatures for SAN/PMMA (20/80) after adding 1.0 wt% GMS at different q ranges, T_s can be obtained by extrapolating the apparent diffusion coefficients to the x-axis when the D_{app} became zero	67
6.10	Plots of $R(q)$ versus of q for SAN/PMMA (20/80) blends at five temperatures used.....	70
6.11	Plots of $R(q)$ versus of q for SAN/PMMA (20/80) blends after adding CBC33 at 217 °C.....	71
6.12	Plots of $R(q)$ versus of q for SAN/PMMA (20/80) blends after adding 1.0 wt% CBC33 and CBC53 at 217 °C.....	72
6.13	Plots of $R(q)$ versus of q for SAN/PMMA (20/80) blends after adding 1.0 wt% GMS and Zinc Stearate at 220 °C.....	73
6.14	Plots of $R(q)$ versus of q for SAN/PMMA (20/80) blends after adding 1.0 wt% CBC33 and GMS at 217 °C.....	74
6.15	Plots of q_m against temperature for SAN/PMMA (20/80) blends after adding 1.0 wt% CBC53, obtained from calculation and observation methods.....	75
6.16	Plots of $R(q_m)$ against temperature for SAN/PMMA (20/80) blends after adding 0.2, 0.4 and 1.0 wt% CBC33, obtained from calculation and observation methods.....	76

List of Figures (continued)

	Page	
6.17	Plots of $R(q_m)$ against temperature for SAN/PMMA (20/80) blends after adding 0.2, 0.4 and 1.0 wt% GMS, obtained from calculation and observation methods.	76
6.18	Plots of $(R(q_m))^{1/2}$ against temperature for SAN/PMMA (20/80) blends after adding 0.2, 0.4 and 1.0 wt% CBC33, obtained from observation method.....	78
6.19	Plots of $R(q_m)$ against temperature for SAN/PMMA (20/80) blends after adding 1.0 wt% CBC33 and GMS, obtained from calculation and observation methods.....	79
6.20	Plots of D_{app} against temperatures for SAN/PMMA (20/80) blends after adding CBC33 at various compositions.....	80
6.21	Plots of D_{app} against temperatures for SAN/PMMA (20/80) blends after adding CBC53 at various compositions.	81
6.22	Plots of D_{app} against temperatures for SAN/PMMA (20/80) blends after adding GMS at various compositions.....	81
6.23	Plots of D_{app} against temperatures for SAN/PMMA (20/80) blends after adding Zinc Stearate at various compositions.....	82
6.24	Plots of D_{app} against temperatures for SAN/PMMA (20/80) blends after adding 0.2 wt% CBC33, CBC53, GMS and Zinc Stearate.	83
6.25	Plots of D_{app} against temperatures for SAN/PMMA (20/80) blends after adding 0.4 wt% CBC33, CBC53, GMS and Zinc Stearate.	83
6.26	Plots of D_{app} against temperatures for SAN/PMMA (20/80) blends after adding 1.0 wt% CBC33, CBC53, GMS and Zinc Stearate.	84
6.27	A scanning electron micrograph picture of SAN.....	87
6.28	A scanning electron micrograph picture of PMMA.....	87
6.29	A scanning electron micrograph picture of a fractured specimen for a miscible 20/80 melt mixed SAN/PMMA blend.....	88
6.30	A scanning electron micrograph picture of a fractured specimen for a phased separated SAN/PMMA (20/80) at 210 °C.....	88

List of Figures (continued)

		Page
6.31	A scanning electron micrograph picture of a fractured specimen for a miscible 20/80 melt mixed SAN/PMMA blend added with 1.0 wt% of CBC33.....	89
6.32	A scanning electron micrograph picture of a fractured specimen for a phased separated SAN/PMMA (20/80) at 210 °C, added with 1.0 wt% of CBC33.....	89
6.33	A scanning electron micrograph picture of a fractured specimen for a miscible 20/80 melt mixed SAN/PMMA blend, added with 1.0 wt% of CBC53.....	90
6.34	A scanning electron micrograph picture of a fractured specimen for a phased separated SAN/PMMA (20/80) at 210 °C, added with 1.0 wt% of CBC53.....	90
6.35	A scanning electron micrograph picture of a fractured specimen for a miscible 20/80 melt mixed SAN/PMMA blend added with 1.0 wt% of GMS.....	91
6.36	A scanning electron micrograph picture of a fractured specimen for a phased separated SAN/PMMA (20/80) at 210 °C, added with 1.0 wt% of GMS.....	91
6.37	A scanning electron micrograph picture of a fractured specimen for a miscible 20/80 melt mixed SAN/PMMA blend added with 1.0 wt% of Zinc Stearate at larger scale magnification x5,000.....	92
6.38	A scanning electron micrograph picture of a fractured specimen for a phased separated SAN/PMMA (20/80) at 210 °C, added with 1.0 wt% of Zinc Stearate at larger scale magnification x10,000.....	92
7.1	Free successive situations for a reptation chain: (a) the chain is trapped in its original tube; (b) the chain moves to the right and a certain portion (I_0I_1) of the original tube disappears; (c) the chain moves to the left and a portion (J_0J_2) of the original tube disappears [de Gennes 1979].....	98

Nomenclature

Abbreviation

AFM	Atomic force microscopy
AN	Acrylonitrile
DSC	Differential scanning calorimeter
LCST	Lower critical solution temperature
NG	Nucleation and growth
NMR	Nuclear magnetic resonance spectroscopy
PMMA	Poly(methyl methacrylate)
SAN	Copolymer from polystyrene and acrylonitrile
SANS	Small angle neutron scattering
SAXS	Small angle X-ray scattering
SD	Spinodal decomposition
SEM	Scanning electron microscope
UCST	Upper critical solution temperature
WAXS	Wide angle X-ray scattering

Symbols

$c(\mathbf{r},t)$	Concentration at the position of vector \mathbf{r} and time t
$c(\mathbf{q},t)$	Fourier transformation of $c(\mathbf{r},t)$
$C_o(q)$	Parameter related to elastic energy
D_{app}	Apparent diffusion coefficient
$f(c)$	Volumetric free energy due to concentration fluctuation
F	Free energy of the Flory-Huggins-de Gennes theory
g	Empirical term
Δg	Volumetric change in Gibbs free energy between the new and present phase
ΔG_m	Gibbs free energy of mixing
ΔH_m	Enthalpy of mixing
$I(q,t)$	Scattered intensity
M	Molecular mobility
\bar{M}_n	Number average molar mass

\bar{M}_w	Weight average molar mass
n	Refractive index of the blend
n_i	number of molecule of component i in the lattice model
P	Particular properties such as elastic modulus or thermal conductivity of blend
P_i	Particular properties of component I
P^*	Critical pressure
\tilde{P}	Reduced pressure
q	Scattering wave number
q_c	Critical value of q
q_m	Maximum value of q
\bar{q}_m	Reduced maximum scattering wave number
r_i	Number of segment per chain molecule of polymer i
\bar{r}	Average number of segment
R	Gas constant; 8.31432 J/mole-degree
$S(q,t)$	Structure function
ΔS_m	Entropy of mixing
t	time
T	Temperature
T^*	Critical temperature
\tilde{T}	Reduced temperature
T_g	Glass transition temperature of blend
T_m	Melting temperature
V	Volume of the system
V^*	Critical volume
\tilde{V}	Reduced volume
X_i	Weight fraction of component i

Greek alphabets

α_T	Thermal expansion coefficient
A	Helmoltz free energy
β	The exponent of time evolution of the maximum intensity I_m

γ	Thermal pressure coefficient
δ	Solubility parameter
θ	Scattering angle
k	Boltzmann constant
K	Gradient energy
λ	Wavelength of the radiation
Λ	Inter-domain distance of each percolating domain
$\Lambda(q)$	Onsager coefficient
$\Delta\mu$	Chemical potential
ϕ_i	Volume fraction of component i
ϕ_0	Average volume fraction of the system
$\chi(q,t)$	Susceptibility of the system
χ_{12}	Flory-Huggins interaction parameter
ψ_i	Segment fraction of polymer I
ψ_0	Total number of segment

สถาบันวิทยบริการ
จุฬาลงกรณ์มหาวิทยาลัย

Chapter I

Introduction

The concept of polymer blending, the physical mixing of two or more polymers, has been the area of interest in the field of polymer science and technology. Interest in polymer blends arises from the potential to achieve a product featuring properties that are not available in a single homopolymer with relatively low expenditure in comparison to the invention of a new polymer. By simply varying the composition in the blend, a virtually new mixture of unique properties can be obtained due to the change in the level of mixing or morphology. The relationship between morphology and properties of polymer blends has been extensively investigated. It is well known that many properties of polymer blends are determined by their morphology.

Polymer blends can be classified into three categories; immiscible, miscible and partially miscible blends depending on their micro-phase structure. In an immiscible system, one can always observe multi-phase domains each of which contains different proportion of constituents whereas a miscible blend only occurs as a single-phase system. In contrast, partially miscible blends may exhibit either single- or multi-phase microstructures, depending on the conditions.

Phase separation from an initially homogeneous mixture is considered to be one possible route to generate irregular spatial patterns in the samples. A partially miscible polymer blend generally undergoes spinodal decomposition after exposure to temperatures in the unstable two-phase regime. The rates of phase separation and the resulting morphology depend on many parameters, e.g., time of heat treatment, temperature, concentration, and physical properties of the blend constituents. Many publications have reported on three stages of the growth of the spatial composition fluctuations [Hashimoto 1993]; early stage, intermediate stage, and late stage.

As the spinodal decomposition proceeds, the concentration fluctuations in the blend increases in amplitude. The scattered intensity grows exponentially with time in

the early stage of phase separation, the dynamics can be well described over this limited range of time by the linearised Cahn-Hilliard theory as reported by several authors [Hashimoto 1993; Jinnai *et al.* 1993].

1.1 Literature Review of Liquid Crystal and Polymer Blends

Liquid crystal polymers (LCP) are materials that offer a unique combination of high tensile strength, unusual barrier properties, and excellent thermal stability. In recent years, significant interest has been generated in the study of liquid crystal polymers and their blends with thermoplastics. Blending a high-performance liquid crystal polymer with a conventional plastic is an attractive route to create a novel high-performance plastic. Concepts such as self-reinforcing composites and molecular composites have been developed to describe immiscible and miscible polymer blends [Nakai *et al.* 1998]. Blizard *et al.* [1987] characterized the morphology of the blends of both polycarbonate and nylon 6,6 with a liquid crystal polyester, found that some extensional flow or shear flow is required for the coalescence and extension of the particulated liquid crystal polymer phase.

Lin *et al.*[1993] studied the miscibility and viscoelastic properties of blends of a liquid crystal polyester and poly(ethylene terephthalate). They found that the melt viscosity decreased exponentially with the liquid crystal polymer content in the range of composition where the blends are miscible. The phase behavior and rheology of binary blends of polycarbonate and a liquid crystal polymer were investigated by Lee *et al.*[1996]. Differential scanning calorimetry (DSC) and optical microscopy have indicated that the liquid crystal polymer is soluble in the mixture for weight fractions of liquid crystal polymer less than 0.05 and shows partial miscibility with polycarbonate over the rest of the composition range. The phase-separated structure formed in polymer mixtures consisting of liquid crystal polymer and poly(ethylene terephthalate) were investigated by Nakai *et al.*[1996]. Phase separation during isothermal annealing at various temperatures after rapidly heating the as-prepared thin

films was investigated using real-time in situ polarized light microscopy and light scattering.

Dorgan *et al.*[1998] studied processing effects on the phase separation morphology of liquid crystal polymers. The effects of processing on morphology, varying quench temperature, composition and molecular weight were presented. Simulations of some examples of quenching experiments demonstrated that increased liquid crystal polymer concentration, decreased molecular weight, increased solvent, and decreased quench depth all lead to an increase in the domain size. Turcott *et al.*[2001] studied microstructure development during the injection molding of poly(ethylene terephthalate) and liquid crystal polymer blends. The morphology was directly related to the amount and type of liquid crystal polymer in the blend. 10% LCP, three morphological layers were found across the thickness of the molded part, while at 30% LCP, five morphological layers could be identified. The LCP structure can be classified into four types: droplets, thick rods, thin fibrils and ribbons.

Many studies on the phase behavior, miscibility and thermal properties in polymer and liquid crystal (LC) mixtures have been reported in recent years. Ballauff [1986] developed the theory for the phase behavior of mixtures of a thermotropic liquid crystal and a flexible polymer within the framework of the Flory lattice model. Ahn *et al.*[1992] studied the thermodynamic and phase behavior of blends of LC, 4-cyano-4'-heptylbiphenyl (7CB) and each of two amorphous polymers, poly(methyl methacrylate)(PMMA) and polystyrene(PS) as a function of temperature or LC concentration. Phase diagrams for both the binary PMMA/7CB and PS/7CB blends were constructed from DSC and optical microscope observation showing that 7CB was partially miscible in both PMMA and PS.

Kim *et al.*[1993] used the light scattering technique to study the kinetics of polymerization-induced phase separation in a LC and polymer mixtures. They observed a cascading phenomenon where phase separated domains become unstable and undergo phase separation for a second time. The Lebwohl-Lasher model of LC and the Flory-Huggins lattice model of liquid crystal polymers were combined by Zhang *et al.*[1995] to calculate the phase diagram of the mixtures of low molar mass

liquid crystal and flexible polymers. It was shown that the isotropic interactions between polymer segments and the liquid crystals are important and this results in isotropic/isotropic demixing before isotropic/nematic demixing. Shen *et al.*[1995], Chiu *et al.*[1995; 1996] and Kyu *et al.* [1996] computed the phase diagrams in the mixtures of polymer and LC by combining Flory-Huggins theory for isotropic mixing and Maier-Saupe theory for nematic ordering. Rodrigues *et al.*[1998] studied the microscopic behavior of blends of poly(ethylene oxide)(PEO) with two different LC in order to evaluate miscibility. The LC were 4-cyano-4'-n-heptylbiphenyl (7CB) and p-cyanophenyl-p-pentyloxy-benzoate (pCP). Thermal analysis and morphology evaluation showed the influence of each component on the other and suggested that they are miscible at all ranges of concentration. The pCP dispersed in the PEO-rich-phase of the matrix, and shifted the transition temperature. Scanning microscopy analysis of the PEO/7CB system indicated that the blend components were uniformly mixed because of chemical interactions between the constituent groups of PEO and 7CB. These results are in agreement with the DSC analysis. Chuenchaokit[1998] studied the properties of the blend systems of poly(bisphenyl-A-carbonate)(PC) with two LCs in the cyclohexyl-biphenylcyclohexanes group (CBC33 and CBC53) at low concentration range of LCs. The shear viscosities of pure PC and their blends were investigated using a capillary rheometer and the glass transition temperatures were measured by Differential Scanning Calorimeter (DSC). Experimental results showed that the viscosity of the blends with only a small weight fraction (1 percent) of LCs is about 90 percent lower than that of the pure polycarbonate. Powanusorn[2000] investigated the rheological, thermal and mechanical properties of LCs and polymer blends in order to compare with these of the base polymer. The results show that LC may improve the processability of the base polymer by reducing the melt viscosity while the LCs did not affect the thermal and mechanical properties of the polymer.

It has long been known that a LC can reduce the melt viscosity of polyolefins and polyester blends [Buckley *et al.* 1984]. However these effects are very similar to these induced by other small molecule addition especially the lubricant additives such as Zinc stearate. In an extensive series of experiments on blends with LCs [Chuenchaokit 1998; Powanusorn 2000] we have observed a reduction in the blend viscosity under shear, using twin-plate and capillary rheometers. We have found that

very small amounts of LC can dramatically reduce the shear viscosity of the melt blend, but the mechanisms are still under investigation. If the addition of LC contributes to the non-shear dynamics of the polymer molecules, the mechanism of the reduction in melt viscosity would be different from that of the normal lubricants. The LC blends are usually transparent and this may imply the miscibility at the molecular level. This is in contrast with normal lubricants, which are likely to phase separate at the molecular level.

1.2 Literature Review of Miscible Polymer Blends

For the last decade, the study of the miscibility window for blends containing random copolymer has been carried out extensively. A homopolymer forms a miscible blend with random copolymer in a certain copolymer composition and temperature range, when there is a strong unfavourable interaction between comonomer units of copolymer, though all segmental interactions are positive. Therefore, the ellipsometric studies are very suitable for evaluating the miscibility of copolymer blends showing miscibility window behaviour, which show a broader interface than homopolymer pairs. The miscibility window behaviour has been reported for some blends, e.g. poly(methyl methacrylate) (PMMA) and styrene–acrylonitrile random copolymer (SAN) [Stein *et al.* 1974]. Higashida *et al.* [1992] reported the temperature dependence of all three segmental interaction parameters by ellipsometry [Kressler *et al.* 1993]. It was indicated that the phase behaviour of PMMA/SAN blends could be explained by a simple mean field model considering the difference of the temperature dependence [Higashida *et al.* 1995]. Shimomai *et al.* [1996] also showed that this phase behaviour could be explained by the equation of state theory applied for the mixture of homopolymer and random copolymer.

1.3 Objectives

In this present work the light scattering was used to study miscibility of melt mixed SAN/PMMA (20/80) blends after adding LCs or lubricants at various compositions.

1.4 Organization of Thesis

This thesis comprises 7 chapters. The first chapter introduces general ideas and scope of this work. The next chapter deals with thermodynamics of polymer blends while the kinetics of phase separation is described in Chapter 3. Liquid crystals and lubricants are detailed in Chapter 4, followed by the manifestation of materials and preparation method in Chapter 5. Miscibility and kinetics of phase separation of SAN/PMMA Blends with liquid crystals or lubricants as well as morphological investigations are coped with in Chapters 6. Conclusions and recommendation are reviewed in the last chapter.



สถาบันวิทยบริการ
จุฬาลงกรณ์มหาวิทยาลัย

Chapter II

Miscibility and Thermodynamics of Polymer Blends

The general models that can describe properties of polymer blend is introduced in this chapter. Starting from the classical thermodynamics, followed by other related theories based on the lattice model, such as classical Flory-Huggins theory, Flory equation of state is described briefly. The differences between nucleation-growth and spinodal decomposition with respect of the free energy change during phase separation are manifested, and finally the blending techniques and determination of miscibility are verified.

2.1 Principles of Polymer-Polymer Miscibility

The basic and very useful thermodynamic equation that can describe the miscibility of two polymers is the Gibbs free energy equation:

$$\Delta G_m = \Delta H_m - T\Delta S_m \quad (2.1)$$

where ΔG_m is the Gibbs free energy of mixing

ΔH_m is the enthalpy of mixing

ΔS_m is the entropy of mixing

T is the temperature in Kelvin

The enthalpy and entropy of mixing are generally both positive for a pair of polymers so that the two-polymer mixtures will form a single phase only when the enthalpy term is less than the entropy term ($T\Delta S_m$). The Gibbs free energy of mixing is usually controlled by the enthalpy term which has to be very small positive or even negative in order to be favorable to mixing. Equation 2.1 apparently can predict whether a blend is miscible, immiscible, or partially miscible by taking into account the sign of ΔG_m as seen in Figure 2.1. With the positive sign of Gibbs free energy, the blend is immiscible whereas the negative sign indicates a miscible blend. Nevertheless,

some can exhibit partially miscible, even with the negative sign of ΔG_m . Thus, the second criteria required for complete miscibility is that the second derivative of the Gibbs free energy of mixing with respect to the compositions is always positive.

$$\frac{\partial^2 \Delta G_m}{\partial \phi_i^2} > 0 \quad (2.2)$$

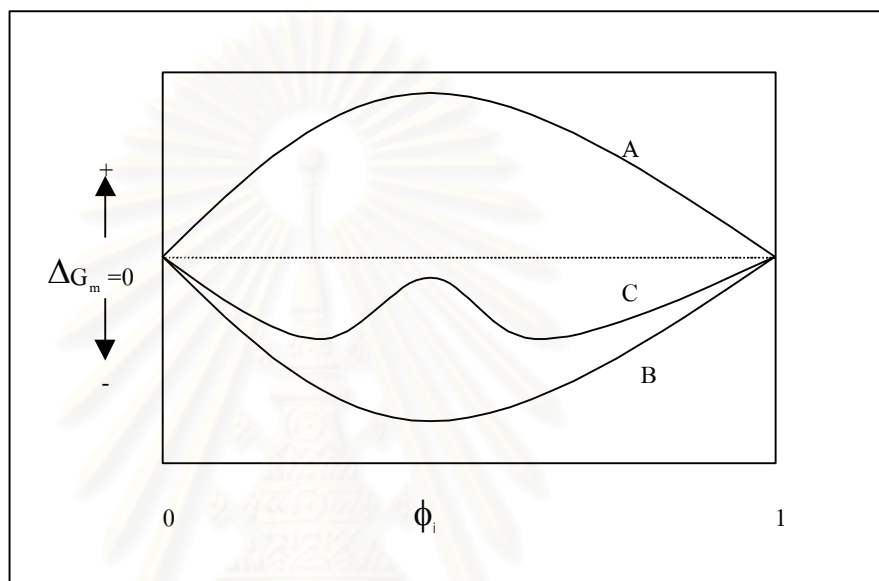


Figure 2.1: Plots of Gibbs free energy of mixing as a function of composition for a binary mixture exhibiting three types of mixing behaviour; immiscibility (A), complete miscibility (B) and partial miscibility (C).

Two examples of the phase diagrams of binary polymer mixtures related to curve C in Figure 2.1 are shown in Figure 2.2. In Figure 2.2(a), the phase separation occurs due to an increase in temperature, and this behaviour is known as the *lower critical solution temperature* (LCST) [Bernstein *et al.* 1977]. On the other hand, the behaviour shown in Figure 2.2(b) where the phase separates when decreasing the temperature is called the *upper critical solution temperature* (UCST). In the former, the phase separation proceeds upon heating in the blend exhibiting LCST behaviour which is typically observed in high molecular weight polymer blends. On the contrary, the blend is normally miscible at high temperature and becomes immiscible as the temperature decreases.

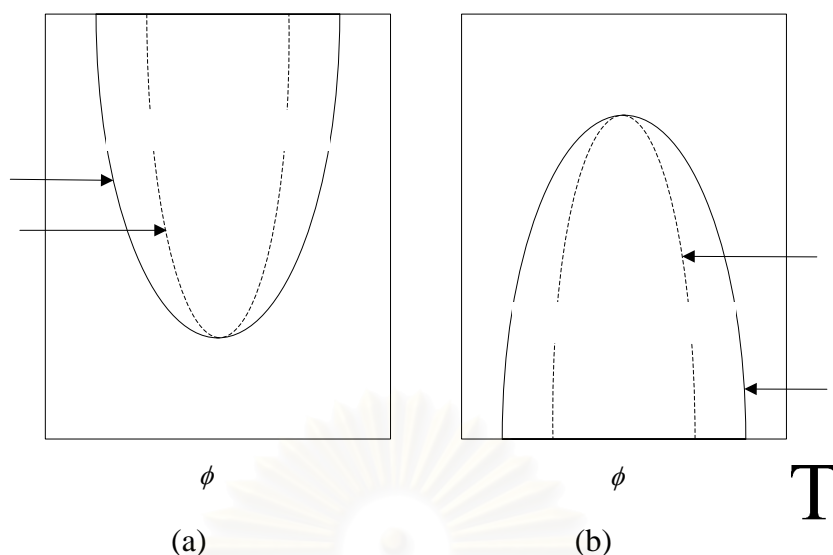


Figure 2.2 (a) The corresponding LCST-type phase diagram for a binary mixture, (b) The corresponding UCST-type phase diagram for a binary mixture.

For polymer blends it appears that not only the UCST and LCST phase diagrams have been found, but other types of phase diagrams can also be observed. Figure 2.3 presents a schematic representation of various types of phase diagrams for polymer mixture, and for the sake of clarity, the discussion here will be restricted to monodisperse binary mixture. As can be seen from Figure 2.3a, there is no instability regime indicating that the blend appears completely miscible. Figures 2.3 b-c clearly show that the UCST and the LCST exist separately, whereas in Figures 2.3 d-f, the UCST merges with the LCST.

สถาบันวิทยบริการ
จุฬาลงกรณ์มหาวิทยาลัย

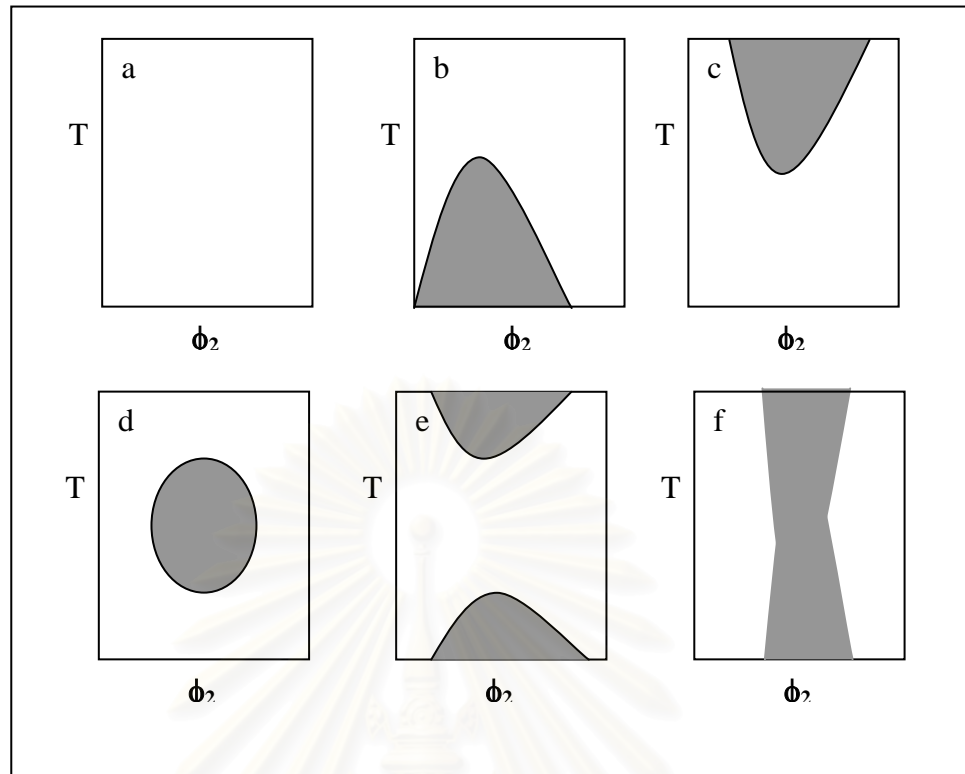


Figure 2.3 Presents a schematic representation of various types of phase diagrams for polymer mixtures [Olabisi *et al.* 1979].

2.2 Mechanism of Phase Separation

If the temperature of a partially miscible blend is raised from the one-phase region to the two-phase region, then concentration fluctuations become unstable which results in phase separation via spinodal decomposition. The driving force for this process is provided by the gradient of the chemical potential. Figure 2.4 is a typical dependence of ΔG_m on ϕ for a system that is partially miscible at the temperature T_0 . The main diagram in Figure 2.4 shows the corresponding miscibility limits in temperature and composition. Clearly, for any composition between ϕ_1 and ϕ_2 the system can reduce ΔG_m by separating into two phases with composition ϕ_1 and ϕ_2 . The solid line is called the *binodal* limit and is defined by the points of common tangent to ΔG_m at that temperature. At these compositions the chemical potentials μ_1 and μ_2 are equal and the two phases can coexist. The dashed line is the *spinodal* limit, defined by the points of inflection where $\frac{\partial^2 \Delta G_m}{\partial \phi_2^2} = 0$, these points are ϕ'_1 and ϕ'_2 . For

the compositions between ϕ'_1 and ϕ'_2 , $\frac{\partial^2 \Delta G_m}{\partial \phi_2^2} < 0$ and the system is unstable to all small concentration fluctuations. The phase separation process is called spinodal decomposition. Between ϕ_1 and ϕ'_1 , ϕ'_2 and ϕ_2 , $\frac{\partial^2 \Delta G_m}{\partial \phi_2^2} > 0$ so that small fluctuations are damped out and the phase separation proceeds by a nucleation and growth process. For $\phi < \phi_1$ and $\phi > \phi_2$, the system is a stable single phase.

In addition, the point where the spinodal limit meets the binodal limit in such a system is called the critical point corresponding to the critical temperature and the critical composition. This point is defined as:

$$\frac{\partial^3 \Delta G_m}{\partial \phi^3} = 0 \quad (2.3)$$

สถาบันวิทยบริการ
จุฬาลงกรณ์มหาวิทยาลัย

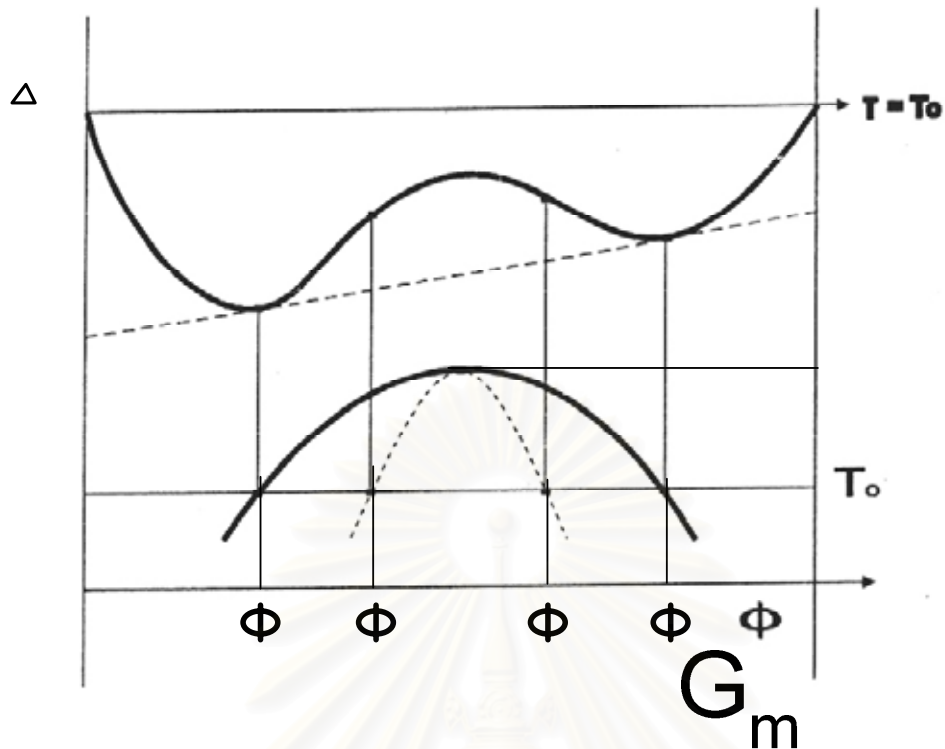


Figure 2.4 Illustration of the corresponding miscibility limits in temperature and composition.

Considering Figures 2.5(a) and (b), it can be seen when the original system composition is laid in unstable phase as shown with C_0 . The tie lines C_a-C_a' , C_b-C_b' , and C_c-C_c' connect the points on the free energy curves representing the two compositions of the nonhomogeneous system whose average composition is C_0 . In Figure 2.5(a), the free energy of the homogeneous phase of composition C_0 is point O. Any small perturbation on composition about C_0 resulting in two phase also results in moving of the free energy of homogeneous phase toward the lower free energy, making system more stable. In Figure 2.5(b), the homogeneous system needs activation energy to overcome the boundary hill and moves toward the lowest energy state, i.e. point C_a and C_a' in Figure 2.5(b). The limit of metastability is the lowest free energy represented by the tie line C_a-C_a' , and it is defined as the binodal, whereas the unstable change is called spinodal.

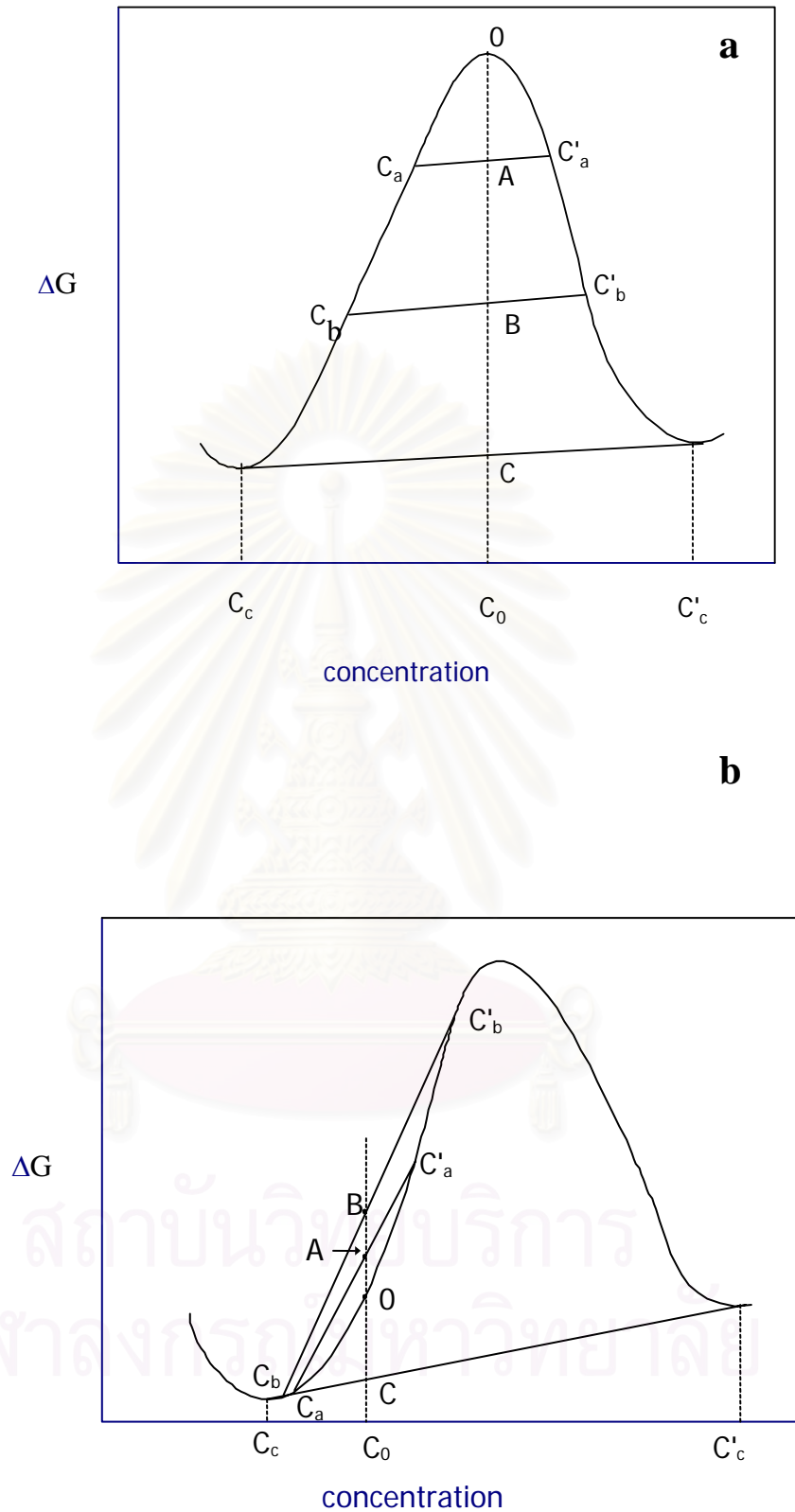


Figure 2.5 Schematic illustration of the free energy –concentration diagrams: (a) unstable region, (b) metastable [Olabisi *et al.* 1979]

2.2.1 Nucleation and Growth

Nucleation and growth is a process which starts within the metastable state. The system begins with the activated sites called nuclei. The nuclei are different from an equal number of nearest neighbour molecules because they possess an excess of surface energy which produces the aggregate as a new phase [Olabisi *et al.* 1979]. The nuclei grow in their sizes and number with a decrease in free energy; however, their concentration still remains constant. The growth process can be represented by Figure 2.6.

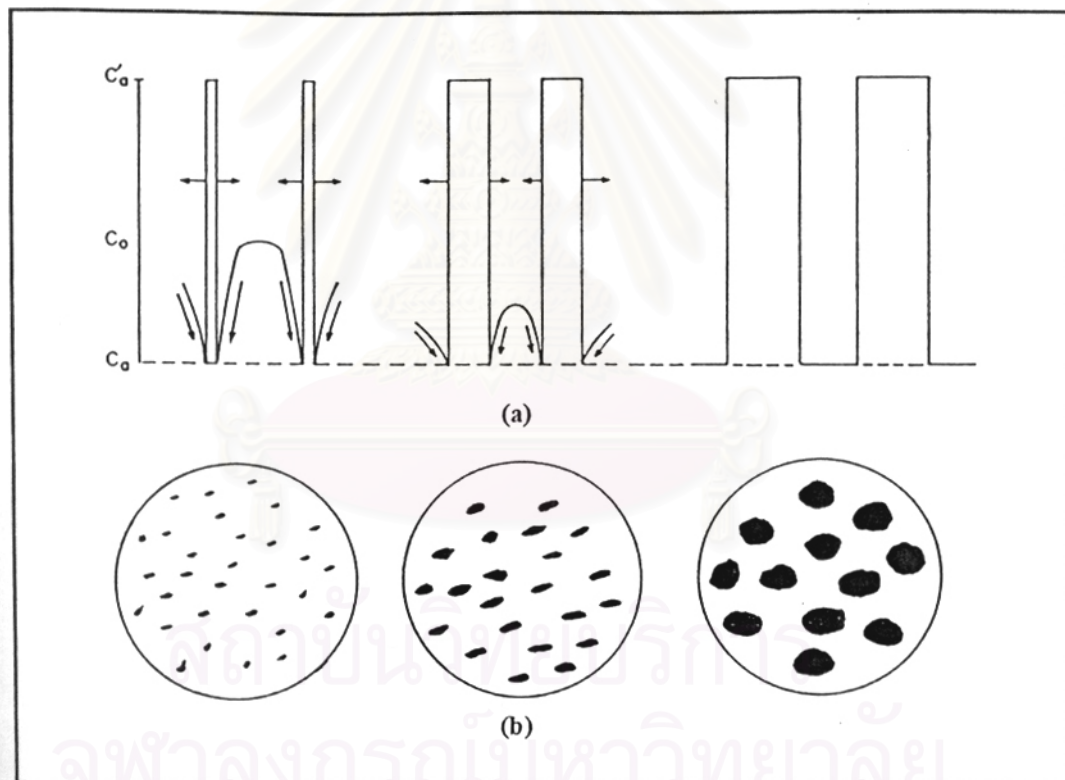


Figure 2.6 Schematic illustration of a phase separation by the nucleation and growth mechanism: (a) one-dimensional evolution of concentration profiles, (b) two-dimensional pictures of the phase structure [Olabisi *et al.* 1979].

2.2.2 Spinodal Decomposition

Spinodal decomposition is a kinetic process that occurs within an unstable region. The spinodal decomposition process is associated with a reduction in the free energy of mixing therefore the phase separation can occur spontaneously. No activation energy is required for this process. The growth originates, not from nuclei, but from small amplitude which statistically modulation with a certain maximum wavelength. The interwoven structures at the beginning become coarser and larger as the spinodal proceeds, and eventually turn into droplet in order to reduce the surface energy. The amplitude and the wavelength of the concentration fluctuation continue growing until reaching the equilibrium. The growth process and corresponding phase structure are shown in Figure 2.7.

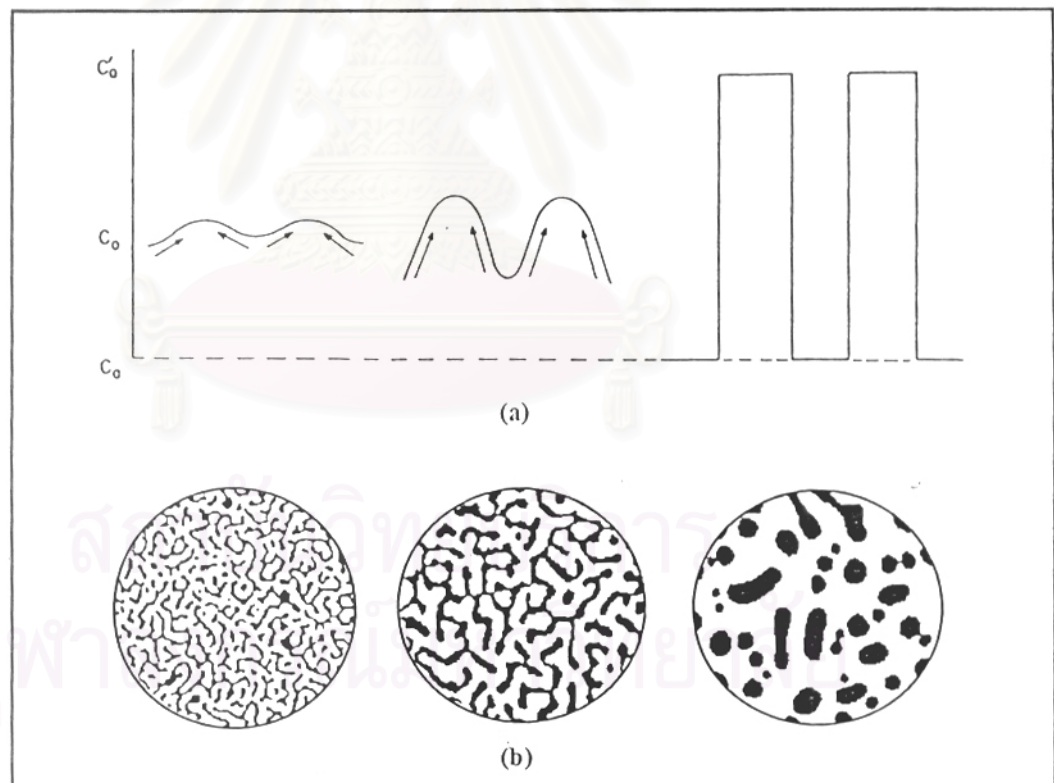


Figure 2.7 Schematic illustration of a phase separation by the spinodal decomposition mechanism: (a) one-dimensional evolution of concentration profiles, (b) two-dimensional pictures of the phase structure [Olabisi *et al.* 1979].

Several theories have been developed to describe both mechanisms of phase separation. Among these theories, the most important and well-known one is Cahn-Hilliard theory. The kinetics of phase separation via spinodal and nucleation and growth will be discussed in more detail in the following chapter.

2.3 Thermodynamic Theories

2.3.1 The Flory-Huggins Theory

This theory is based on the idea of arranging chains of small molecules inside the lattice free cell. Flory and Huggins [Flory 1941, 1942; Huggins 1941, 1942] have independently formulated a lattice model which was successfully able to treat theoretically the changes of the entropy and the enthalpy of mixing. Flory and Huggins suggested the entropy equation for the thermal mixing of monomer and chain molecule liquid. This then has been extended to the polymer-polymer mixture, and experimented. The entropy equation, which was derived is

$$\frac{\Delta S_m}{k} = - \left[\left(\frac{\psi_1}{r_1} \right) \ln \psi_1 + \left(\frac{\psi_2}{r_2} \right) \ln \psi_2 \right] \psi_0 \quad (2.4)$$

where ψ_i is the segment fraction of polymer i

ψ_0 is total number of segment

r_i is the number of segment per chain molecules of polymer i

k is the boltzman constant (1.38×10^{-23} J/K)

Note that there were several assumptions for this equation, e.g. the molecular weights of polymers were much higher than that of solvent, polymer molecules comprised uniform flexible segments which can be put into the lattice. By substitution ψ_i , r_i in Equation 2.4 with the volume fraction, ϕ_i , the general equation can be obtained.

$$\frac{\Delta S}{k} = -(n_1 \ln \phi_1 + n_2 \ln \phi_2) \quad (2.5)$$

where n_i is number of molecules of component i

To calculate the Gibbs free energy for polymer-polymer system, the enthalpy of mixing which shows the interaction between the adjacent molecules should be known. From the Van Laar expression the enthalpy of mixing can be written [Olabisi *et al.* 1979] as:

$$\frac{\Delta H_m}{kT} = \Psi_1 \Psi_2 \chi_{12} \Psi_0 \quad (2.6)$$

where χ_{12} is Flory-Huggins interaction parameter (dimensionless). The χ_{12} is negative in exothermic mixing, while the χ_{12} is positive in endothermic mixing.

The Gibbs free energy is then written as

$$\Delta G_m = kT \left[\left(\frac{\Psi_1}{r_1} \right) \ln \psi_1 + \left(\frac{\Psi_2}{r_2} \right) \ln \psi_2 \right] \Psi_0 + kT \Psi_1 \Psi_2 \chi_{12} \Psi_0 \quad (2.7)$$

Equation (2.7) is known as the classical Flory-Huggins equation which can be applied to a mixture of two polymers as well. The theory can be successfully used to describe the blend of polymers exhibiting UCST behaviour. Furthermore, the Flory-Huggins theory cannot explain all the shape of phase diagram including the temperature and the composition dependence of the interaction parameter. From Equation (2.7), since the entropic contribution to free energy generally is marginal and if χ_{12} becomes negative or the system is exothermic, the system will be miscible in all temperature range. This clearly shows that the Flory-Huggins theory fails to explain the LCST behaviour. In addition, the original interaction parameter χ_{12} was supposed to be independent of concentration, temperature, and molecular weight.

However, many later works have found that the Flory-Huggins interaction parameter in fact depended on temperature, composition and pressure.

Tompa [1956] suggested that the χ_{12} should also depend on the composition and suggested the extensive expression of Flory-Huggins interaction parameter as,

$$\chi = \chi_1 + \chi_2\Psi + \chi_3\Psi^2 + \dots \quad (2.8)$$

Further developments were introduced by Koningsveld *et al.* [1971]. A parameter 'g' as a function of composition, temperature, pressure and molecular weight has been used in the lattice model instead of χ_{12} . The free energy of mixing has then been modified to be in a simple form as:

$$\frac{\Delta G}{RT} = \frac{\Psi_1}{r_1} \ln(\psi_1) + \frac{\Psi_2}{r_2} \ln(\psi_2) + g\Psi_1\Psi_2 \quad (2.9)$$

The parameter 'g' was used in various forms as an adjustable term to fit the data. Therefore, the equation was limited to a specific system and the values of 'g' from different experimental conditions can be different. Equation (2.9) can be fit to experimental curves very well by manipulating the constants. However, these equations are empirical and the constants cannot be directly related to the molecular origin.

Because of the inadequacies of the lattice theory, Flory *et al.* [1964] have developed a new so-called equation of state theory to correct the contribution of the entropy and enthalpy of mixing. However, the Flory-Huggins theory is still widely use as a basic description for polymer mixing thermodynamics due to its simplicity.

2.3.2 The Flory Equation of State Theory

In this theory, the polymer molecules were treated as hard spheres with equivalent volumes. The hard core properties of the pure components and the mixtures were characterized by three equation of state parameters V^* , T^* and P^*

which can be evaluated from the pure component data such as density, thermal expansion coefficient and thermal pressure coefficient.

Flory and his workers described the equation of state for two pure components and their mixtures as:

$$\frac{\tilde{P}\tilde{V}}{\tilde{T}} = \frac{\tilde{V}^{1/3}}{\tilde{V}^{1/3} - 1} - \frac{1}{\tilde{V}\tilde{T}} \quad (2.10)$$

where \tilde{P} , \tilde{V} , \tilde{T} are the reduced pressure, volume and temperature, respectively. These reduced values are defined as:

$$\tilde{P} = \frac{P}{P^*} \quad (2.11)$$

$$\tilde{V} = \frac{V}{V^*} \quad (2.12)$$

$$\tilde{T} = \frac{T}{T^*} \quad (2.13)$$

where P^* , V^* , T^* are the characteristic pressure, volume and temperature respectively.

Those three reduced properties apparently are difficult to measure directly. So let first consider three measurable fundamental coefficients, namely the thermal expansion coefficient α_T , the thermal pressure coefficient γ , and the compressibility κ , which can be written in reduced expressions as:

$$\alpha_T = \frac{1}{V} \left(\frac{\partial V}{\partial T} \right)_P = \left(\frac{\tilde{T}}{T\tilde{V}} \right) \left(\frac{\partial \tilde{V}}{\partial \tilde{T}} \right)_{\tilde{P}} \quad (2.14)$$

$$\gamma = \left(\frac{\partial P}{\partial T} \right)_V = \left(\frac{\tilde{T}P}{T\tilde{P}} \right) \left(\frac{\partial \tilde{P}}{\partial \tilde{T}} \right)_{\tilde{V}} \quad (2.15)$$

$$\kappa = \frac{\alpha_T}{\gamma} = -\frac{1}{V} \left(\frac{\partial V}{\partial P} \right)_T = - \left(\frac{\tilde{P}}{P\tilde{V}} \right) \left(\frac{\partial \tilde{V}}{\partial \tilde{P}} \right)_{\tilde{T}} \quad (2.16)$$

The thermal expansion coefficient and the thermal pressure coefficient are related by the compressibility, κ , as:

$$\alpha = \kappa\gamma \quad (2.17)$$

In the limit of pressure going to zero, the equation of state can be reduced to the simplest form

$$\frac{(\tilde{V}^{1/3} - 1)}{\tilde{V}^{4/3}} = \tilde{T} \quad (2.18)$$

The thermal coefficient is therefore can be written via temperature and the reduced volume as:

$$\alpha_T \tilde{T} = \frac{3(\tilde{V}^{1/3} - 1)}{1 - 3(\tilde{V}^{1/3} - 1)} \quad (2.19)$$

The thermal pressure coefficient is similarly obtained as follows,

$$\gamma = \frac{P^*}{T\tilde{V}^2} \quad (2.20)$$

Considering a binary system and by making an assumption that the characteristic volumes of both components are equal, let them be where V^* :

$$V_1^* = V_2^* = V^* \quad (2.21)$$

The advantage of the Flory's equation of state theory over the Flory-Huggins theory is that both LCST and UCST behaviour can be predicted. There are many theories that came out lately. However the equation of state that widely accepted is the equation by Flory.

2.4 Blending Techniques

To blend polymers, there are three main methods – mechanical blending, solution blending, and in-situ polymerization. Mechanical mixing is the popular method in commercial blending. Solution blending usually is adopted for small amounts of materials and in academic studies. The in-situ polymerization needs special kinds of polymer and special processes.

2.4.1 Mechanical Blending

The mechanical mixing or so-called the melt mixing process has long been known to be the most well-known appropriate method and dominates the usage of blends due to the economical reason and high scale production. Polymer blends can be obtained by applying heat or force to two pure components however many parameters are needed to be taken into account such as viscosity, phase separation temperature, glass transition temperature (T_g), melting point temperature (T_m), etc.

2.4.2 Solution Blending

The solution casting or sometimes called solvent casting is another main method. In fact it is also popular, not even less than the previous one. Nonetheless this method can be applied only in small scale especially in laboratory work. Polymer blend can be prepared by dissolving two pure components in a common soluble solvent. The solvent is later eliminated. Generally three methods have been widely utilized to remove solvent. The first one is the common technique and mostly used, starting by allowing solvent to evaporate at room temperature, then putting in a vacuum oven and continually increasing temperature. The optimum heating rate

depends on polymer system. The second methods result in powder product by freezing and storing the mixture under vacuum. The last method is used for the high boiling point common solvent [Thongyai 1992]. Putting polymer solution in non-solvent can lead to the precipitation of the polymer and the products are also in powdered form.

2.4.3 In-situ Polymerization

In-situ polymerization is the polymerization process that polymerizes one monomer in the process of another polymer. The mixing process happens during the polymerization. This method is used in the production of partially miscible blends such as high impact polystyrene. The advantage of this method is that it can be used with polymers that cannot be melt mixed because of a high T_g , low thermal stability or low phase separation limit.

2.5 Determination of Miscibility

It is clear that polymer blends have different properties from their pure components. Among those blends, there are still differences between miscible blends and immiscible blends as well. It should also be noted that the miscibility of the system might appear to be homogeneous when using one method for determination but inhomogeneous when using another method, depending on the nature of each method and the size scale accessible by each technique. The approximate limit ranges of experimental techniques are shown in Figure 2.8. So far a large number of methods have been introduced in order to study polymer blends more easily and accurately. Three main groups with respect to the ways of study are briefly discussed herein; T_g study, scattering study, morphology study.

2.5.1 Glass Transition Temperature Study

Measurement of T_g which marks the characteristic transition of the amorphous region of a polymer or blend from a glassy state to a rubbery state, is the most convenient and popular way to investigate the miscibility or immiscibility of polymer

blends. It is generally known that miscible blend always exhibits one T_g whereas immiscible blend has two T_g 's. In the case of partial miscibility, two shifted T_g 's can be observed. The T_g can be measured using the technique of differential scanning calorimetry (DSC), dynamic mechanical thermal analysis (DMTA) and dielectric relaxation. The details of DSC technique which is used in this work are given in Chapter 5.

2.5.2 Scattering study

For amorphous systems, homogeneous mixtures are usually transparent whereas heterogeneous mixtures are cloudy that results from the reflective indices difference of two mixtures. The variations of temperature, pressure and compositions of the mixture can change the miscible blends from being transparent to cloudy. The first appearing of cloudiness denotes the cloud point. Using light scattering technique, one can investigate phase separation phenomena, namely nucleation & growth and spinodal decomposition. So far it should be noted that to employ scattering technique, not only laser light source can be used, x-ray and neutron is available as well. However, since the operation cost is very high and there are few equipments in the world, those methods are uncommonly used.

2.5.3 Morphology study

Using highly powerful microscopic techniques, it can reveal the internal structure, e.g., interpenetrating phases which are impossible to see with bare eyes can be revealed. The normal technique which can be used to observe phase boundary under normal light is optical microscope. However, as some blends have very tiny components, other more powerful techniques are required, i.e. transmission electron microscopy (TEM), scanning electron microscopy (SEM), atomic force microscopy (AFM). It should be noted that in order to see the structure clearly, preliminary treatments such as etching or staining are sometimes necessary.

Domain size	1	2	3	4	5
Microscopy		TEM		SE	optical
Spectroscopy	IR				
Thermal		DSC			
Mechanics					
Dielectric					
Diffraction	WAX	SAXS	SANS		light

Figure 2.8 Approximate ranges of experimental techniques to study blend morphology of: (1) interatomic; (2) molecular, spherulites; (3) filler aggregates, compatibilised blends; (4) reinforcements, noncompatible blends; (5) voids [Utracki 1989].

2.6 Conclusions

In summary, the principle of thermodynamics has been described in Section 2.1. The general Gibbs free energy of mixing equation can easily be used to estimate the miscibility and phase separation curve with respect to ordinary thermodynamic functions. In Section 2.2, the mechanism of phase separation has been illustrated. It appears that phase separation in polymer blends can take place via 2 routes, spinodal decomposition and nucleation and growth depending on the free energy curves. If the temperature of a partially miscible polymer blend is raised from the one-phase region to the two phase region, then concentration fluctuation becomes unstable and results in phase separation via spinodal decomposition. The driving force for this process is provided by the gradient of the chemical potential. While in the case of nucleation and growth once a blend is quenched into metastable state, it requires activation energy such as impurity. The line that separates the metastable state and stable state is called the binodal line, while the spinodal line divides the metastable state and unstable

state. In Section 2.3, applications of statistical thermodynamics on polymer system have been presented. Two main theories namely Flory-Huggins theory and the Flory equation of state as well as other recently developed theories have been shown. The Flory-Huggins theory is very general and can be extended to several other theories. It appears that this theory is still used nowadays, albeit a number of flaws. In Section 2.4, three main methods for blending of polymers have been described. The first one is the mechanical blending which is popularly used in commercial scale blending. The second one is the mixing in the common solvent which has some limitations due to their various ways in elimination of the solvent. The last one is the in-situ polymerization which produces special kind of polymers under good conditional control. In Section 2.5, the methods for determination the blend miscibility by detecting the changes in the properties caused by the phase separation has been exhibited. The most common property that can be detected is the T_g . By using the fact that a pure component exhibits one T_g , the mixed system that shows one T_g can likely conclude as a miscible blend.



Chapter III

Kinetics of Phase Separation in Polymer Blends

Phase separation kinetics of polymer blends has been an increasingly interesting subject in recent years because of its fundamental and practical importance. A number of studies have been made on the coarsening kinetics of the phase-separated structure of polymer mixtures. The results have shown that the coarsening process of the polymer mixtures with a critical composition can be classified into the following three stages; [Hashimoto *et al.* 1991; Takenaka *et al.* 1992; Cummings *et al.* 1992; Hashimoto 1993; Edel 1995] (i) early stage, (ii) intermediate stage, and (iii) late stage. In the early stage of spinodal decomposition, the time evolution of concentration fluctuations is well-described by the linearized theory proposed by Cahn-Hilliard [1958; 1959 ; Cahn 1961; 1965; 1968] for small molecule systems, and the concentration fluctuation grow exponentially with time. In the intermediate stage of spinodal decomposition, the time evolution of the concentration fluctuations becomes increasingly nonlinear with time, as a consequence, both the wavelength and amplitude of the dominant mode of concentration fluctuations grow with time. In the late stage of spinodal decomposition, the amplitude of concentration fluctuations reaches an equilibrium value, but the size of the phase-separated structure continuously growing with time.

Regarding the spinodal decomposition mechanism, many works so far studied the theory of spinodal decomposition. de Gennes [1979; 1980] and Pincus [1981] presented calculation subjected on spinodal decomposition in polymer blend systems by adapting the original Cahn-Hilliard [1958 ; 1959 ; 1965] theory which has been developed for low molecular weight systems. Later on, Binder [1983] extended the developed Cahn-Hilliard theory by including thermal fluctuations which were originally introduced by Cook [1970]. These two theories have introduced different viewpoints to describe the fluctuations which have wavelengths smaller than the dimension of a polymer coil. For those larger than the polymer coil, their results led to the same expressions as those of the linearized theories for low molecular weight systems, namely Cahn-Hilliard and Cahn-Hilliard-Cook theories. They used the Flory-Huggins description for free energy term with modification for the interfacial

free energy term. Recently, Strob [1985; 1997] carried out numerical calculations based on Binder's calculation and demonstrated the influence of the fluctuation term. Later, Okada *et al.* [1993; 1995] included the first time, the thermal fluctuation into the linearized theory of the Cahn-Hilliard-Cook theory. For experiments of deeper quench, the virtual structure factor a small in q range, and the time dependent static structure factor, $S(q,t)$, reduced back to the original Cahn-Hilliard theory.

As shown in Figure 3.1a, only the amplitude of the concentration fluctuation grows with time in the early stage of spinodal decomposition, while the wavelength remains constant. The concentration distribution was described well by the linearised theory [de Gennes 1980; Binder 1974; 1983; 1986; 1991; 1998]. During the intermediate stage both the wavelength and amplitude of concentration fluctuation grow with time. In the late stage, the local concentration reaches equilibrium, only the wavelength change then can be observed. The scaling analysis has been recently developed for this stage.

In this chapter the fundamental theories of phase separation via spinodal decomposition are discussed, beginning with the Cahn-Hilliard linearised theory, followed by its limitation.

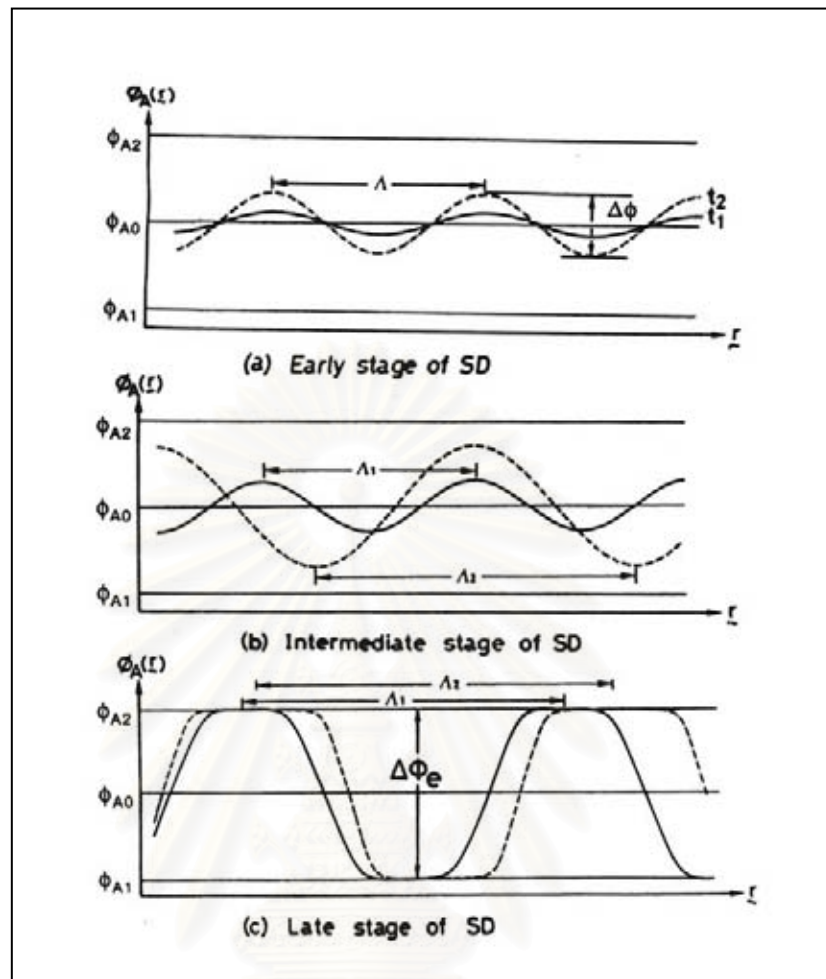


Figure 3.1 Schematic diagrams show the concentration fluctuation in the early (a), intermediate (b) and late stage of spinodal decomposition(c). $\Delta\phi = \phi_{A1} - \phi_{A0}$ is the amplitude of fluctuation, Λ is the wavelength of concentration fluctuation [Hashimoto 1993].

3.1 Spinodal Decomposition

Spinodal decomposition is a phase separation process that occurs within an unstable regime and grows from small amplitude composition fluctuations. The spinodal decomposition process is associated with a reduction in the free energy of mixing therefore the phase separation can occur spontaneously. The growth of the amplitude of wavelike composition fluctuations increases with time which results in continuous diffusion creating interconnected phase.

The spinodal decomposition process can be classified into three stages; an early stage where the amplitude of the concentration fluctuation increases with time at constant wavelength, an intermediate stage where both the amplitude and the wavelength increase with time and a late stage where the amplitude reaches its steady state while the wavelength still increases with time. This classification, in general, depends on each blend system. An important feature of this process is the kinetics of the early stage which is studied in this work. The well-known theory used to predict the early stage kinetic behaviour is described in this section.

Several theories have been developed in order to explain spinodal decomposition correctly. The first well-known theory is the Cahn-Hilliard linearised theory. This is rather general and considered to be a fundamental theory of later developed theories like the role that the Flory-Huggins theory does to the thermodynamic polymer field. The other important theory is Cahn-Hilliard-Cook theory.

3.1.1 Cahn-Hilliard Linearised Theory

The Cahn-Hilliard theory [1958 ; 1959 ; 1965] is based on the linearization of a generalized diffusion equation and is considered to be only applicable to the early stage of spinodal decomposition. Basically the linearised theory of Cahn and Hilliard is based on deriving and solving a general diffusion equation. They firstly neglected the effect of material flow and estimated the total free energy of an incompressible and isotropic binary system as a function of order parameter, which herein referred to the composition using Taylor's expansion and neglected the third and higher-order terms.

They related thermodynamics to the diffusion equation by introducing the chemical potential $\mu(r,t)$ as a driving force for diffusion of the system once developing spinodal decomposition into the general diffusion equation. It is assumed that there is no reaction and free movement, the inter-diffusion flux $J(r,t)$ can be expressed as:

$$\mathbf{J}(\mathbf{r},t) = -M \nabla \mu(\mathbf{r},t) \quad (3.1)$$

where M is the diffusion mobility and for the sake of simplicity, it was assumed constant.

The chemical potential $\mu(\mathbf{r},t)$ is defined as

$$\mu(\mathbf{r}, t) = \frac{\partial F}{\partial c} \quad (3.2)$$

$$\begin{aligned} \frac{\partial c}{\partial t} &= -\nabla \mathbf{J}(\mathbf{r}, t) \\ &= M \nabla^2 \mu(\mathbf{r}, t) \end{aligned} \quad (3.3)$$

This equation can be solved if the chemical potential $\mu(\mathbf{r},t)$ is known. They again were estimated it using Taylor expansion, and neglected the third and higher-order term [Cahn *et al.* 1958]. The Fourier transform was applied to equation 3.6 in order to make it easier to solve. However, unfortunately, the Fourier amplitudes cannot be measured. The structure function $S(\mathbf{q},t)$, which can be related to scattering experiments is defined as:

$$S(\mathbf{q}, t) = \langle |c(\mathbf{q}, t)|^2 \rangle \quad (3.4)$$

where $c(\mathbf{q},t)$ is the Fourier transform of $c(\mathbf{r},t)$ which is defined as:

$$c(\mathbf{q}, t) = \frac{1}{(2\pi)^{3/2}} \int c(\mathbf{r}, t) e^{-i\mathbf{q}\cdot\mathbf{r}} d\mathbf{r} \quad (3.5)$$

The scattering wave vector q is the magnitude of \mathbf{q} :

$$q = \frac{4n\pi}{\lambda} \sin\left(\frac{\theta}{2}\right) \quad (3.6)$$

where λ is the wavelength of the radiation source,

θ is the scattering angle,

n is the refractive index of the blend calculated from:

$$n = \phi_1 n_1 + \phi_2 n_2 \quad (3.7)$$

With those assumptions, eventually the modified equation of motion for the structure function can be written as:

$$\frac{\partial S(\mathbf{q}, t)}{\partial t} = -2Mq^2 \left[\left(\frac{\partial^2 f}{\partial c^2} \right)_{c_0} + 2Kq^2 \right] S(\mathbf{q}, t) \quad (3.8)$$

where M is mobility, $\left(\frac{\partial^2 f}{\partial c^2} \right)_{c_0}$ is the second derivative of free energy f at the initial composition c_0 , and κ is a positive coefficient. The Cahn-Hilliard theory can be applied to a polymer blend system.

The solution of Equation 3.8 is a general Cahn-Hilliard linearised equation, which can be written in an exponential function,

$$S(\mathbf{q}, t) = S(\mathbf{q}, 0) \exp(2R(\mathbf{q})t) \quad (3.9)$$

where $R(\mathbf{q})$ is the q dependent growth rate of concentration fluctuations, given by,

$$R(\mathbf{q}) = -q^2 M \left[\left(\frac{\partial^2 f}{\partial c^2} \right)_{c_0} + 2Kq^2 \right] \quad (3.10)$$

The leading term on the right hand side of equation 3.10 leads to a definition of an apparent diffusion coefficient, D_{app} , which is the coefficient of the q^2 term. Because the second derivative of the free energy (f) becomes zero at the spinodal temperature (T_s) it can be seen that D_{app} also becomes zero at T_s . Generally, the growth or decay with time depends on whether $R(q)$ is positive or negative. In the metastable region, $R(q)$ is always negative; consequently concentration fluctuations always decay. On the other hand, in the unstable region where the blend undergoes spinodal decomposition, $R(q)$ is positive for q less than the critical value (q_c), indicating that the fluctuation grows with time. The critical value q_c can be expressed as,

$$q_c = \sqrt{-\frac{(\partial^2 f / \partial c^2)_{c_0}}{2K}} \quad (3.11)$$

Equation 3.12 as a maximum at

$$q_m = \frac{1}{2} \sqrt{-\frac{(\partial^2 f / \partial c^2)_{c_0}}{K}} \text{ or } \frac{q_c}{\sqrt{2}} \quad (3.12)$$

Inserting the maximum wave vector q_m into equation 3.12, the growth rate $R(q_m)$ is:

$$R(q_m) = \frac{M}{8K} \left(\frac{\partial^2 f}{\partial c^2} \right)_{c_0}^{-2} \quad (3.13)$$

It is obvious from equation (3.12) and (3.13) that q_m depends on the thermodynamics characteristics ($\frac{\partial^2 \Delta G_m}{\partial c^2}$) while the $R(q_m)$ are controlled by both the thermodynamic driving force and the mobility.

In addition, from equation (3.10), the Cahn-Hilliard theory has predicted that a plot of $R(q)/q^2$ versus q^2 should give a linear relationship with a slope of $(-MK)$. The $R(q)/q^2$ value at $q = 0$, i.e. the intercept of this plot, yields the apparent diffusion coefficient, D_{app} are defined as,

$$D_{app} = -M \left(\frac{\partial^2 f}{\partial c^2} \right)_{c_0} \quad (3.14)$$

or

$$D_{app} = \frac{2R(q_m)}{q_m^2} \quad (3.15)$$

Concerning equation 3.10, a plot of $R(q)/q^2$ vs q^2 yields a straight line with a slope of $2MK$ and an intercept of D_{app} . Furthermore q_m and $R(q_m)$ also can be obtained by those slopes and intercepts as follows,

$$q_m = \sqrt{\frac{\text{intercept}}{-2\text{slope}}} \quad (3.16)$$

$$R(q_m) = \frac{(\text{intercept})^2}{-4\text{slope}} \quad (3.19)$$

The critical wave vector, q_c at which the $R(q)$ is zero is defined as

$$q_c = \sqrt{2}q_m \quad (3.20)$$

In terms of the wavelength of the dominant concentration fluctuation, Λ_m , and the critical wavelength, Λ_c ;

$$\Lambda_m = \frac{2\pi}{q_m} \quad (3.21)$$

The mobility term M in the equations above deserves some discussion. It is a combination of the dynamic properties of the components of the blend and the exact

way that combination is formed that has been the subject of considerable discussion in the literature. (See for example Meier *et al.* [1993] and more recently, Kamath *et al.* [2003])

In the case of an intimate mixture of the LC with the blend, M may be expected to be sensitive to the LC addition. Other ways to observe this effect would include a direct measurement of the viscosity though the confusing effect of surface segregation have been remarked, and a direct observing of the local dynamics using various spectroscopic techniques. However, as we were particularly interested in the miscibility behavior, it seemed worthwhile to investigate the mobility effect of the LCs by this route.

Many experimental investigations have been shown that the Cahn-Hilliard linearized theory was applicable only to the extremely early stage of phase separation and failed to describe the characteristic behaviour in the intermediate stage [Synder *et al.*, 1983; Hashimoto *et al.*, 1983; Okada *et al.*, 1986; Guo *et al.*, 1990]. Most of these early stage spinodal studies have reported a good agreement with Cahn-Hilliard theory while some have observed some discrepancies from the simple Cahn-Hilliard theory. The discrepancies normally found were that $R(q)/q^2$ versus q^2 plots were curved instead of linear as predicted in the theory. For example, Binder [1983] and Synder *et al.* [1985] pointed out that the nonlinear terms in the diffusion equation must be included in order to provide a quantitative description for the spinodal decomposition process. The decrease of $R(q)/q^2$ was not linear with q^2 [Sasaki *et al.* 1984], q_m was found shifted toward low q after spinodal decomposition has taken place for a long time [Hashimoto *et al.* 1986; Tomlins *et al.* 1989] and the calculated q_m and $R(q_m)$ was found to deviate from the observed values [Hill *et al.* 1985; Sato *et al.* 1988; Onuki *et al.* 1989], etc.

3.2 Conclusions

The most widely used theoretical treatment of the behaviour of a mixture undergoing spinodal decomposition consists of a phenomenological statistical theory based on a diffusion equation. This approach was used by Cahn and Hilliard, who

employed a simple linear model which retained only the lowest-order term of the composition dependence of the free energy and was considered to be only applicable to the early stage of spinodal decomposition. In this theory, for an inhomogeneous mixture of small molecules the time dependence of the static structure factor after the system was quenched into the two-phase region followed an exponential growth. It showed that the scattering intensity kept growing while the maximum wave vector was constant as time proceeded. This fitted quite well with a number of experiments especially at the certain range of time in the early stage of phase separation. Consequently, it has been suggested that the linearised theory might be used to approximately indicate the early stage of phase separation while beyond that the effect of thermal fluctuation, nonlinearity of the approximate chemical potential and the droplet growth should be taken into consideration. These are presented in Cahn-Hilliard-Cook and Langer-Baron-Miller theories.



สถาบันวิทยบริการ
จุฬาลงกรณ์มหาวิทยาลัย

Chapter IV

Liquid Crystals & Lubricants

4.1 Liquid Crystals

Liquid crystals were discovered more than a hundred years ago. They are defined as liquid material, which also have the high degree of anisotropy. One of the important manifestations of LCs is their melting behavior. When normal crystalline solid is heated, it changes from solid phase directly to isotropic liquid at its crystalline melting point (T_m). In liquid crystalline materials, several different mesophases are formed after their T_m and the mesophases will become isotropic at the higher transition temperature called clearing temperature. The transition properties of liquid crystals come from the rigid parts of their molecules, which are called mesogens. Mesogens consist of low molecular weight compounds. They are arranged along the main polymer chain or on side branches of the graft molecules.

4.1.1 Classification of Liquid crystals

Liquid crystals can roughly be divided into two areas:

4.1.1.1 Lyotropic liquid crystals which are formed from compounds having amphiphilic properties. Between the pure amphiphile and its isotropic solution in an excess of the solvent there exists, at intermediate concentrations, anisotropic properties characteristic of liquid crystal structured phases, consisting of ordered arrangements of micelles composed of amphiphile and solvent. Common examples of such lyotropic liquid crystals are those produced from soaps and other detergent systems and water.

4.1.1.2 Thermotropic liquid crystals which are formed from compounds whose molecules are mainly either rod-shaped or disc-shaped by thermal effects, i.e. by heating the crystalline solid or by cooling the isotropic liquid. Several materials exist in a liquid crystal phase at room temperature, and many other cases of this type can be produced by using mixtures of compounds.

4.1.2 Types of Liquid Crystals

4.1.2.1 Rod-Like Liquid Crystals

The most common type of liquid crystals, is composed of rod-like molecules with one molecular axis much longer than the other two. In the nematic liquid crystal phase for rod-like molecules, the long axis of the molecules tend to point along a certain direction as they move from one location to another.

Both positional order and orientational order are necessary for a smectic liquid crystal phase. There are a number of such phases, but two important cases are when its director is parallel to the normal layer (smectic A phase) and when its director is at an angle to the normal layer (smectic C phase). In both of these phases, there is no positional order within the plane of the layers.

4.1.2.2 Discotic Liquid Crystals

In addition to rod-shaped molecules, disc-like molecules also form liquid crystals. The anisotropic phases formed by disc-like molecules are called discotic liquid crystals and the simplest type is the nematic phase in analogy with the nematic phase formed by rod-like molecules. A time snapshot is shown in Figure 4.1, where it is seen that the short axes of the molecules maintain a preferred orientation. This simple phase of disc-like molecules has no positional order, just like nematic liquid crystals. Other discotic liquid crystal phases exist in analogy with smectic liquid crystals.

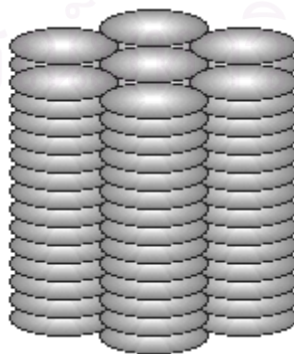


Figure 4.1 Discotic liquid crystal phases [Motong 2002].

Molecules that form discotic liquid crystal phases usually are comprised of a core based on benzene or triphenylene group have been added. These groups often resemble the molecules that form rod-like liquid crystals, with part of the “rigid core” pointing toward the center of the molecule and a terminal group pointing away from the center.

4.1.2.3 Lyotropic Liquid Crystals

It is possible to form liquid crystals by dissolving certain molecules in solution. These differ from the liquid crystal phases previously described because they are multi-component systems and the concentration of the various components is a new and important parameter. These liquid crystals are called lyotropic liquid crystals to differentiate them from the thermotropic liquid crystals. Thus in the case of lyotropic liquid crystals, concentration plays the role that temperature does in thermotropic liquid crystals; the transformation from one phase to another can be accomplished by changing the concentration.

A typical lyotropic liquid crystal molecule has two parts, one that is polar and therefore hydrophilic, and another that is nonpolar and therefore hydrophobic. Such molecules are called amphiphilic and form ordered phases when mixed with either a polar or nonpolar solvent.

4.1.3 Phase Structures of Liquid Crystals

In a discussion concerning the structures of liquid crystal phases formed by rod-like molecules, a point is often reached where the arguments centre on which structural features actually define the liquid-crystal-line state.

4.1.3.1 Nematic Structure

The nematic phase is essentially a one-dimensionally ordered elastic fluid in which the molecules are orientationally ordered, but there is no long range positional ordering of the molecules. In this phase the rod-like molecules tend to align parallel to

each other with their long axes all pointing roughly in the same direction. The average direction along which the molecules point is called the director of the phase. The rod-like molecules in the nematic phase are free to rotate about their long axes and to some degree about their short axes.

The molecular organization, classified as a nematic mesophase, involves in the irregular alignment in one dimension. Molecules remain parallel to each other in the nematic structure (Figure 4.2), but the position of their gravitational centers are disorganized. Molecules of nematic liquid crystals can be orientated in one dimension. Their mobilities can be reduced by the attraction to supporting surfaces. For examples, nematic molecules tend to lie parallel to the rough surface of a glass slide. A bright satin-like texture is observed when nematic liquid crystals are viewed between crossed polaroids. Characteristic dark threads appear at lines of optical discontinuity. These wavering filaments give the mesophase its name; take from the Greek word *nematos*, meaning fiber.

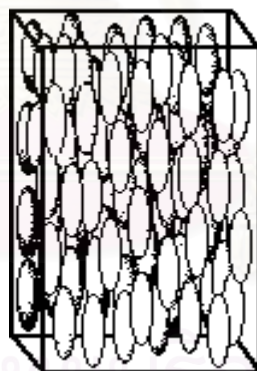


Figure 4.2 Nematic structure [Motong 2002].

The typical nematic liquid crystal can be represented by the structure in Figure 4.3(a). The bridging group B together with the two ring structures O_1 and O_2 form the “rigid core” of the rod-like molecule. This rigidity is necessary to make the interactions with the other molecules anisotropic and therefore favorable for the formation of liquid crystal phases. Modifications to the “rigid core” which ruin its linear structure or increase its flexibility tend to reduce or eliminate liquid crystalline behavior. The two terminal groups R_1 and R_2 are usually necessary for the formation

of liquid crystal phases, but may be quite short, a methoxy group for example, or nonexistent if the “rigid core” section is long enough. Figure 4.3(b) is an example of a molecule that forms a nematic liquid crystal phase.

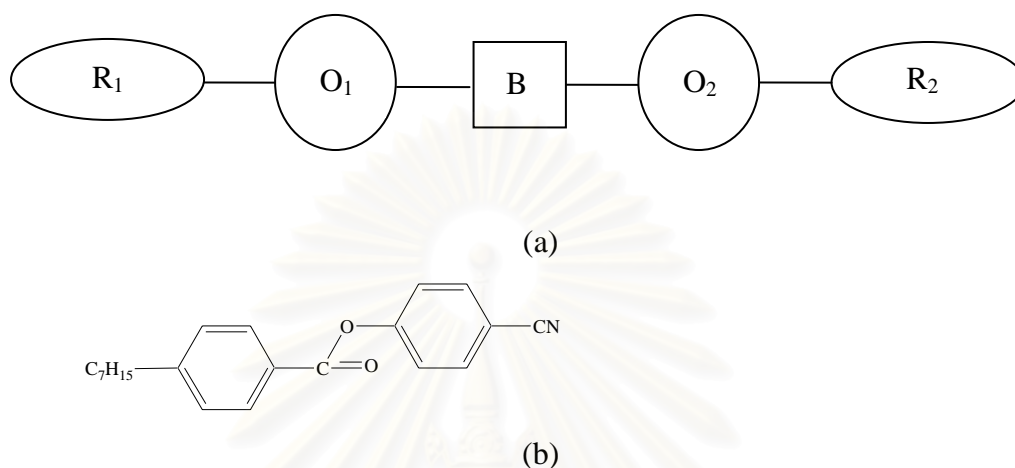


Figure 4.3 Typical rod-like liquid crystal forming molecule. (a) a schematic which R denotes an end group, O a ring structure, and B a bridging group, and (b) an example [Sperling 2001].

A number of different groups have been used as bridging groups. Some examples are diazo and azoxy compounds, esters, and biphenyls. The ring structures are frequently aromatic rings, but cyclohexane and other ring structures can be included. When synthesizing nematic liquid crystals with strong electrical properties, a polar terminal group is typically added to one end of the molecule such as cyano and nitrous oxide groups.

4.1.3.2 Smectic Structure

In the smectic structure, long molecules are arranged side by side in layers much like those in soap films. The term smectic (soap like) is derived from the Greek word for grease or slime. The layers are not strictly rigid, but they are flexible. Two dimensional molecular sheets can slide pass each other, see Figure 4.4. Molecular motion is rather slow, so smectic mesophases are quite viscous.

Optically smectic layers behave like uniaxial, birefringent crystals. The intensity of light transmitted parallel to the molecular layer is greater than that transmitted perpendicularly. The temperature dependence of smectic interval tested by birefringence has slightly small effect to internal order.



Figure 4.4 Smectic structure [Motong 2002].

Typical molecules that form smectic phases are very similar to those forming nematic phases but tend to be slightly longer. This can be done by elongating the “rigid core” of the molecule to include three rings or by making the terminal groups longer. This is well illustrated by examining the nature of the phases presented when molecules with the same “rigid core” but with longer terminal groups are investigated. When the terminal groups are very short, the compound melts from the solid to the nematic phase and ultimately to the isotropic liquid phase. As the terminal groups get longer, the compound melts first from the solid to a smectic phase, then to a nematic phase, and finally to the isotropic phase. With even longer terminal groups, the solid melts to a smectic phase and then directly to the isotropic liquid phase.

There is a good evidence to suggest that long terminal groups, especially hydrocarbon chains, are necessary for smectic phases to exist. Long “rigid core” molecules without long terminal groups may have nematic phases but they rarely have smectic phases. Likewise, structures containing strong dipoles perpendicular to the long axis of the molecule favor side-by-side organization and therefore tend to form smectic phases.

4.1.3.3 Cholesteric or Chiral Structure

The cholesteric structure is the third type of liquid crystal behaviors. It is so named because many compounds that form this mesophase are the derivatives of cholesterol. A cholesteric structure (Figure 4.5) is the shape of a nematic phase which is periodically wrapped around the axis. When chiral groups are present, the basic structure is helicoidal.

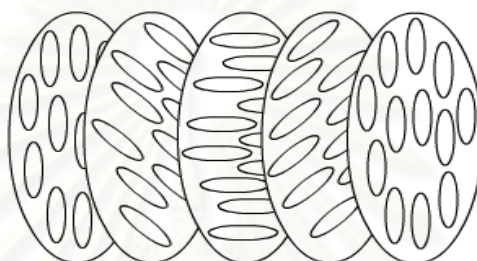


Figure 4.5 A cholesteric structure [Motong 2002].

4.1.4 Mesophasic Transition Temperatures

Liquid crystals can undergo various phase transitions as the temperature increases from the ordered to the least ordered states, as shown in Figure 4.6.

The temperature when liquid crystal changes from crystal to the first liquid crystalline phase, is called “crystalline melting temperature” (T₃).

The temperature when liquid crystal changes from smectic phase to nematic phase, is called “S→N transition temperature” (T₄).

The temperature when the last (or only) liquid crystalline phase gives way to the isotropic melt or solution, is called “clearing temperature” (T₅).

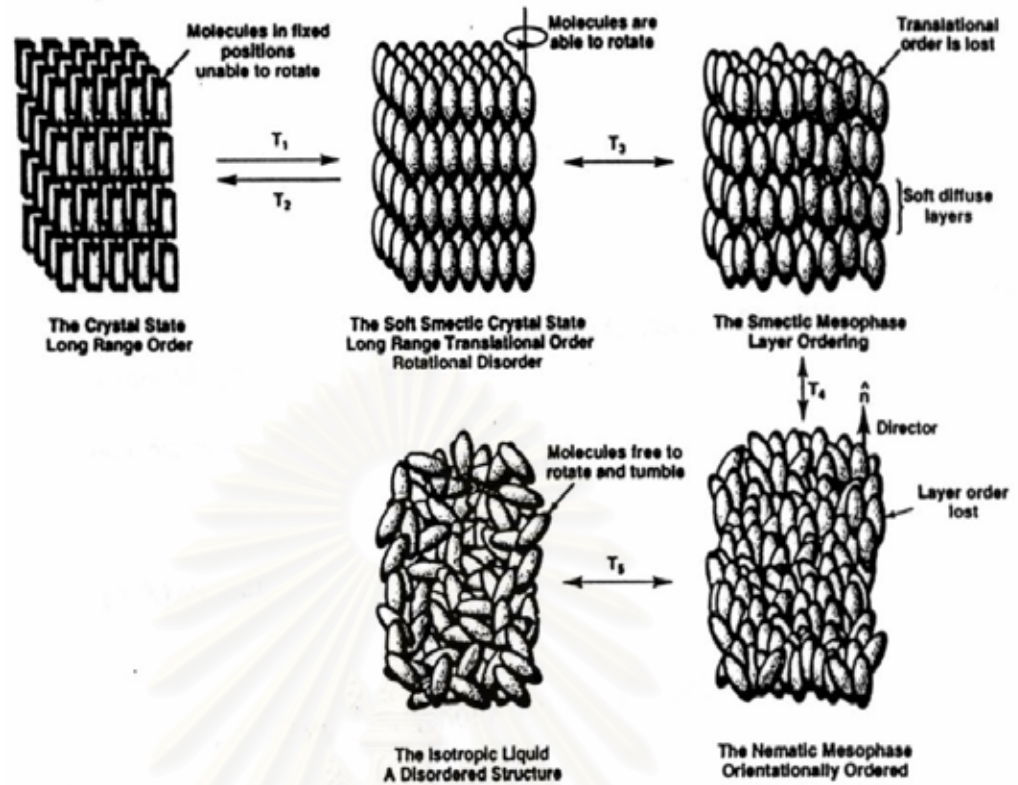


Figure 4.6 Phase transition of Liquid Crystal [Demas *et al.* 1998].

4.1.5 Polymer Liquid Crystals

As the linear molecules increase in length, they can gradually crossover into the realm of polymers, which are formed by small monomeric units linked together. A wide variety of polymers is possible including block copolymer, in which the polymers are composed of flexible parts and rigid parts with the rigid parts resembling the “rigid core” of rod-like liquid crystals.

Thermotropic polymer liquid crystals are polymers that possess at least one liquid crystal phase between the glass transition and the transition to the isotropic liquid. Lyotropic polymer liquid crystals are rigid polymers that form ordered phases when dissolved in solution.

4.2 Lubricants

Additives play quite an important role in the field of polymers either in their processing or during their usage. A lubricant may be defined for most purposes as a substance that reduces the friction, heat and wear between two surfaces. These surfaces might be between polymer molecules and the equipment or between polymer molecules themselves. Lubricants must facilitate processing of plastics in such a way that production runs efficiently without interruption, leading to final articles which are technically and aesthetically acceptable.

4.2.1 The Mechanism of Lubricant Action

When the lubricant is blended with polymer, the lubricant coats the surface of polymer particles. Thus, powder is lubricated and flows easily in the cold parts of the processing equipment. With an increase in temperature, polymer begins to soften and the lubricant melts and penetrates the polymer at which point in the barrel this occurrence. The rate of penetration of the lubricant into the polymer is governed by its solubility, which depends upon the structure of the lubricant molecule, as well as its polarity in relation to the polymers. The mechanism of a lubricant can be discussed in terms of two general classes of lubricants based on function. These are external lubricants and internal lubricants. There are no materials functioning entirely as internal or external lubricants, usually the lubricants exhibit a combination of the properties of the two with one being predominant.

4.2.1.1 *Internal Lubricants*

These materials promote intermolecular flow via a chain slippage mechanism. Such materials are characterized by being somewhat polar and semi-compatible. A plasticizer causes embrittlement at very low concentrations, but internal lubricants are non polar enough to change flexibility or hardness at room temperature. The polar nature of these materials allows them to be accepted into the polymer matrix at high temperatures. The Vander Waal 's forces between chains are reduced by the polar lubricants, which slips in between the polymer chains. This allows the chains a greater ease of movement because it decreases attraction between molecules. As rigid PVC cools, internal lubricant precipitates and becomes non-functional at room temperature.

The clarity is only slightly reduced because the lubricant is very finely divided in the polymer matrix. On the other hand, external lubricants adversely effect the clarity because of its incompatibility and its tendency to organize themselves into large droplets. These pseudoplasticizers can adversely affect the heat distortion of temperature by lowering the glass transition temperature of the polymer, if used in excess.

In real terms, internal lubricants reduce internal friction, which reduces shear burn in injection moulding applications, back pressure in extrusion and roll-parting forces in calendering. They give better gauge control in film, sheets and pipes, shorten cycles and promote better mould filling. Internal lubricants at typical concentrations have minimal adverse effects on fusion time, nor do they contribute significantly to metal release. If the concentration of the internal lubricant exceeds its solubility constant in the polymer, the internal lubricant will act as an external lubricant.

Internal lubricants also perform the following important functions:

- Reduce frictional heat build-up under shear.
- Promote gelation.
- Lower melt viscosity.

4.2.1.2 External Lubricants

External lubricants are responsible for two phenomena: metal release and particulate flow in the melt. External lubricants have low compatibility with the polymers and have a high affinity for metal surfaces. During the processing, they reduce the friction and stick between hot melt polymer and working surfaces of machinery. Hence, easier movement of stocks through the machinery is achieved and adhesion of hot melt to the machine which results in local formation of stagnant layers, overheating and degradation (burn up) in which degraded its material contaminants the stock and promotes further degradation, is prevented. External lubricants have lower compatibility with the polymer and hence they provide better metal-release or anti-sticking properties.

Chapter V

Materials and Experimental Techniques

This chapter explains the characteristics of materials used in this work as well as experimental techniques. Two commercial materials namely the commercial poly(methyl methacrylate) (PMMA) and poly(styrene-co-acrylonitrile) (SAN) are of interest. The chemical structures and the physical behaviours of those materials are firstly discussed. Sample preparation by using melt mixing method is considered, secondly. Lastly, several important techniques which were employed, are manifested ; differential scanning calorimetry, light scattering and scanning electron microscopy.

5.1 Material Characteristics

Poly(methyl methacrylate) is best known as the excellent transparent polymer. In addition, it also exhibits good rigidity, good abrasion resistance, an outstanding weather ability, and good general chemical resistance, except for some organic solvents. Owing to its prominent optic properties, the main products of poly(methyl methacrylate) are used in optic applications, such as automotive tail-light lenses, safety and security glazing, lights sky, illuminated signs and optical fibers. Its applications include coating substances such as floor waxes, and in emulsion latex) paints. The chemical structure of this polymer is shown in Figure 5.1.

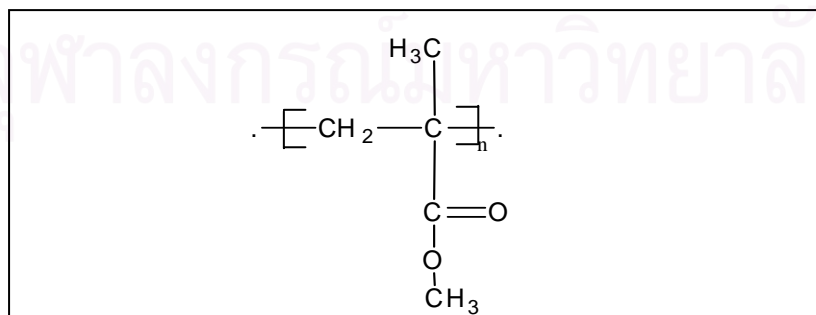


Figure 5.1 The chemical structure of poly(methyl methacrylate) (PMMA).

Copolymerization of styrene and acrylonitrile was discovered and patented by I.G. Farben Industries in the early 1930s, and was first commercialized in 1937. The poly(styrene-co-acrylonitrile) (SAN) with 15-37 %AN have been of most practical interest because they offer the useful combination of mechanical and aesthetic properties. Increasing an amounts of AN tends to produce a more yellow polymer, but improvement in color can be made by carefully excluding oxygen from the monomers and using azo-type initiators. Polymers containing more than 78% acrylonitrile (AN) are less amorphous and have lower strength due to the presence of polyacrylonitrile homopolymer. A styrene/acrylonitrile polymer with weight ratio of 76:24 is preferred because it exhibits an azeotropic mixture in which the concentration in the solution phase is the same as in the copolymer. Composition drift is undesirable during the production of SAN copolymer because of the incompatibility between SAN copolymer with different amount of AN, combined with the change in refractive index. Molau[1963] clearly showed the phase separation of random copolymers of styrene and acrylonitrile, if the variation of AN content exceeds 4% AN content. Three polymerization techniques are used in the manufacture of SAN polymers: emulsion, suspension, and continuous mass processes [Olabisi 1997].

SAN copolymer properties are directly related to the molecular weight of the polymers, molecular weight distribution, and distribution of the highly polar incorporated AN in the polymer chain. SAN copolymers are transparent, hard, rigid materials that have good dimensional stability and offer superior mechanical properties and chemical resistance compared to polystyrene homopolymer. The chemical resistance and mechanical properties are related to AN content and generally increase with incorporated AN. Dilute acids and alkalis, fat, grease, mineral oil, gasoline low in aromatics, and animal fats and oil are among the chemicals to which SAN copolymers are generally considered to be resistant. SAN copolymers are not resistant to concentrated mineral acids, aromatic hydrocarbons, chlorinated hydrocarbons, esters, ethers, and ketones. The chemical structure of this polymer is shown in Figure 5.2.

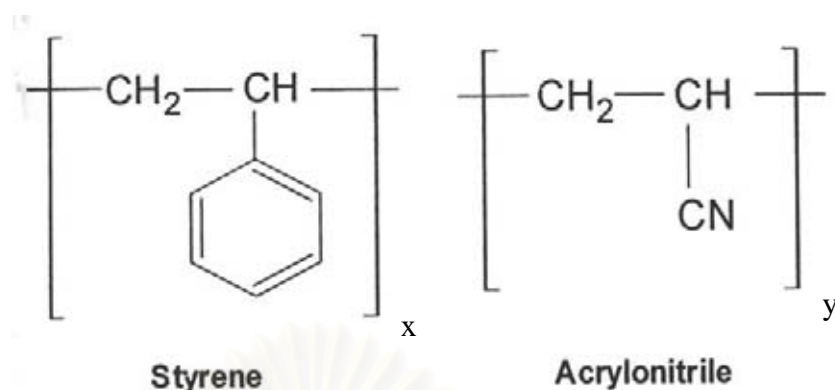


Figure 5.2 The chemical structure of styrene-co-acrylonitrile (SAN)

The random copolymer of styrene acrylonitrile (SAN) containing about 25% by weight of acrylonitrile (AN) was kindly provided by Bayer Polymers Co., Ltd. It appears as slightly yellowish transparent pellets with a glass transition temperatures (T_g) at 105 °C and molecular weight is 149926. The commercial grade Polymethyl methacrylate (PMMA) was kindly provided by TPI Polyacrylate Co., Ltd. Its T_g is 95 °C and molecular weight is 72575. The molecular weight of SAN and PMMA were determined by gel permeation chromatography analysis at National Metal and Materials Technology Centre. Both materials were kept in a dry atmosphere and heated prior to use. SAN and PMMA were heated at 130 °C in a vacuum oven for 4 hours before mixing in order to remove humidity.

Low molar mass thermotropic liquid crystals were purchased from Merck Co., Ltd. CBC33 and CBC53 are in the form of a white powder. Their structures which contain a cyclohexyl-biphenyl-cyclohexane backbone are shown in Figure 5.3 and 5.4 respectively. Molecular weight characteristics, transition temperatures, and other physical properties are shown in table 5.1.

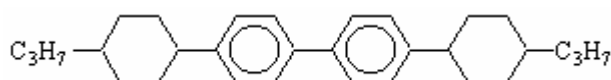


Figure 5.3 Structure of CBC33.

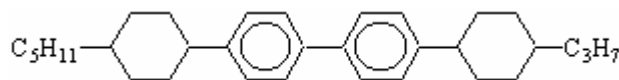


Figure 5.4 Structure of CBC53.

Table 5.1 Properties of low molar mass thermotropic liquid crystals.

Property	CBC33	CBC53
Melting point (°C)	158	164
Smectic-Nematic Temperature (°C)	223	260
Clearing Temperature (°C)	327	317
Molecular weight (g/mol)	403	431

The lubricant, glycerol monostearate (GMS) was kindly provided by RikevitaLtd (Malaysia). The melting point is 65 °C and the molecular weight is 358 g/mol. Zinc stearate with molecular weight 632 g/mol, was supplied by Quality Minerals Co., Ltd. The chemical structure of GMS and zinc stearate are shown in Figure 5.5 and Figure 5.6, respectively.

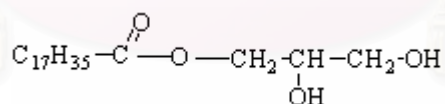


Figure 5.5 Structure of glycerol monostearate (GMS).

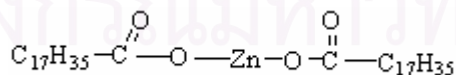


Figure 5.6 Structure of zinc stearate.

5.2. Equipment and Methods

5.2.1. Small Angle Light Scattering (SALS)

The study of miscibility was performed by using light scattering apparatus at the Department of Chemical Engineering, Chulalongkorn University, Thailand. The equipment is shown in Figure 5.7.



Figure 5.7 The light scattering equipment.

A He/Ne laser of 5 mW ($\lambda = 632.8$ nm) was used as an incident light source. Samples were placed on a LINKAM hot stage, which was mounted between the laser and a CCD camera. The temperature of the LINKAM hot stage was controlled by a computer. The light scattering pattern is captured by the CCD camera and analysed using the Image-Pro Plus 3.0 program.

Two different experimental techniques were employed using the light scattering apparatus, viz., a cloud point experiment, and a temperature jump experiment. In the former case, a number of dry films of each composition were heated at different heating rates. The point at which the scattered intensities start to increase is defined as the cloud point. Since cloud point values depend on the rate at which phase separation in the sample responds to the temperature changes, as a rule, the lower the heating rate the lower the cloud point value. Extrapolating heating rate to zero is then used to obtain a value close to the true cloud point. Several heating rates, viz., 0.3 °C/min, 0.5 °C/min and 1.0 °C/min were chosen for the cloud point measurement.

The second set of experiments was designed to determine the D_{app} and the spinodal temperatures, by following the spinodal decomposition process after a temperature jump inside the phase boundary. Homogeneous blends were annealed 20 °C below the desired phase separation temperature or cloud point for at least 15 min and then transferred quickly into the LINKAM hot stage, which was pre-heated to the desired temperature in two phase region. The final temperature was chosen from the cloud point curves, i.e. how deep we wanted to go inside the two phase region. The higher the temperature (bigger quench depth), the bigger the driving force for the concentration fluctuations.

5.2.2 Twin screw extrusion

The samples of SAN/PMMA at various compositions (10, 20, 30, 40, 50, 60, 70, 80, 90 % of SAN) were melt mixed by the PRISM twin screw extruder at Department of Chemistry, Faculty of Science, King Mongkut's Institute of Technology North Bangkok. The extruder machine as shown in Figure 5.8, consists of a twin screws which the raw materials are fed by a controllable feeder. The barrel contains the two intermeshing screws which operate in a co-rotating mode to provide a uniform and controllable stress field suitable for mixing polymers to obtain a regular composition distribution in the products [Utracki 1991]. There are some kneading paddles in the middles of the screws, which are effective in both the melting and the dispersing of the two polymers, in other words, they provide a better well-mixed flow.

The extruder is heated along its length at the variable set point temperatures by electrical heaters. Temperatures are controlled by three temperature sensors. At the end of screw, the slit die viscometer is connected and controlled by the electrically heated along its length to a given set point temperature. Along the midpoint of the vertical wall there are two horizontally aligned pressure transducers, at distance L apart. The die also has two corresponding temperature sensors.

Polymer pellets were first pre-mixed by paddle before feeding to the extruder. The mixed pellets were then put into the extruder, which was operated at torque 60%, screw speed at 30 rpm and the temperature between 190-210 °C. The temperatures used in the extruder here laid inside the phase separation regime hence producing two-phases samples consisting of two mixed phases with different compositions. These samples were cloudy as the consequence, and they were therefore necessary to anneal inside the miscible regime prior to use. The beads were heated overnight at 20 °C above their glass transition temperatures after which they became perfectly transparent. Thin film samples (approximately 0.05-0.10 mm.) for light scattering experiments were obtained by using a hydraulic hot press machine.

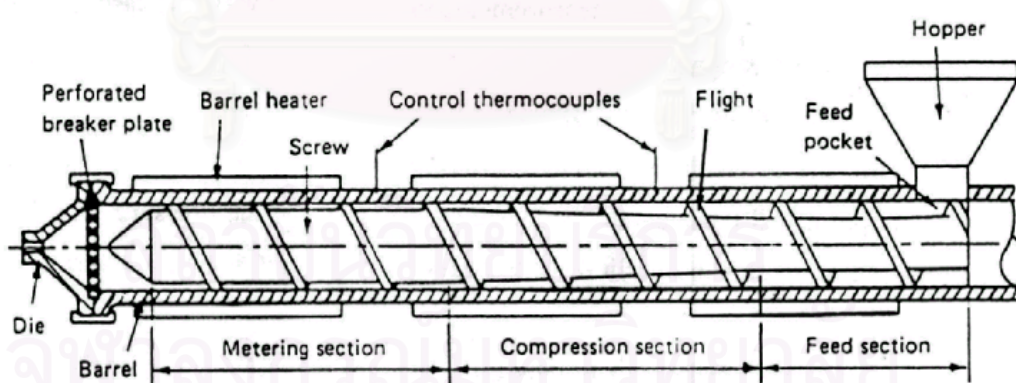


Figure 5.8 Illustration of a plasticating extruder [McCrum *et al.* 1997].

5.2.3 Differential scanning calorimeter (DSC)

DSC was used to examine both the T_g of the blends and the pure polymers. It has been known that a miscible binary blend generally exhibits one T_g which lies

between the T_g 's of the two components while an immiscible blend exhibits two T_g 's at exactly the same temperatures at the individual T_g . A partially miscible blend exhibits two T_g 's which lay between the T_g 's of two constituents.

As shown in Figure 5.9, the sample and the reference are simultaneously heated at a fixed rate until their temperatures reach the set point. Temperatures of both cells are kept similar, temperature differences therefore, exist between two cells when transformations occurs. The heat controller automatically compensates the temperature differences by increasing or decreasing an addition heating power to obtain similar temperatures in both pans. Further details of this technique can be found elsewhere [Wendlandt 1986].

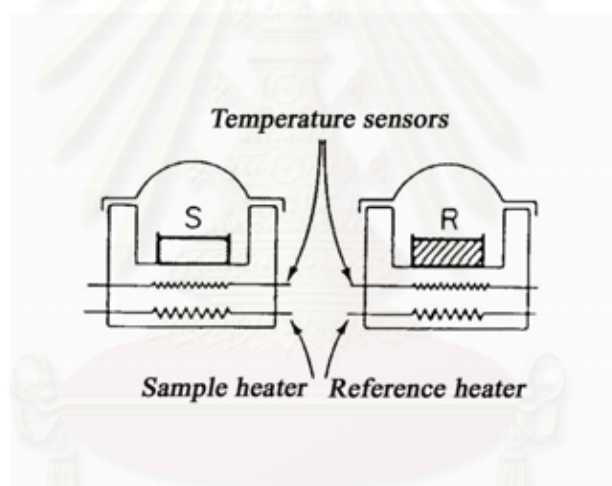


Figure 5.9 A schematic diagram of differential scanning calorimeter [Wendlandt 1986].

A Perkin Elmer (DSC 7) was used as a main T_g detector in this work. The weight of each sample used was in between 15-25 mg. Samples were placed on the aluminium pan and heated at the rate of 10 °C/min from room temperature to approximately 20 degrees higher than the T_g transition and then the pans are quenched to room temperature, held the temperature for 2 minutes and heated again at the same rate. The T_g value was obtained at the mid point of the specific heat changes. The second heating will produce the T_g that is free from the effects of the thermal history.

5.2.4 Scanning Electron Microscopy (SEM)

The scanning electron microscope (SEM) was originally devised in Germany in the 1930s by Knoll & von Ardenne, and has been considered as an original of the early electrical facsimile machine. In SEM, a fine beam of electrons is firstly scanned across the surface of an opaque specimen. Once the electron beam touches the surface of the samples, a difference of electron density in the specimen results in the varieties of scattering electron and photon emissions. Those electrons are detected, modified and modulated the brightness of the second beam scanned synchronously in cathode ray tube (CRT). The large amount of the signals produce a bright spot on the CRT while smaller signals produce a dimmer spot [Rojanapitayakorn 2000].

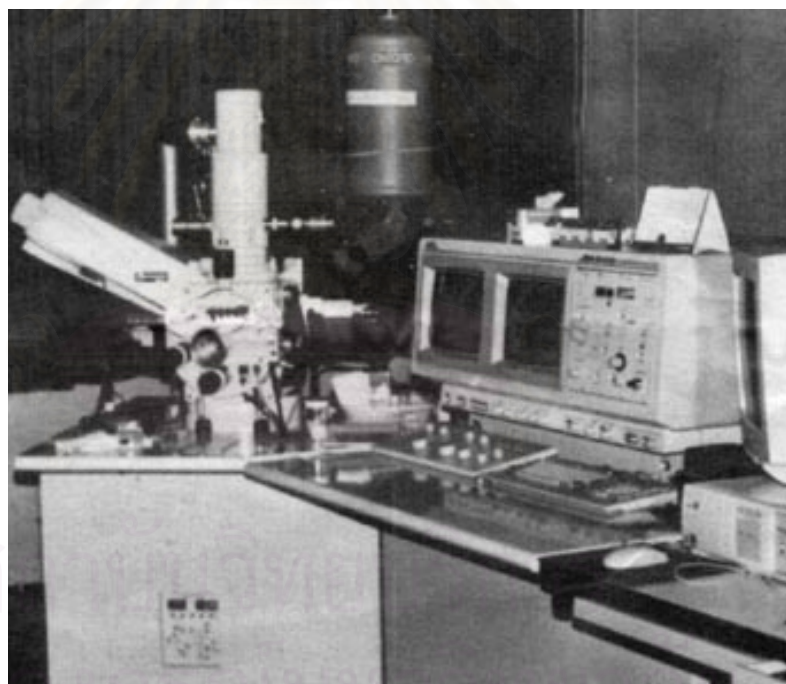


Figure 5.10 A photographic illustration of SEM model JSM-6400.

Phase separated morphologies of the fractured surfaces in this thesis were observed by using a scanning electron microscope JEOL JSM-6400 at the Scientific and Technological Research Equipment Centre, Chulalongkorn university as shown in Figure 5.10. Since this technique requires the sample having a good electron

conducting, it is necessary to provide conduction to specimens by coating a thin metal layer e.g. gold ,as used in this work. The coated specimens were kept in dry place before the experiments.



สถาบันวิทยบริการ
จุฬาลงกรณ์มหาวิทยาลัย

Chapter VI

Miscibility, Kinetics and Morphology of Phase Separation of SAN/PMMA Blends with Liquid Crystals or Lubricants

It has been known for more than a decade that PMMA forms miscible blends with SAN copolymer of a limited acrylonitrile (AN) content [Stein *et al.* 1974; Suess *et al.* 1987; Fowler *et al.* 1987; Cowie and Lath 1988; Kressler *et al.* 1993; Oultaache *et al.* 1994; Higashida *et al.* 1995; Newby *et al.* 2001; Cameron *et al.* 2002] while PMMA is not miscible either with homopolymer of styrene or acrylonitrile. Similar behaviour has been noted for other copolymer-homopolymer mixtures. A number of papers reported a variety of physical studies on blends of PMMA with SAN containing 28% by weight of acrylonitrile [Ohnaga *et al.* 1989] which is right at the upper limit of the composition ranges where miscibility occurs. The miscibility between SAN and PMMA is believed [Fowler *et al.* 1987] to be due to a strong specific intrachain repulsion between the co-monomer units (acrylonitrile and styrene in this case) that is favourable for mixing. Within the miscibility boundaries, the SAN/PMMA blends exhibit lower critical solution temperature (LCST) behaviour, in which phase separation occurs upon heating [McMaster 1975; Bernstein *et al.* 1977; Kressler *et al.* 1986; Fowler *et al.* 1987; Subramanian *et al.* 1990 and Kammer *et al.* 1991]

Stein *et al.* [1974] observed miscibility of SAN/PMMA blends by varying the AN contents in SAN from 9 to 26.5 wt%. Later on, Suess *et al.* [1987] have investigated the miscibility behavior of SAN/PMMA blends with differences in blend ratios and AN contents by small angle light scattering. They observed that SAN that has low AN content of the phase behavior dependent on the AN composition. At below 9.4 wt% of AN, the blends were immiscible and then the blends exhibited a lower critical solution temperature behavior when the AN content higher than 9.8 wt%. In the same year, Fowler *et al.* [1987] have also studied the phase behavior of SAN/PMMA blends which exhibited a lower critical solution temperature behaviour and their phase behaviour depended on the percent weight AN contents in SAN.

Sompradeekul [1998] studied the effects of small molecular solvent on the phase diagrams and tensile strength of SAN/PMMA blends. It was found that the phase diagrams of the blends prepared from different solvents were different and depended on the type of solvent, the boiling point of solvent and the period of drying time in a vacuum oven.

Cameron *et al.* [2002] studied the glass transition and the structure relaxation in blends of SAN/PMMA with different AN content in SAN by using DSC. The results show that SAN/PMMA (50/50) containing 30 wt% of AN in SAN was immiscible, while blends with SAN containing AN between 13 and 26 wt% were miscible. Thus the upper limit condition for miscibility for the PMMA/SAN blends was in the vicinity between 26 and 30 wt% of AN.

6.1 Glass Transition Temperature (T_g) Study

T_g is commonly measured by DSC, but the usage of T_g in determination of blend miscibility has its own limitations. As it is known that T_g region curves cover about at least a 15-20 °C range. Thus, if the difference of the T_g of the two polymers is within 15 °C, it is almost impossible to detect the extent of mixing by observing the two adjacent T_g s using DSC. This is the case for PMMA-SAN blends which the difference of the T_g 's of PMMA and SAN ranges between 8 and 15 °C depending on the copolymer composition of SAN. In this study, the T_g of the blends of PMMA and SAN copolymer before and after adding LCs and lubricants has been investigated.

The T_g 's of SAN and PMMA used in this research are in the same vicinity (SAN: 102.7°C, PMMA: 97.4°C) and quite far from the binodal limit (cloud point at about 205°C). The plasticizing effect which is expected to lower down T_g of the blends after blending with LCs are not discovered. The samples in the one-phase region were analyzed in order to determine the T_g values of the blends before and after adding 1.0 wt% CBC33, CBC53, Zinc stearate and GMS. It can be seen in Table 6.1 that T_g values of the blends after adding LCs were insignificantly different from the original blends. The T_g of The blends after adding lubricants either Zinc Stearate or GMS were slightly lower than the origin blends. It was appeared that the addition

of lubricants might reduced T_g of the polymer blends while the addition of LCs had no effect on these thermal properties.

Table 6.1 T_g of SAN/PMMA (20/80) blends after adding 1.0 wt% of Zinc Stearate, GMS, CBC33 and CBC53.

Sample	T_g ($^{\circ}\text{C}$)
20:80 SAN/PMMA	96.2
20:80 SAN/PMMA+ 1.0% Zinc Stearate	95.2
20:80 SAN/PMMA+ 1.0% GMS	92.3
20:80 SAN/PMMA+ 1.0% CBC33	96.4
20:80 SAN/PMMA+ 1.0% CBC53	96.2

6.2 Phase Behavior

The first part of this chapter illustrated the studies of miscibility and kinetics of phase separation of SAN/PMMA blends with and without LCs and lubricants from the early stage of spinodal decomposition. It started with phase boundaries investigation, followed by miscibility and kinetic discussion. Then the test of Cahn-Hilliard theory for phase separation was dealt with.

6.2.1 Cloud Point Determination

The phase diagrams were obtained by observing the light intensity while heating up samples very slowly for at least three different heating rates from the one-phase region into the two-phase region. The point at which the scattered intensities started to increase in the same way to that shown in Figure 6.1 is defined as the cloud point (T_c). It has been found that the observed cloud point temperatures were dependent on the heating rate as shown in Figure 6.2. As a result, the faster the heating rate, the higher the apparent cloud point temperature was observed. This was in agreement with other works which suggested that this phenomenon might be the result of the viscous and highly entangled nature of polymer blends [Guo 1990;

Thongyai 1994; Pavawongsak 1996; Soontaranun 1997; Rojanapitayakorn 2000; 2001]. In order to diminish the effect of relaxation and heating rate dependence, the method of extrapolation to zero heating rate was used to obtain the lowest cloud point temperatures. For our cloud point measurements, several heating rates (0.3, 0.5, 1.0 °C/min) were chosen. Extrapolating to zero heating rate as shown in Figure 6.2 was utilized in order to obtain the cloud point.

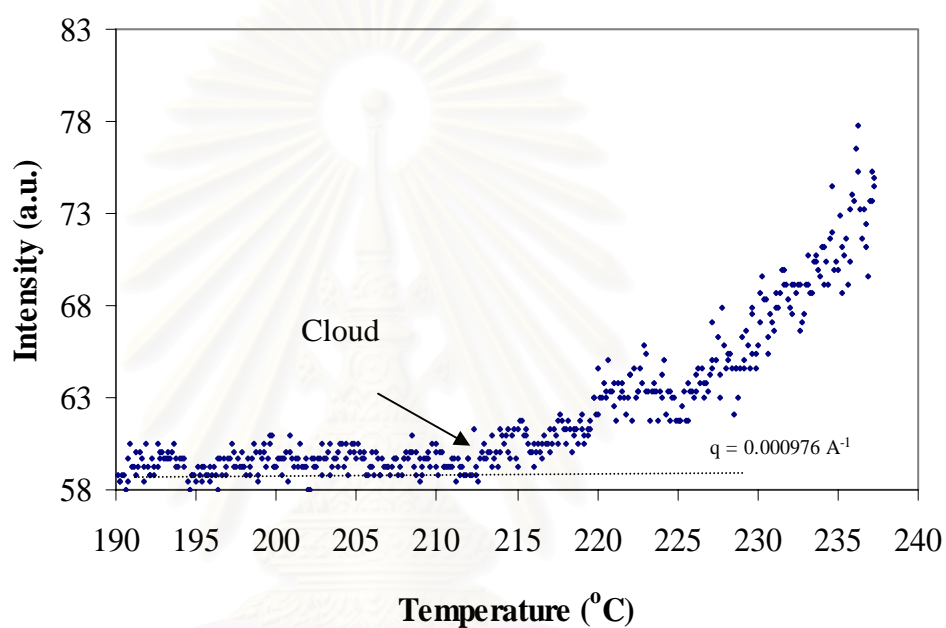


Figure 6.1 A plot of intensity against temperature for SAN/PMMA (40/60) blend at the heating rate of 1.0 °C /min.

สถาบันวิทยบริการ
จุฬาลงกรณ์มหาวิทยาลัย

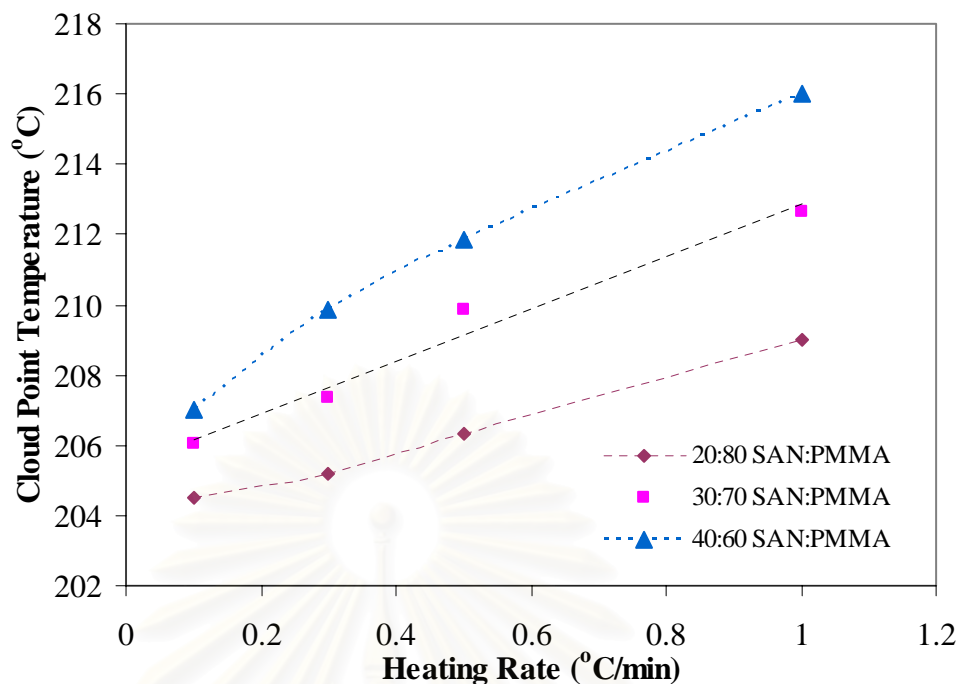


Figure 6.2 The observed cloud point temperatures at different heating rate.

As shown in Figure 6.2, the observed cloud point temperatures do not change linearly over the whole ranges of heating rate. This has been reported recently by Soontaranun [1997] that for some systems there was a distinct change in the slope of the curve of cloud point with heating rate, and it has been suggested that two mechanisms may be detected. The faster process, which showed up at the higher heating rate could then be spinodal decomposition, while the slow response could be nucleation and growth (NG).

Cloud point curves for SAN/PMMA blends are shown in Figure 6.3. The blends, which were first clear became cloudy after heating, indicating lower critical solution temperature (LCST) behavior. At temperatures below the cloud point curve, the samples are transparent and homogeneous. In other words, at temperatures above this curve, phase separation occurs. Figure 6.3 shows the cloud point temperatures for blends containing SAN copolymers with varying AN content, all extrapolated to zero heating rate. It has previously been noted that the phase behavior depended not only on \overline{M}_w but also on the amount of AN in SAN copolymer [Suess *et al.* 1987]. The SAN copolymer used in this study contained about 25 wt% of AN in SAN. The lower the

AN content in the copolymer, the lower the SAN wt% at the critical point of the blends. The data for the cloud points and the spinodal of the 25% AN blend in Figure 6.3, suggest that the critical composition should be between 10 and 20 wt% of SAN. The separation temperatures are falling as we reduce the amount of SAN in the blend, but while we can detect a cloud point at 20%, we cannot find any phase separation as we raise the temperature for concentration of 10%. Moreover, from Suess *et al.* [1987], SAN/PMMA blends usually have a critical point below 20 wt% SAN as shown by some literature values in Figure 6.3. For these reasons we chose this composition to study the effects of molecular movement of polymer after adding LCs and normal lubricants.

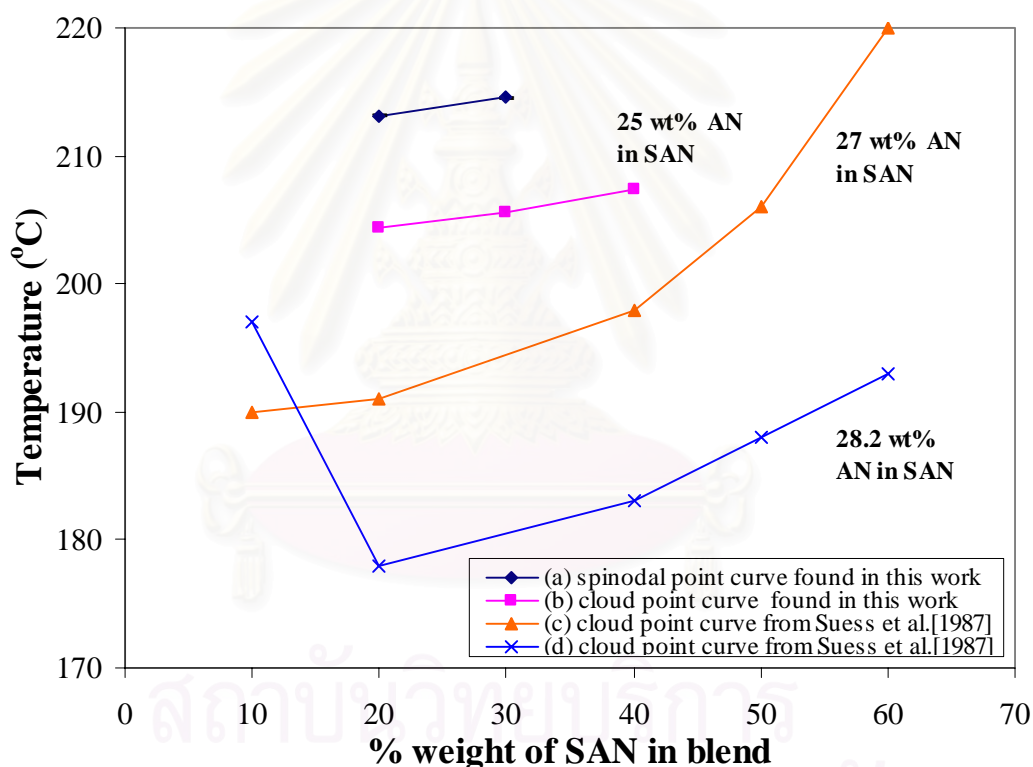


Figure 6.3 Phase diagram of SAN/PMMA determined by light scattering technique.

The cloud points were obtained from zero heating rate method. (a)-(b) \overline{M}_w of PMMA is 72575, \overline{M}_w of SAN is 149926, (c) \overline{M}_w of PMMA is 167000, \overline{M}_w of SAN is 82000, (d) \overline{M}_w of PMMA is 178000, \overline{M}_w of SAN is 83000.

6.2.2 Spinodal Determination

Light scattering technique is utilized in order to indicate whether a blend undergoes spinodal decomposition or NG mechanism. Sasaki *et al.* [1984] suggested that for the blend phase separating via NG, the scattered intensity did not increase exponentially with time, whereas the blend undergoing spinodal decomposition exhibited a contrary result. The changes of the scattered intensity ($I(q,t)$) as a function of scattering wave number (q) can also be used to determine the mechanisms of phase separation. For spinodal decomposition, the scattered intensity should develop a maximum peak at a particular angle and then the peak will move toward lower angles as phase separation proceeds, while no maximum peak can be observed in NG [Lefebvre *et al.* 1999; Mazumder *et al.* 1999].

According to temperature jump (215, 217, 220, 222 and 225 °C) experiments, the blends were suddenly heated and kept at constant temperature and inside the spinodal region. Surprisingly, the intensity did not change at the beginning of phase separation but delay for some time before linearly increasing as called in this work as the delay time deviated from the Cahn-Hilliard-Cook theory. However, after that distinctive period, the scattered intensity increases exponentially which can be explained by the linearised theory as shown in Figure 6.4.

The rate of change of \ln (intensity) with time (after any delay time) of scattered light patterns provides the Cahn-Hilliard growth rate ($R(q)$) [Hashimoto 1991; Jinnai *et al.* 1993] from equation (3.9). A D_{app} can then be obtained as in equation (3.10) from the y-intercept of a plot of $R(q)/q^2$ versus q^2 as shown in Figure 6.5.

$$S(q, t) = S(q, 0) \exp(2R(q)t) \quad (3.9)$$

where $R(q)$ is the q dependent growth rate of concentration fluctuations, given by,

$$R(q) = -q^2 M \left[\left(\frac{\partial^2 f}{\partial c^2} \right)_{c_0} + 2Kq^2 \right] \quad (3.10)$$

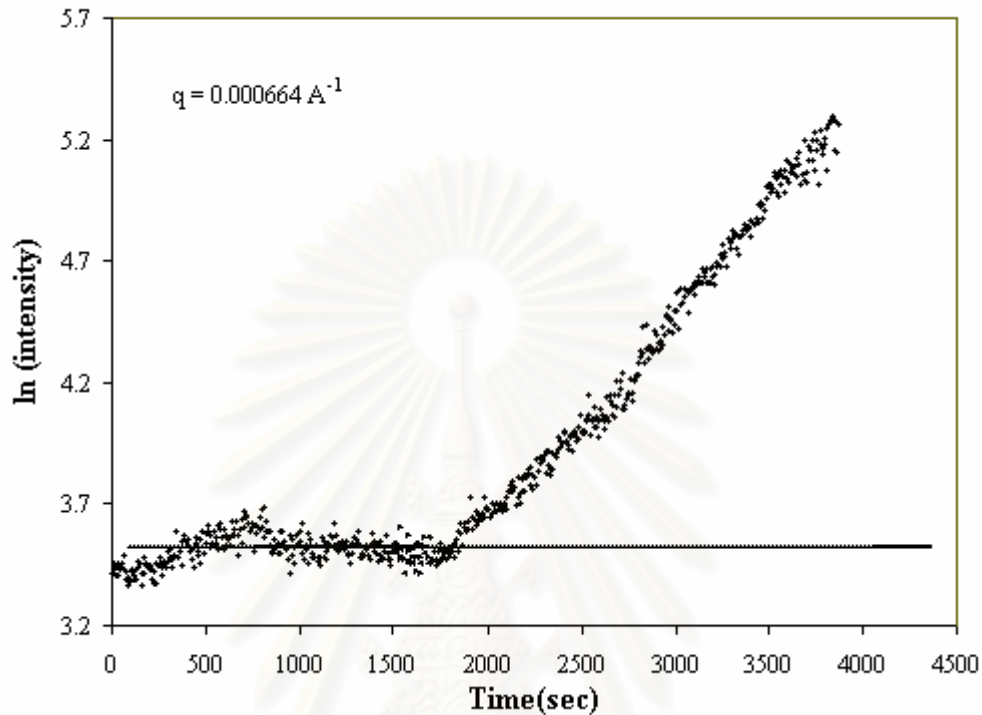


Figure 6.4 A plot of $\ln(\text{Intensity})$ against time for SAN/PMMA (20/80) blends, obtained from a temperature jump experiment at 217 °C. As seen in this Fig., the delay time is approximately 1700 s.

In Figure 6.5, it appears that $R(q)/q^2$ versus q^2 curve at various quench depth ($T-T_S$; 4, 6, 9, 11, 14 °C) becomes nonlinear at higher temperature. This is in agreement with what have been found in other systems [Cook 1970; Pincus 1981; Binder 1983; Binder *et al.* 1986; Clarke *et al.* 1997; Rojanapitayakorn 2002]. These effects have been attributed to thermal fluctuations or to polymer relaxation [Rojanapitayakorn *et al.* 2001]. They are more likely to arise because we are not observing at the very early stages of spinodal decomposition – as witnessed by the apparent time delay before growth in Figure 6.4. According to Cahn-Hilliard theory, the phase separation via spinodal decomposition should occur spontaneously after heating into the phase separation regime. The response time of the light scattering used in this work is not causing such a long delay times. A number of references [Cabral *et al.* 2000; 2002] showed that, for at least, some blends have the spinodal

growth domain in a wavelength range that light scattering cannot be observed. This might be another reason that can explain this system. While this will lead to the data that cannot be explained by Cahn-Hilliard theory (as discussion later on). We will argue that the conclusions about observed *changes* in the growth rates $R(q)$ when adding small molecules can be still measurable.

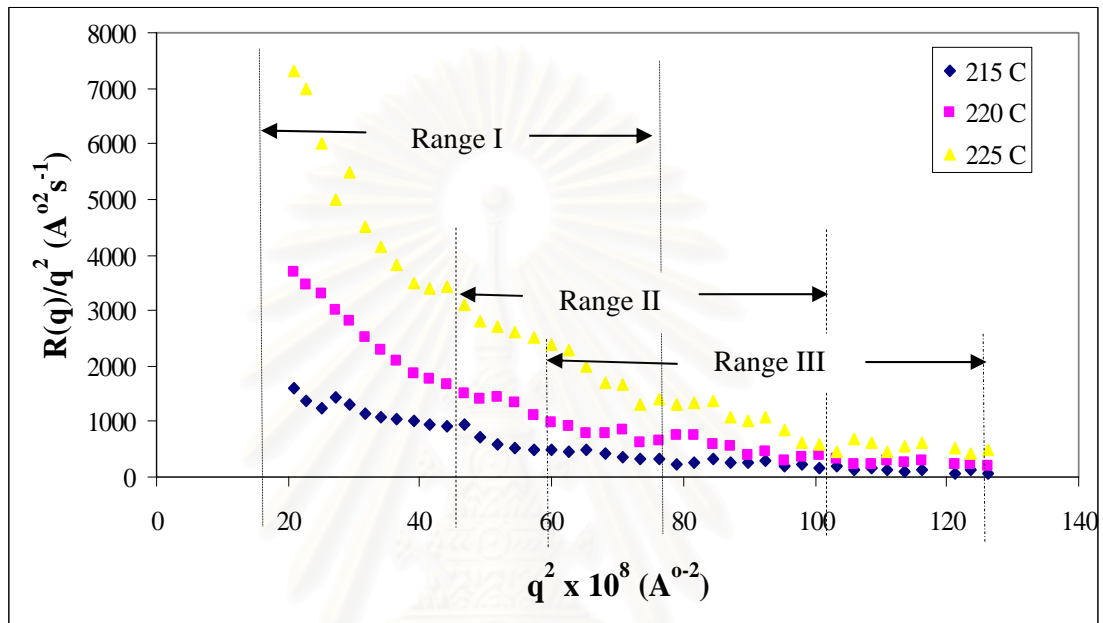


Figure 6.5 Plots of $R(q)/q^2$ against q^2 for SAN/PMMA (20/80) obtained from different temperatures.

The values of D_{app} were obtained by extrapolating $R(q)/q^2$ to obtain y-intercept using the values in the high q -data range ($q = 0.000756$ - $0.000114 \text{ \AA}^{-1}$) in order to avoid scattering from the contamination by any initial inhomogeneities in the sample such as dust. Spinodal temperatures, T_s (or apparent values of T_s) can be obtained by extrapolating the apparent diffusion coefficients to the x-axis when the D_{app} became zero as shown in Figure 6.6. However it should be noted that phase separation becomes possible once the temperature of the samples laid higher than the binodal curve. Thus for off critical blends in a continuous heating experiments, the cloud point detected may represent either the binodal point or some points apparently between the binodal and spinodal limits.

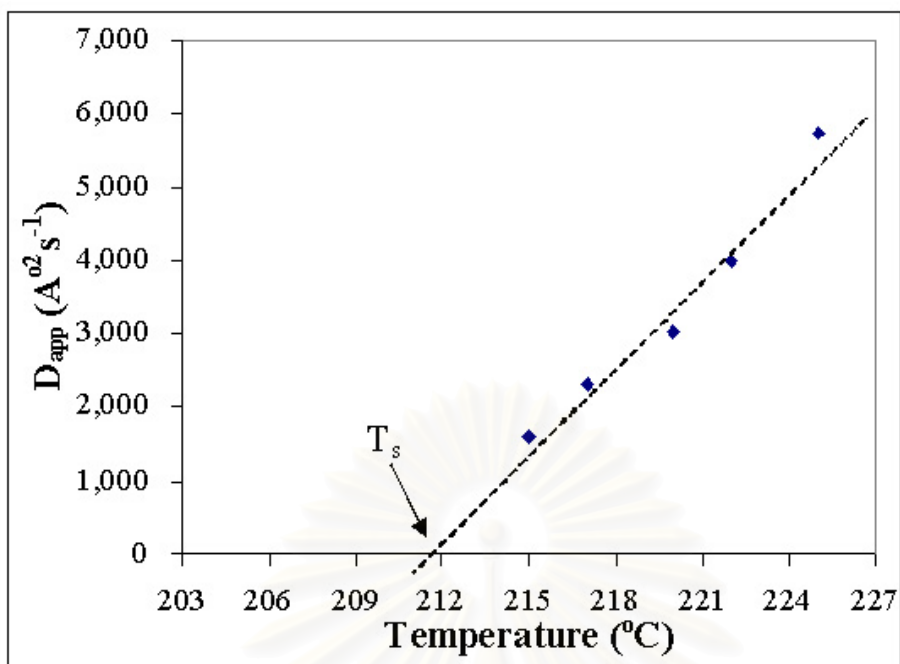


Figure 6.6 Plots of D_{app} against temperatures for SAN/PMMA (20/80) after adding 1.0 wt% CBC33, Spinodal temperatures, T_s can be obtained by extrapolating the apparent diffusion coefficients to the x-axis when the D_{app} became zero.

In order to test the effect of using a limited linear range of $R(q)/q^2$ versus q^2 plots. Three small q ranges were divided as follows: $q = 0.000342 - 0.00082 A^{-1}$ (range I), $q = 0.000664 - 0.00099 A^{-1}$ (range II) and $q = 0.000756 - 0.000114 A^{-1}$ (range III), as shown in Figure 6.5. A linear relationship can be obtained with a fairly good fit in all small ranges. The values of D_{app} for different temperatures in each q range can be obtained from the y-intercepts of the linear lines at $q^2 = 0$. The temperature dependence of D_{app} obtained from different q ranges is shown in Figure 6.7-6.9, and the extrapolation of the linear relationship between the D_{app} and the temperature can be made to yield the spinodal temperature (T_s). The spinodal temperature obtained from different q ranges are close to each other. These results were discussed later in this chapter.

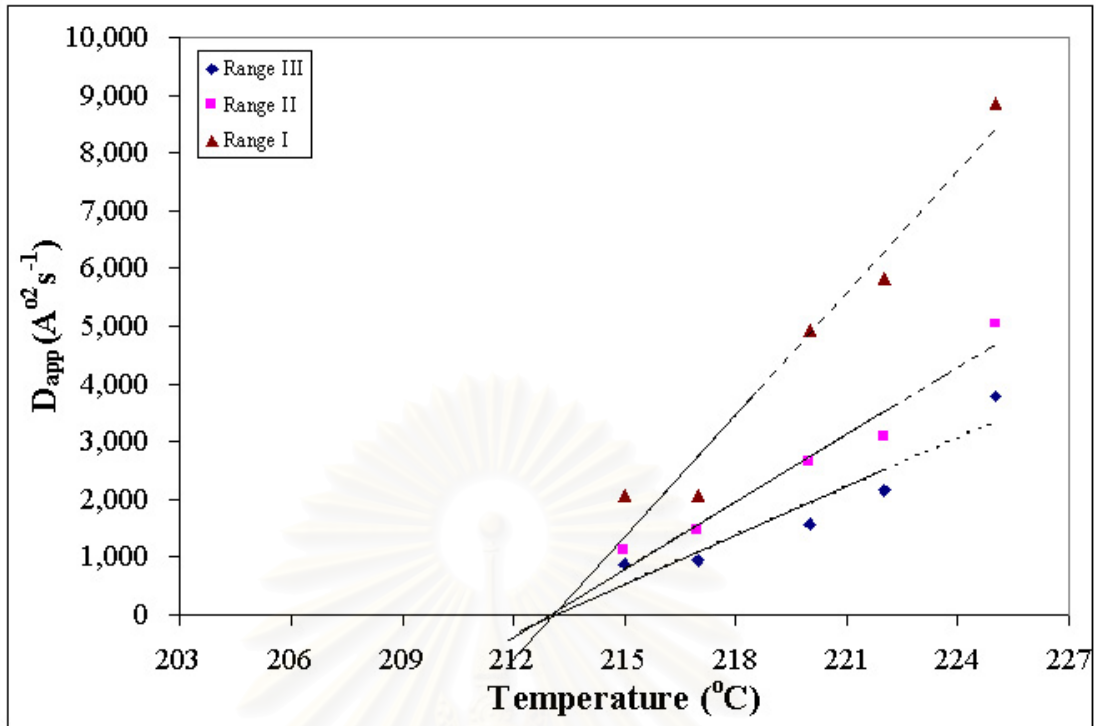


Figure 6.7 Plots of D_{app} against temperatures for SAN/PMMA (20/80) at different q ranges, T_s can be obtained by extrapolating the apparent diffusion coefficients to the x-axis when the D_{app} became zero.

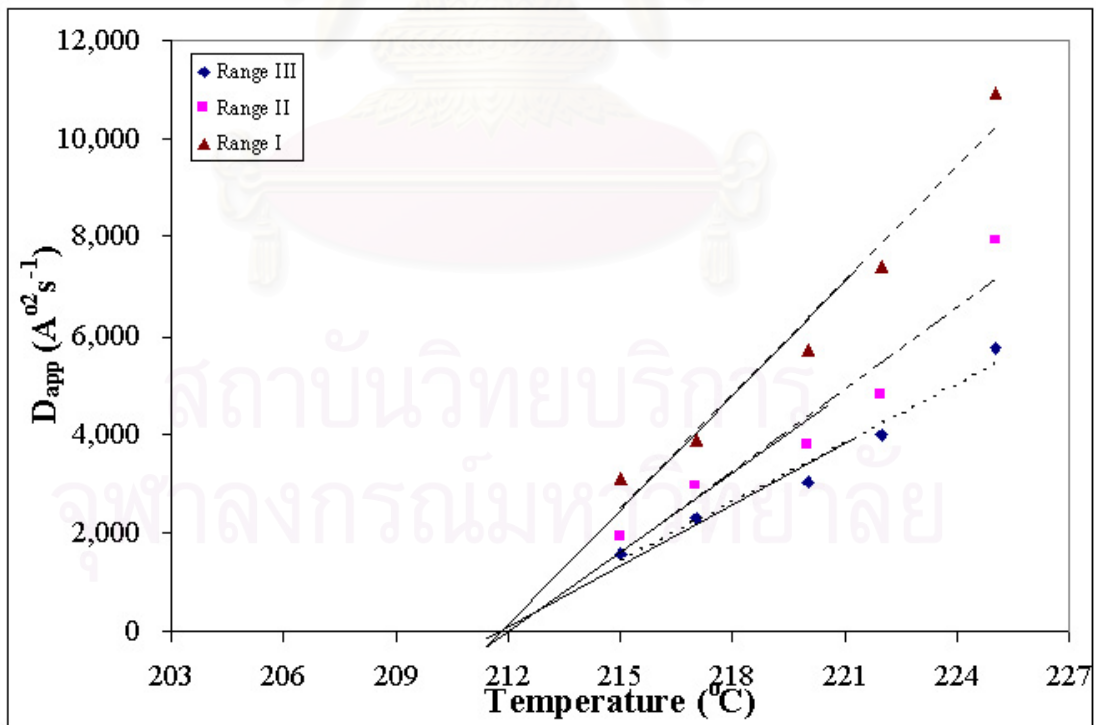


Figure 6.8 Plots of D_{app} against temperatures for SAN/PMMA (20/80) after adding 1.0 wt% CBC53 at different q ranges, T_s can be obtained by extrapolating the apparent diffusion coefficients to the x-axis when the D_{app} became zero.

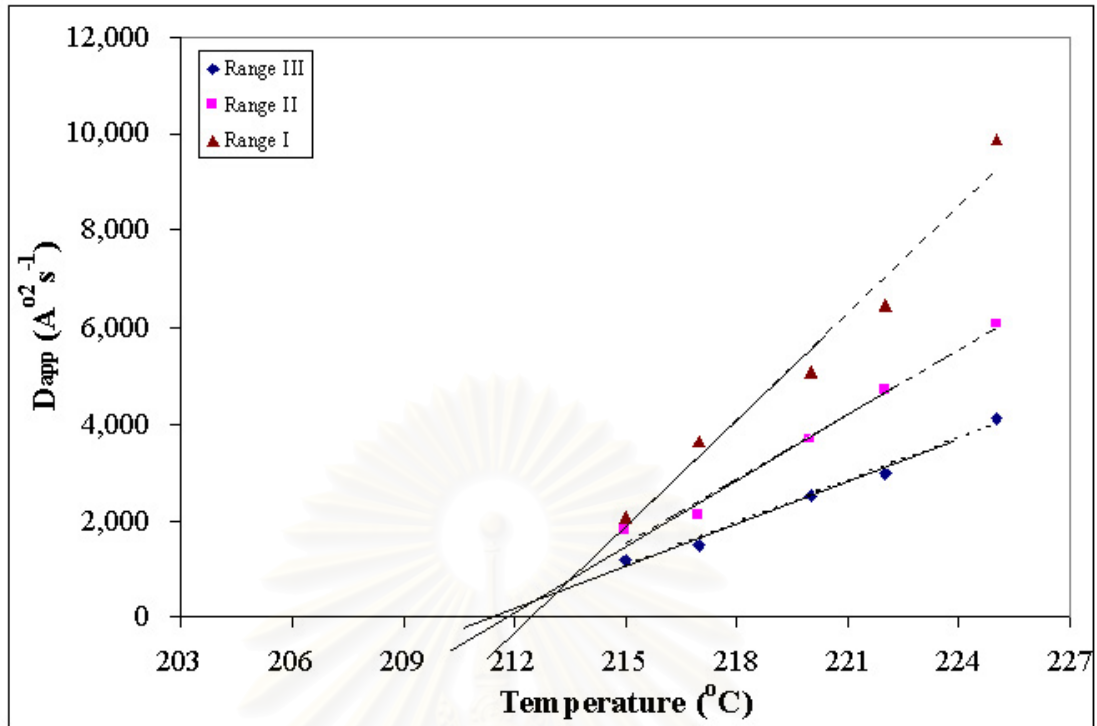


Figure 6.9 Plots of D_{app} against temperatures for SAN/PMMA (20/80) after adding 1.0 wt% GMS at different q ranges, T_s can be obtained by extrapolating the apparent diffusion coefficients to the x-axis when the D_{app} became zero.

The results of spinodal temperatures at different q ranges are shown in Table 6.2. From these results, we chose q range III (high q ranges) to find the values of D_{app} in order to avoid scattering from the contamination. Moreover, the trend of D_{app} curve at different q ranges of the original blends and the blends with LCs and lubricants are similar, so we chose to compare the D_{app} results only in small high q range III.

Table 6.2 Spinodal temperatures of SAN/PMMA (20/80) blends after adding 1.0 wt% of Zinc Stearate, GMS, CBC33 and CBC53 at different q ranges.

Sample	Range I	Range II	Range III
20:80 SAN/PMMA	213.2	212.9	213.1
20:80 SAN/PMMA+1.0 wt% CBC33	211.5	212.1	211.8
20:80 SAN/PMMA+1.0 wt% CBC53	212.5	212.5	212.3
20:80 SAN/PMMA+1.0 wt% GMS	211.4	211.6	212.5
20:80 SAN/PMMA+1.0 wt% Zinc Stearate	212.1	213.6	212.7

6.2.2.1 Spinodal Temperature Results

As seen in Figure 6.10, we found that spinodal temperatures after the addition of 0.2, 0.4, 1.0 wt% of CBC33, CBC53, GMS and Zinc stearate consecutively are only slightly different. Since the D_{app} is composed of the mobility (M) and the second derivative of Gibbs free energy (G''), the same spinodal temperature indicated that the G'' of all the systems become zero at the same temperature and might not be affected by the addition of additives. The differences in the slopes of the D_{app} and temperature mostly come from the change in M according to the different additives. So we might assume that the thermodynamic term (G'') is unaffected by the added additives and that changes in D_{app} are determined mostly from the changes in the molecular mobility term (M).

Table 6.3 Spinodal temperatures of SAN/PMMA (20/80) blends before and after addition of 0.2, 0.4, 1.0 wt% of CBC33, CBC53, GMS and Zinc Stearate.

Sample	Spinodal Temperature (°C)	Standard Derivation
20:80 SAN/PMMA	213.4	1.2
20:80 SAN/PMMA+0.2 wt% CBC33	211.1	1.2
20:80 SAN/PMMA+0.4 wt% CBC33	210.9	0.7
20:80 SAN/PMMA+1.0 wt% CBC33	211.4	1.3
20:80 SAN/PMMA+0.2 wt% CBC53	211.2	0.8
20:80 SAN/PMMA+0.4 wt% CBC53	212.0	0.8
20:80 SAN/PMMA+1.0 wt% CBC53	212.5	0.8
20:80 SAN/PMMA+0.2 wt% GMS	211.2	0.5
20:80 SAN/PMMA+0.4 wt% GMS	210.5	1.2
20:80 SAN/PMMA+1.0 wt% GMS	211.4	0.7
20:80 SAN/PMMA+0.2 wt% Zinc Stearate	211.5	1.2
20:80 SAN/PMMA+0.4 wt% Zinc Stearate	211.8	1.2
20:80 SAN/PMMA+1.0 wt% Zinc Stearate	213.0	0.7

6.3 Effects of Liquid Crystals and Lubricants on Kinetics of Phase Separation

It is clear that the scattered intensity of our system increases exponentially with time in the early stage of spinodal decomposition and the growth rate of spinodal decomposition during this time can be represented by the Cahn-Hilliard growth rate ($R(q)$).

6.3.1 The Cahn-Hilliard Growth Rate ($R(q)$)

The Cahn-Hilliard growth rate ($R(q)$) is derived from the half value of the slope from the plot between $\ln(\text{intensity})$ and time.

As already remarked, these samples showed an apparent induction period after being abruptly heated to the temperature inside the spinodal region as seen in Figure 6.4. We estimated growth rates $R(q)$ from the slopes of $\ln(\text{intensity})$ versus time plots after this induction period.

The growth rates, $R(q)$ as a function of q are shown in Figure 6.10 for SAN/PMMA (20/80) blends at various temperatures. The $R(q)$ values obtained from the phase separated blends at higher temperatures are clearly higher than that obtained at lower temperature, which are the results of the faster spinodal decomposition process. The maximum growth rate ($R(q_m)$) and maximum wave number (q_m), can be clearly identified and can be calculated from the slope and intercept of $R(q)/q^2$ versus q^2 plots, in another ways.

The plots of $R(q)$ versus q at five experimental temperatures for the blends added with CBC33, CBC53, GMS and Zinc Stearate have the similar trend as shown in Figure 6.10. Likewise, all plots exhibit an increment of the growth rate as experimental temperature increases.

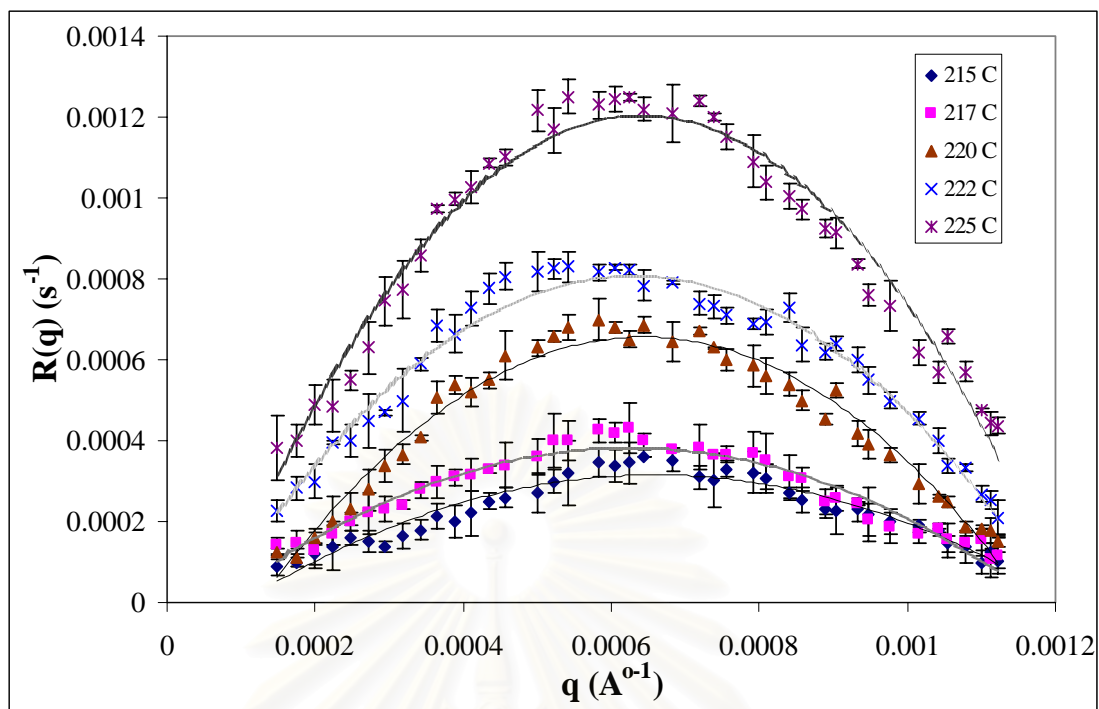


Figure 6.10 Plots of $R(q)$ versus of q for SAN/PMMA (20/80) blends at five temperatures used.

6.3.1.1 Concentration Effects of Liquid Crystals and Lubricants

The $R(q)$ results of the pure and the blends with 0.2 and 1.0 wt% CBC33 is shown in Figure 6.10 indicate that the $R(q)$ of the blends after adding 1.0 wt% CBC33 is higher than those of the blends after adding 0.2 wt% CBC33. The $R(q)$ results of all the blends after adding LCs and lubricants at different three compositions indicate that $R(q)$ values of high composition of LCs or lubricants are higher than those from the blends mixed with low composition of LCs or lubricants.

Those results indicate the effects of composition of LCs and lubricants on molecular movements of polymer blends. The higher content of LCs makes the molecule moving faster. It seems that addition of LCs has a greater effect on mobility than the addition of lubricants, which will be further discussed.

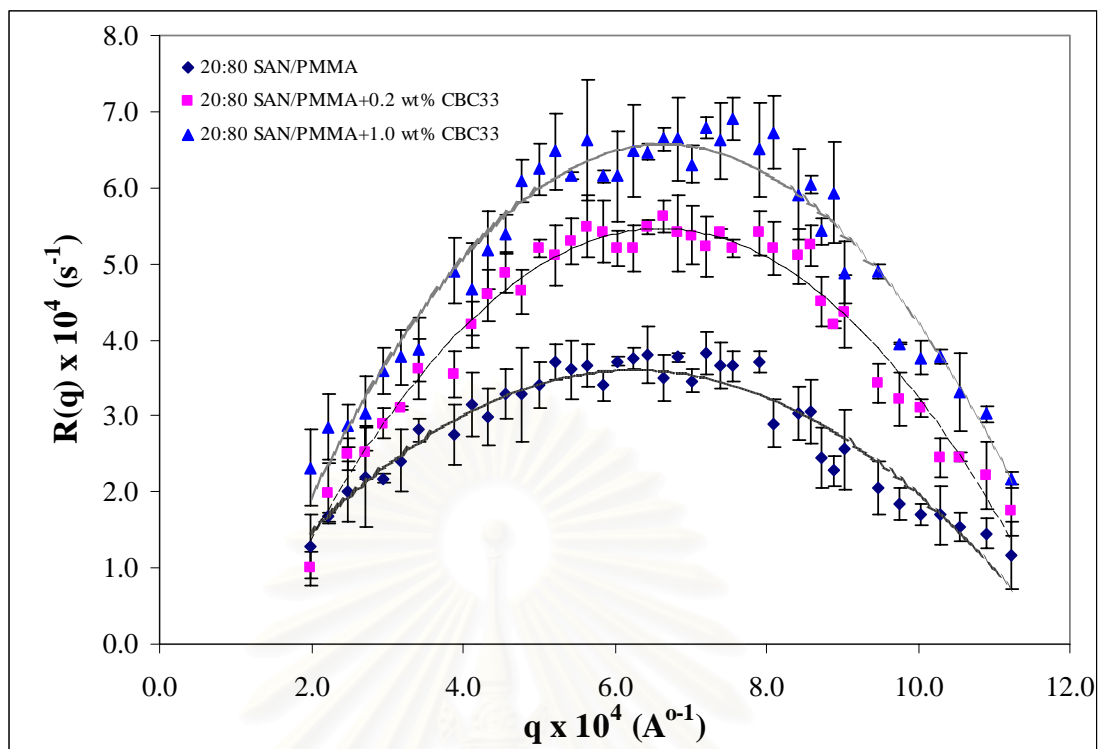


Figure 6.11 Plots of $R(q)$ versus of q for SAN/PMMA (20/80) blends after adding CBC33 at 217 °C.

6.3.1.2 Molecular Structure Effects of Liquid Crystals

The effects of chemical structure of LC on the kinetic results will be concentrated. CBC33 and CBC53 have the same main rigid rod structures, but differ in the alkyl end group and molecular weight, as shown in Figure 5.3 and 5.4.



Figure 5.3 Structure of CBC33.

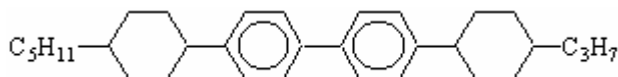


Figure 5.4 Structure of CBC53

The comparison of the $R(q)$ values curves at the fixed temperatures for the blends after adding CBC33 and CBC53 is shown in Figure 6.12 as an example. It can

be seen that the $R(q)$ values of the blends with CBC53 are higher than the blends with CBC33. This might indicate that adding CBC53 lead to the faster movement of the blends than adding CBC33.

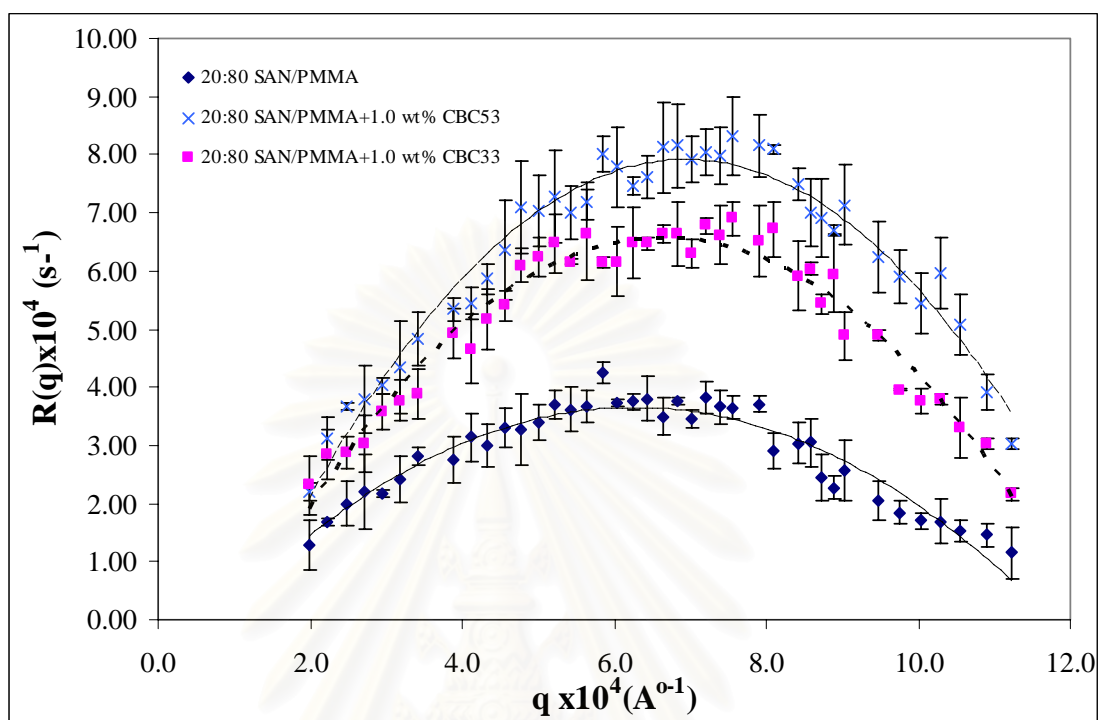


Figure 6.12 Plots of $R(q)$ versus of q for SAN/PMMA (20/80) blends after adding 1.0 wt% CBC33 and CBC53 at 217 °C.

6.3.1.3 Molecular Structure Effects of Lubricants

The results of $R(q)$ values from the change of chemical structure of lubricants; GMS, Zinc Stearate are studied. The chemical structures of GMS and Zinc Stearate are shown in Figure 5.5 and 5.6.

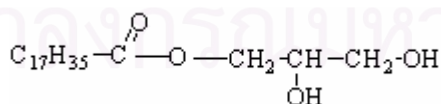


Figure 5.5 Structure of glycerol monostearate (GMS).

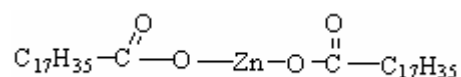


Figure 5.6 Structure of zinc stearate.

The plots of $R(q)$ versus q at 220 °C for the blends added GMS and Zinc Stearate are compared in Figure 6.13. It seems that $R(q)$ values obtained from the phase separated blends added with GMS, are higher than that with Zinc Stearate, although the curves show rather small difference at higher q ranges.

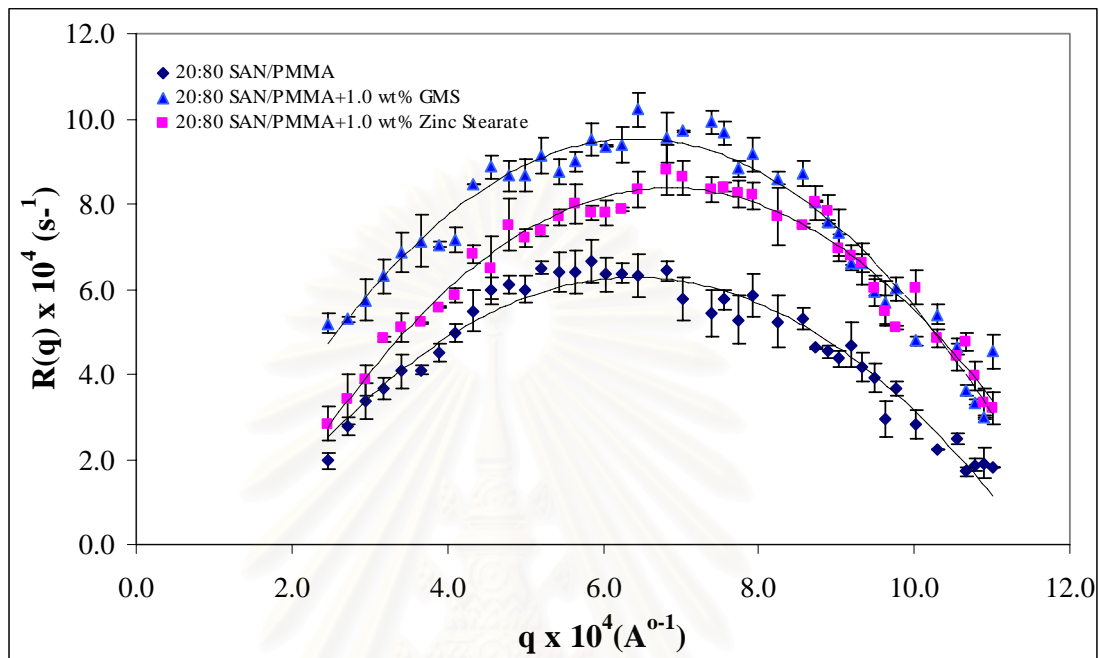


Figure 6.13 Plots of $R(q)$ versus of q for SAN/PMMA (20/80) blends after adding 1.0 wt% GMS and Zinc Stearate at 220 °C.

6.3.1.4 Comparison of Effects of Liquid Crystals and Lubricants

The $R(q)$ values of the blends added with LCs and lubricants are compared. The $R(q)$ curves of the original blend and the blends added with 1.0 wt% CBC33 and GMS are shown in Figure 6.14 as an example. The other concentrations of the blends also have similar results. The $R(q)$ values obtained from the phase separated blends with added LCs, both CBC33 and CBC 53, are clearly higher than those obtained from the original blends and the blends with lubricants, both GMS and Zinc Stearate. These results indicate that adding LCs lead to the faster molecular movement of the blends than adding lubricants.

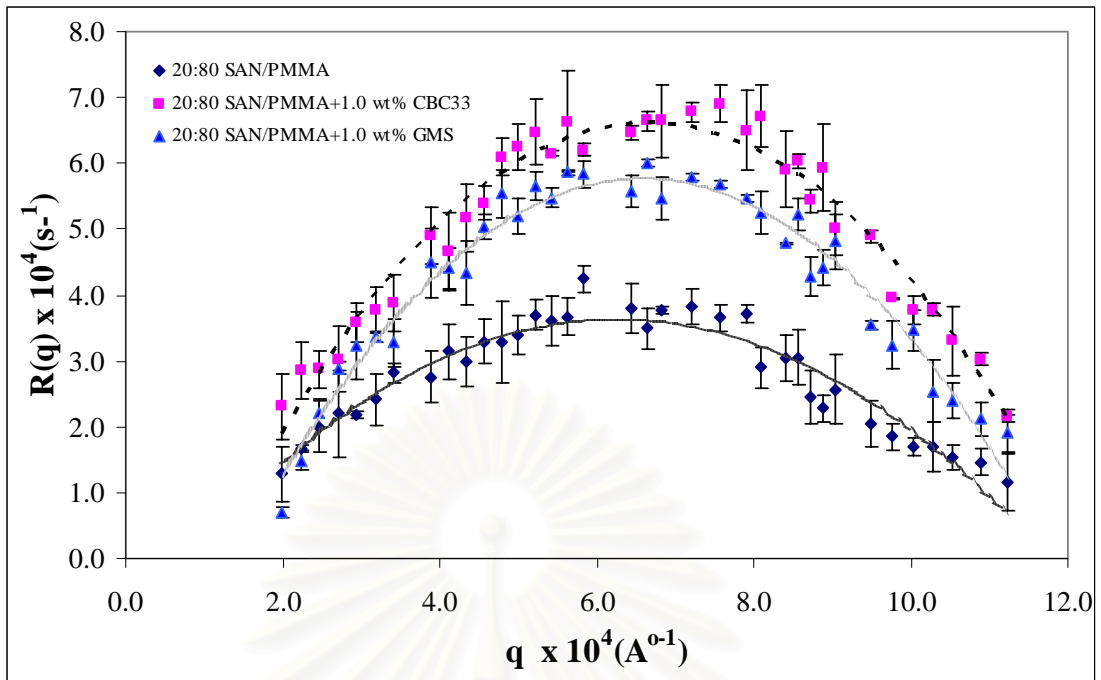


Figure 6.14 Plots of $R(q)$ versus of q for SAN/PMMA (20/80) blends after adding 1.0 wt% CBC33 and GMS at 217 °C.

6.3.2 The maximum scattering wave number (q_m)

The maximum wave number, q_m , can be obtained either directly from the q that gave the maximum $R(q)$ of the plots of $R(q)$ versus q or calculated from the slope of $R(q)/q^2$ versus q^2 plots according to the Cahn-Hilliard theory.

The q_m results of all the blends after adding LCs and lubricants at three compositions are compared. Figure 6.16 shows plots of the q_m values as a function of temperature for the blends with and without CBC33 and GMS as an example of all the blends. It can be seen that the calculated q_m values are slightly higher than the values obtained directly from the plots, but both values are essentially independent of temperature. This might be because of the range of q that we obtained the calculated values are narrower than the range that we obtained directly from the plotted values. However, these differences are in the close vicinity. The plots of q_m versus temperature of the other blends are similar to that shown in Figure 6.15.

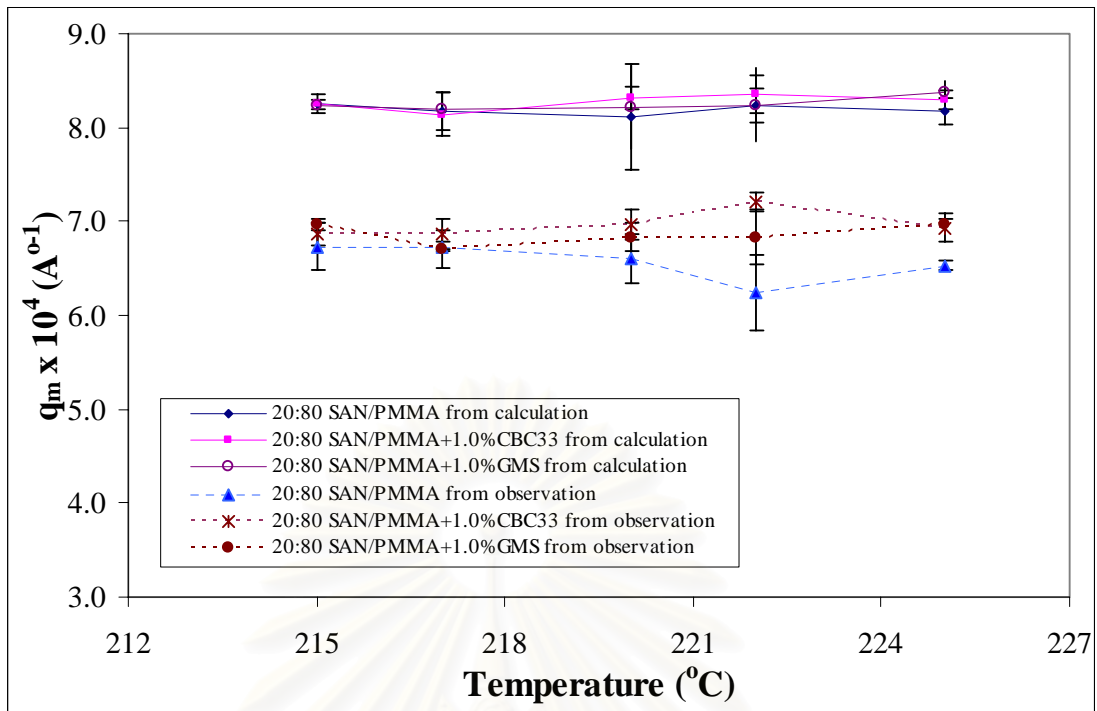


Figure 6.15 Plots of q_m against temperature for SAN/PMMA (20/80) blends after adding 1.0 wt% CBC33 and GMS, obtained from calculation and observation methods.

6.3.3 The maximum growth rate ($R(q_m)$)

6.3.3.1 Concentration Effects of Liquid Crystals and Lubricants

The $R(q_m)$ results of all the blends after adding LCs and lubricants at three compositions are compared. Figure 6.16 and 6.17 show plots of the $R(q_m)$ values as a function of temperatures for the blends after adding 0.2, 0.4 and 1.0 wt% CBC33 and GMS respectively, obtained directly from the $R(q)$ versus q plots. The $R(q_m)$ values of the blends after adding LCs and lubricants increase when increasing the concentration of LCs and lubricants. It can be seen that $R(q_m)$ increases with temperature, as expected due to an increase in molecular mobility and thermodynamic driving potential at higher temperature.

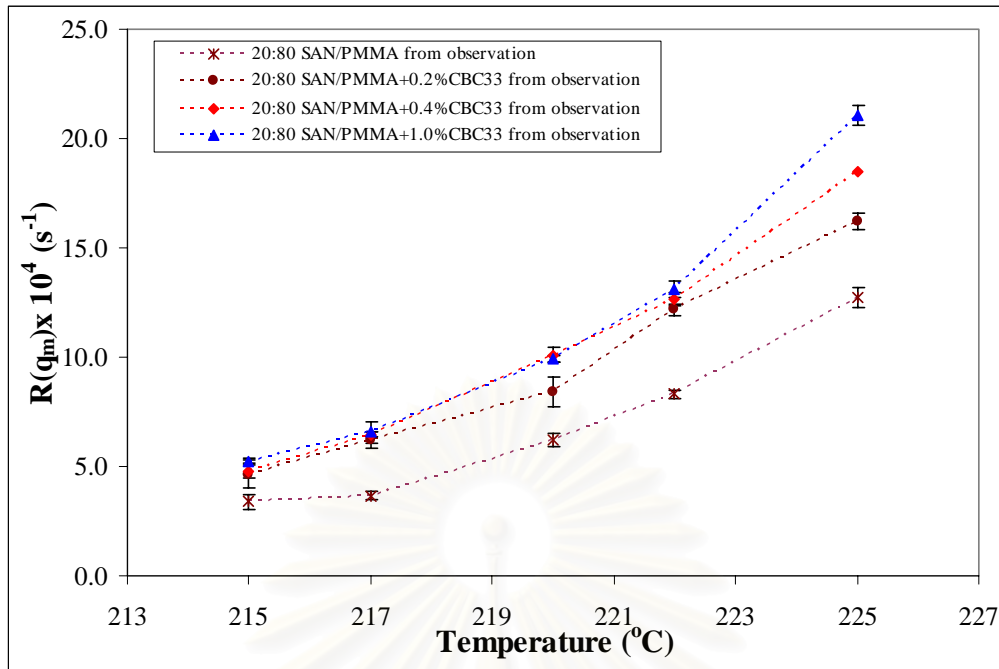


Figure 6.16 Plots of $R(q_m)$ against temperature for SAN/PMMA (20/80) blends after adding 0.2, 0.4 and 1.0 wt% CBC33, obtained from observation method.

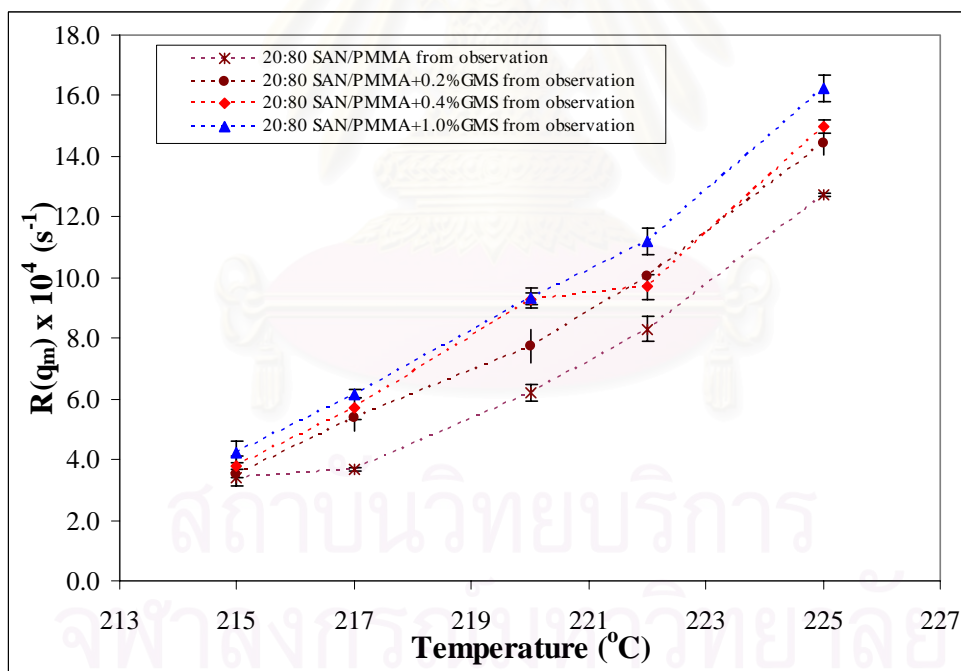


Figure 6.17 Plots of $R(q_m)$ against temperature for SAN/PMMA (20/80) blends after adding 0.2, 0.4 and 1.0 wt% GMS, obtained from observation methods.

Likewise the maximum wave number, the comparison of maximum growth rate $R(q_m)$ from direct observation is illustrated as the plot of $\sqrt{R(q_m)}$ with temperature. As can be seen from Figure 6.18, $\sqrt{R(q_m)}$ increases linearly with temperatures and follows the prediction from Cahn-Hilliard theory. However, since it changes with temperature, this is in contrast to the behaviour of q_m described in the previous section. $R(q)$ is determined much more closely by the final temperature at which the phase separation develops. From the classical Cahn-Hilliard linearised theory, the growth rate ($R(q)$) can be rewritten in the alternative form as,

$$R(q) = -q^2 M [\chi_s - \chi + \kappa q^2] \quad (6.1)$$

where M is mobility constant and χ_s is the interaction parameter at the spinodal temperature (T_s).

From Equation 6.1, the maximum relative growth rate ($R(q_m)$) can be expressed as,

$$R(q_m) = \frac{M[\chi - \chi_s]^2}{2K} \quad (6.2)$$

Inserting the usual $\chi \propto 1/T$ variation into Equation 5.11, we then obtain

$$R(q_m)^{1/2} \propto (T - T_s) \quad (6.3)$$

Which clearly manifests how $R(q_m)$ relates to square of the quench depth or temperature and mobility.

It is obvious from equation (3.12) and (3.13) that q_m depends on the thermodynamics characteristics ($\frac{\partial^2 \Delta G_m}{\partial c^2}$). From Figure 6.15 indicates that the q_m values for the blends with and without LCs and lubricants, are essentially independent of temperature. So, the addition of LCs and lubricants are less effect on

thermodynamics driving force. Moreover, it can indicate that the mobility is more effective on the $R(q_m)$ values than the thermodynamic driving force.

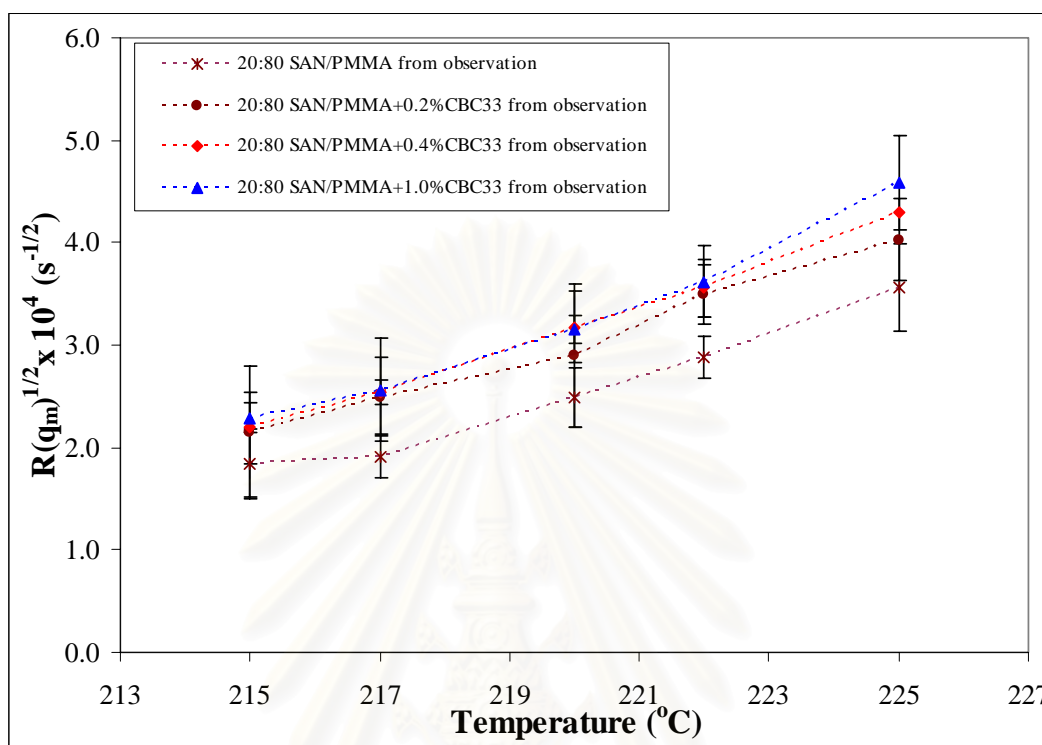


Figure 6.18 Plots of $(R(q_m))^{1/2}$ against temperature for SAN/PMMA (20/80) blends after adding 0.2, 0.4 and 1.0 wt% CBC33, obtained from observation method.

6.3.3.2 Comparison of Effects of Liquid Crystals and Lubricants

An example of the values of the maximum growth rate, $R(q_m)$, obtained from observation and calculation methods as a functions of temperature for the blends before and after adding CBC33 and GMS is shown in Figure in 6.19. It can be seen that $R(q_m)$ increases fairly linearly with temperature and the $R(q_m)$ values of the blends after adding LC both CBC33 and CBC53 are higher than those after adding lubricants both GMS and Zinc Stearate. This is in agreement with observed previously that the addition of LCs results in the faster movement of molecule than the addition of lubricants.

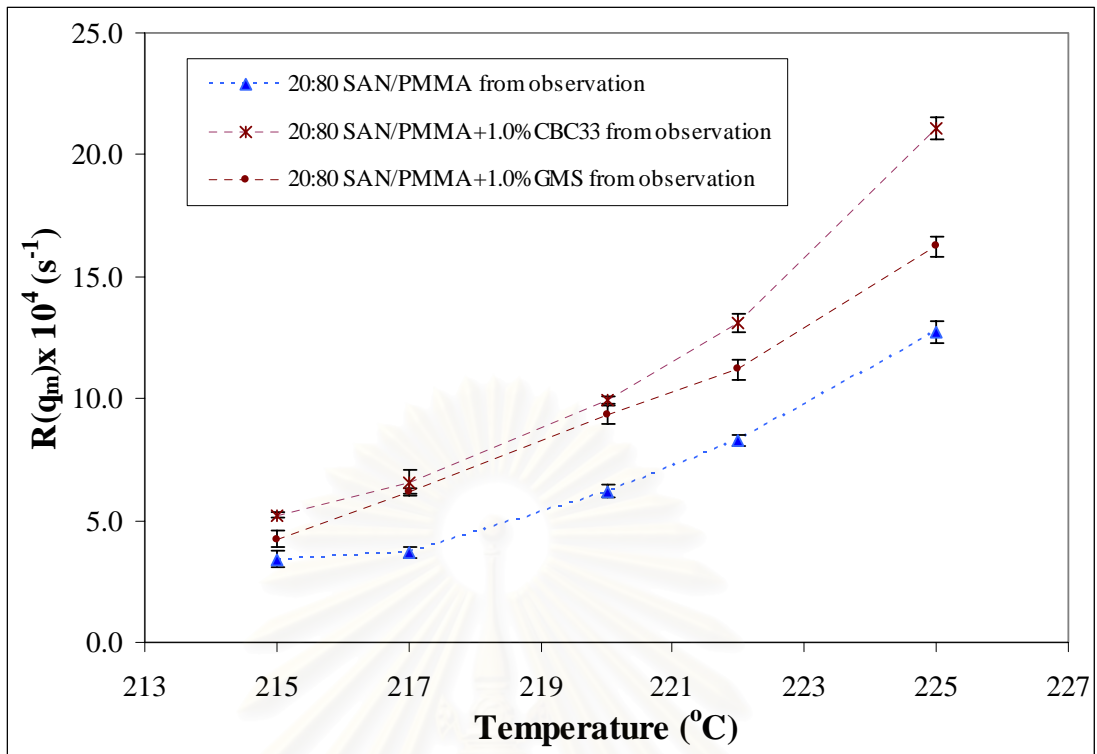


Figure 6.19 Plots of $R(q_m)$ against temperature for SAN/PMMA (20/80) blends after adding 1.0 wt% CBC33 and GMS, obtained from calculation and observation methods.

6.3.4 The apparent diffusion coefficient (D_{app})

Three criteria delimit the early stage spinodal decomposition, namely an exponential growth in the intensity of scattered light, time independence of q_m and the consistency of the data with Cahn-Hilliard theory through equation (3.10). As remarked above, we believe that there are the discrepancies with C-H theory such as in Figure (6.4). The occurrence of a sizeable delay time indicate that we may be missing the true early stages because the domain sizes are too small to be detected by light. Nevertheless we believe that D_{app} values obtained by applying equations 3.1 to 3.13 to analyse the data allow us to make a qualitative comparison of results from different samples, even if the numerical values are themselves can not be compared quantitatively.

D_{app} becomes zero at the spinodal temperature. Interestingly even if we have estimated D_{app} from $R(q)$ data after the earliest stages we have generally found that the

values extrapolate to zero at or close to the true spinodal. Although in this case we have obtained D_{app} from data after the apparent induction period and therefore probably not falling in the early stages – as described above. It is believed that the values of the spinodal temperatures will not be far from the true values.

The spinodal decomposition temperatures obtained in this way thus did not vary outside the experimental accuracy, indicating that the thermodynamics in the blends might not be significantly altered by the addition of the small percentage of lubricants or LCs.

6.3.4.1 Concentration Effects of Liquid Crystals and Lubricants

The D_{app} results of all the blends before and after adding LCs and lubricants at three compositions are compared. Figure 6.20-6.23 shows the values of the D_{app} of SAN/PMMA (20/80) blends at various phase separation temperatures after adding CBC33, CBC53, GMS and Zinc at various of compositions. The obtained D_{app} values are increased both with compositions and with phase separation temperatures.

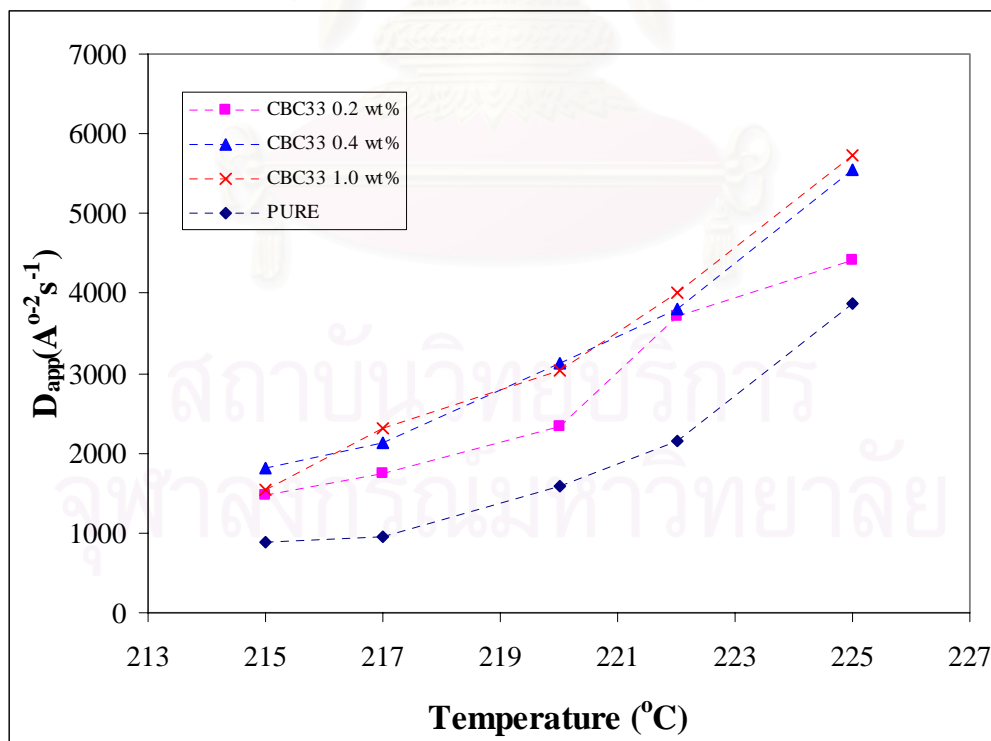


Figure 6.20 Plots of D_{app} against temperatures for SAN/PMMA (20/80) blends after adding CBC33 at various compositions.

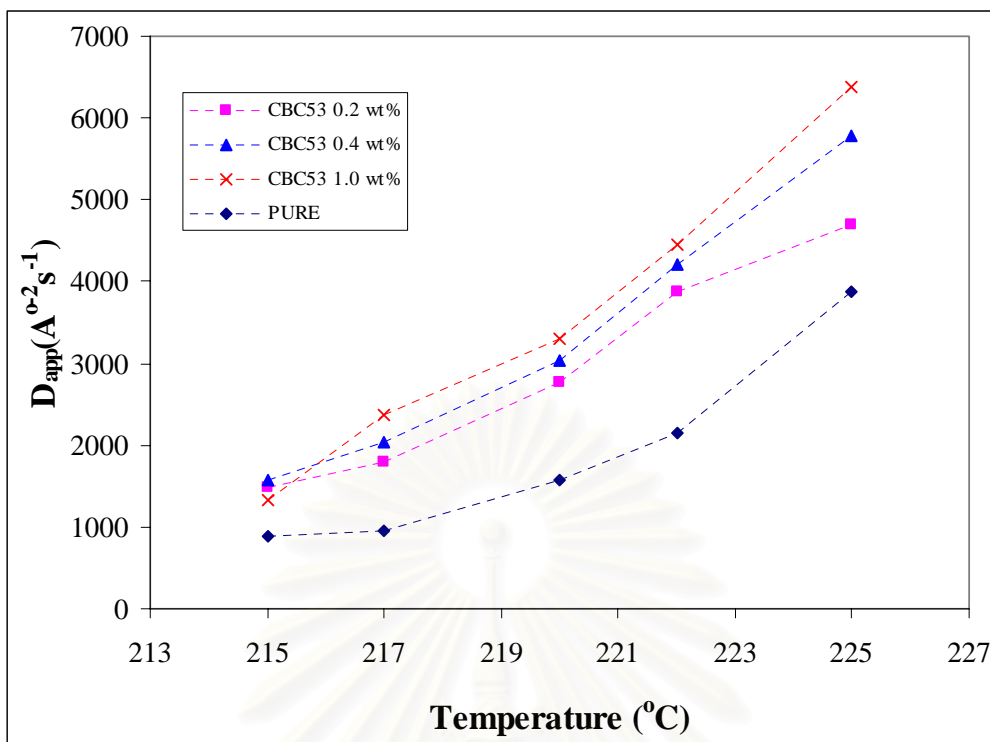


Figure 6.21 Plots of D_{app} against temperatures for SAN/PMMA (20/80) blends after adding CBC53 at various compositions.

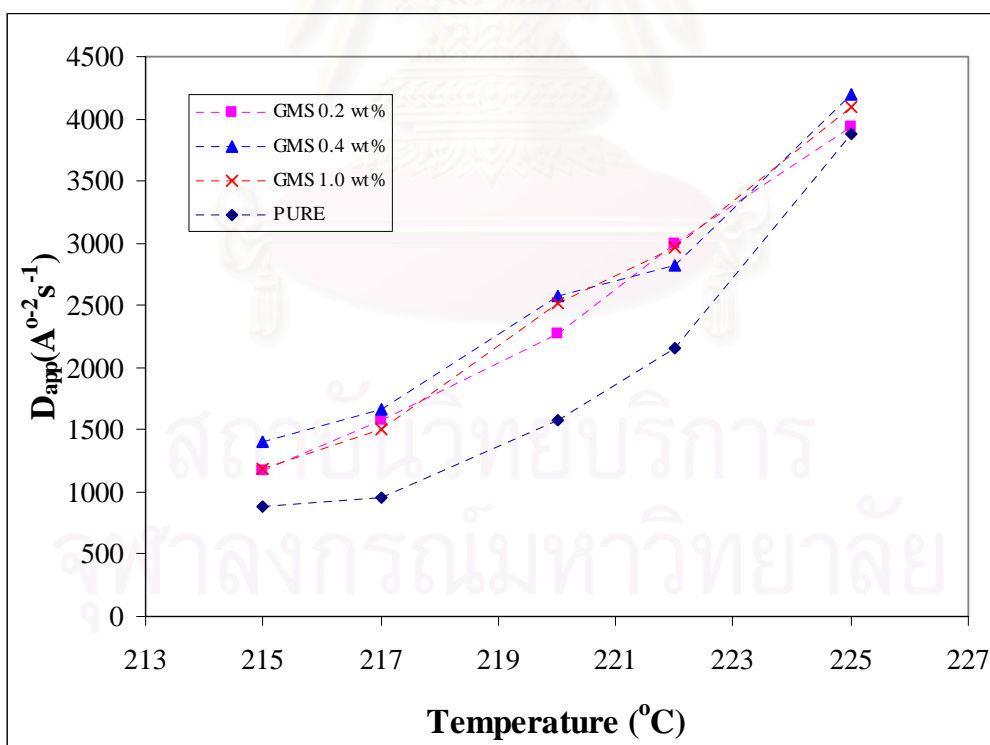


Figure 6.22 Plots of D_{app} against temperatures for SAN/PMMA (20/80) blends after adding GMS at various compositions.

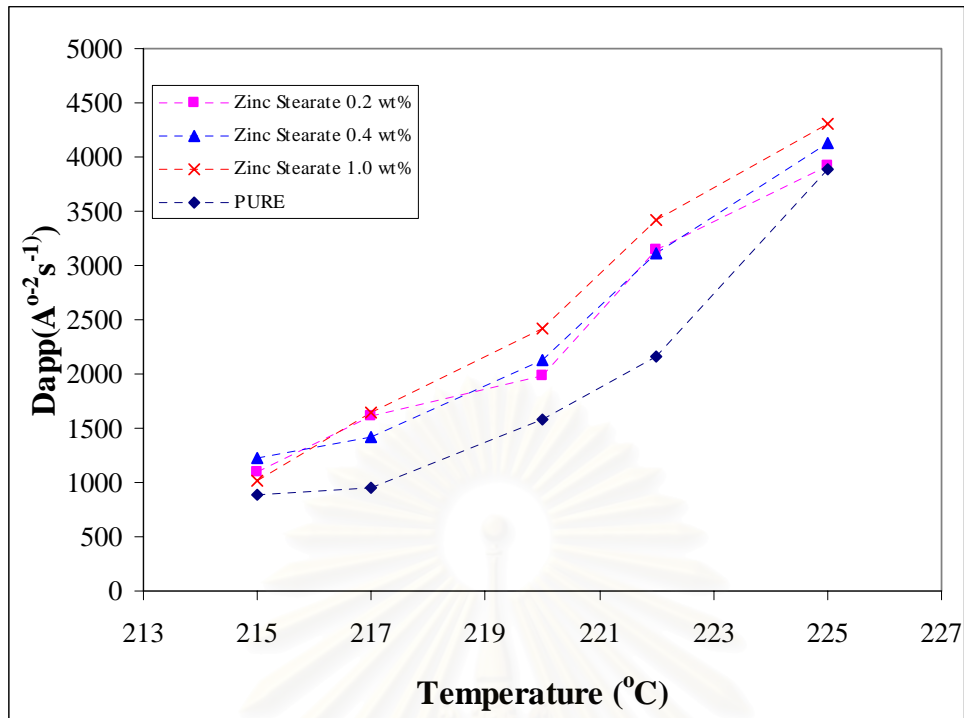


Figure 6.23 Plots of D_{app} against temperatures for SAN/PMMA (20/80) blends after adding Zinc Stearate at various compositions.

6.3.4.2 Comparison of Effects of Liquid Crystals and Lubricants

Figure 6.24-6.26 showed the comparison of D_{app} for SAN/PMMA (20/80) blends and the blends with LCs and lubricants at 0.2, 0.4 and 1.0 wt% respectively. The D_{app} for samples containing CBC53 are significantly higher than those for the pure blends, particularly at larger quench depths.

If the thermodynamic term in equation (3.10) was assumed that is essentially unaffected by adding LCs (as witnessed by the fact that the spinodal temperatures do not shift), then D_{app} is determined by the molecular mobility term M . The implication is that small additions of LC significantly increase M . Addition of CBC33, GMS and zinc stearate causes the same results, i.e. increasing of D_{app} values as the amount of additives and temperature increase. However, for deeper quenches, the LC addition appears to significantly increase molecular mobility while the effects from the lubricants is very small. As argued above, since the spinodal temperature, and therefore the thermodynamic term in D_{app} are unaltered by addition of small

molecules, we are led to the conclusion that the mobility term M is significantly increased, in effect that the LC additives are aiding molecular motion.

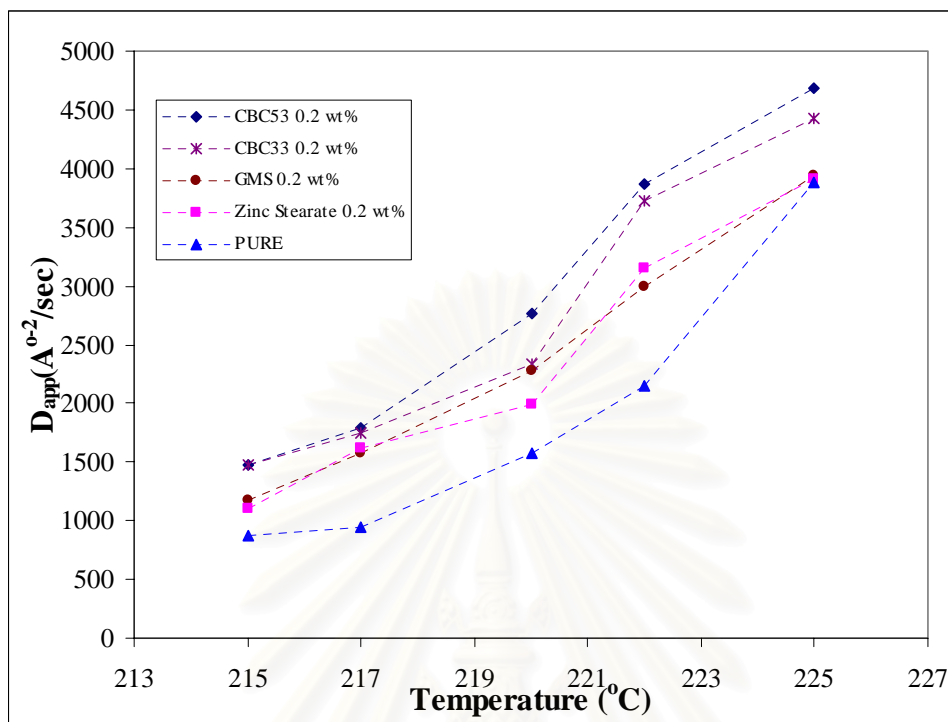


Figure 6.24 Plots of D_{app} against temperatures for SAN/PMMA (20/80) blends after adding 0.2 wt% CBC33, CBC53, GMS and Zinc Stearate.

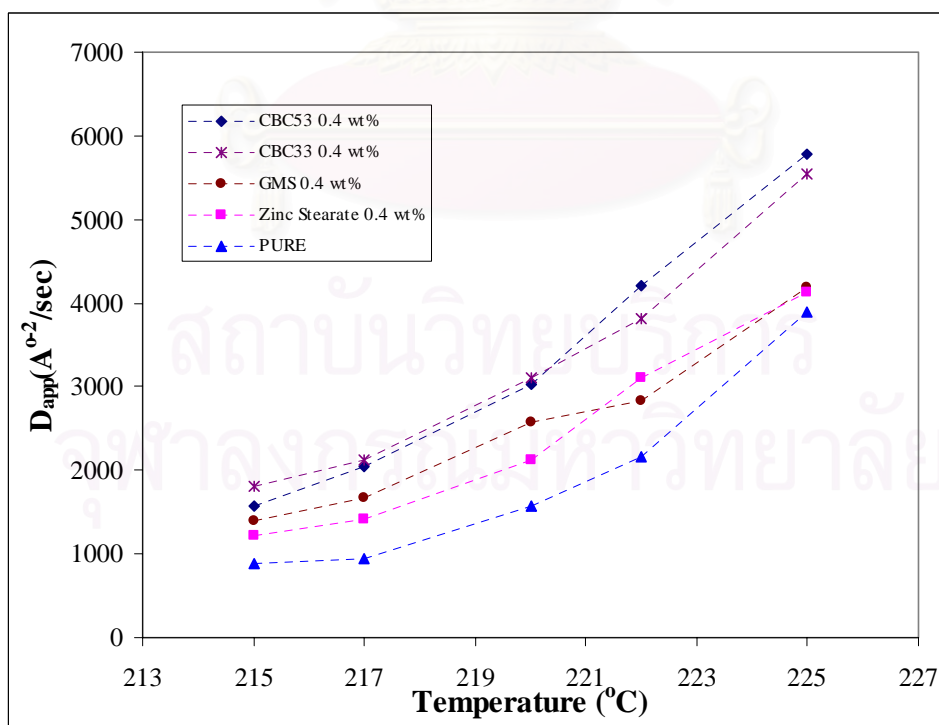


Figure 6.25 Plots of D_{app} against temperatures for SAN/PMMA (20/80) blends after adding 0.4 wt% CBC33, CBC53, GMS and Zinc Stearate.

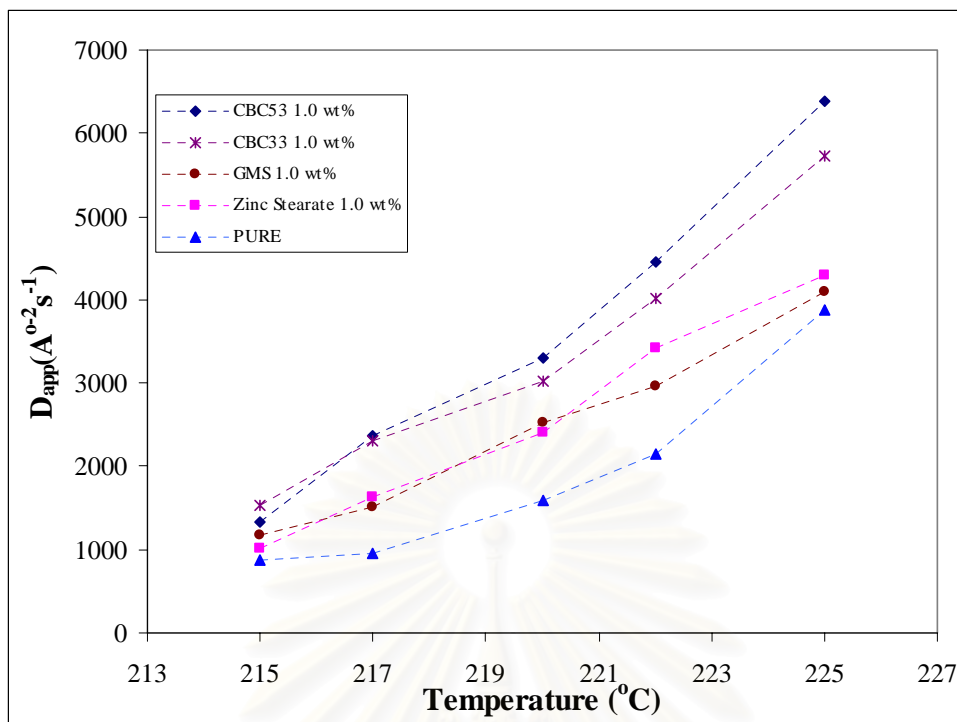


Figure 6.26 Plots of D_{app} against temperatures for SAN/PMMA (20/80) blends after adding 1.0 wt% CBC33, CBC53, GMS and Zinc Stearate.

6.4 Morphology

In polymer blends, properties are related with their morphology directly. It has been reported about morphology studies in polymer blends [Hobbs *et al.* 1988]. In general four types of structures are observed for two-phase polymer systems; sea-island structure, co-continuous structure, salami structure and modulated structure. Among them, the modulated structure is formed via spinodal decomposition from a single-phase mixture.

The morphology and the coarsening behavior with and without LCs and lubricants were investigated by using a scanning electron microscope.

6.4.1 Scanning Electron Microscopy Results

From the SALS results, the D_{app} values of the blends after adding LCs showed higher than those of the blends after adding lubricants, it is anticipated that phase separation in LC blends will have advanced further during the same heating period so that the phase separated structure are more clearly developed.

The measurements of the apparent diffusion coefficients highlights the differences between the pure blend, LC blend and blend with added lubricant. It has been assumed that if the molecules are moving faster, this will result in clearer structures characteristic of early stage spinodal phase separation in the SEM morphologies. The fracture surfaces of the blends and the phase separated blends (all of pure SAN/PMMA and their blend with CBC33, CBC53, GMS and Zinc Stearate blends) at different concentrations of the added small molecules were investigated by SEM, in order to explore the structure away from the surface of the mould and the treated condition at the surfaces. The early stage spinodal decomposition phenomenon was selected because of the simplicity of comparison of the molecular mobility, which are easily obtained from Cahn-Hilliard's analysis. However, it has not been possible to observe the small domain sizes of the early stage spinodal decompositions with SEM even where we use high magnification. The different domain morphology of the phase separated and miscible blends were compared. Although we can

distinguish differences in the morphologies between a miscible blend and its phase separated blend, careful comparisons are needed. However, the PMMA can be automatically eroded by the electron beam in SEM which might affect samples which are in the intense beam of electrons for a long time. The sensitivity of the micrograph was tested and we did not observe any serious changes in the morphologies observed within our experiment times under the electron beam of SEM (9 minutes). We believe therefore that, the erosion effects of PMMA by the beam can be ignored.

Figure 6.27 and 6.28 demonstrated morphological structures of fractured surfaces of SAN and PMMA, respectively. Both polymers show very smooth surfaces with numerous fracture layers as expected for general brittle materials. In the fractured surfaces micrograph of the miscible SAN/PMMA (20/80) and of phase separated blends at the early stages of phase separation, before and after added LC and lubricant are compared. In the following micrograph, Figure 6.29 and 6.30 the fracture surfaces of the miscible SAN/PMMA (20/80) and of phase separated blends at the early stages of phase separation. The surface of the miscible blend is smoother, and shows more fracture layers than the phase separated blends.

Figure 6.31 showed the fractured structure of the blends after added with CBC33 and the fractured structure of this blends after phase separated as shown in Figure 6.32. It can be seen that the fractured structure are quite similar when compared between before and after phase separated, however it seems that miscible blends are likely smoother.

Figure 6.33 showed the fractured structure of the blends after added with CBC53 and the fractured structure of this blends after phase separated as shown in Figure 6.34. The fractured structures of these blends are quite similar.

Figure 6.35 and 6.36 showed the fractured structure of the blends and phase separated blends added with GMS lubricant. The fractured surfaces are very similar to those added with LC.

The fractured structures of the blends and phase separated blends with added Zinc Stearate are shown in Figure 3.37 and 3.38. The morphology of the blends with

added Zinc stearate can be seen at larger scale magnification (x5,000) instead of (x10,000). The blends with added Zinc Stearate show large fibrils and smooth surfaces, differ from its phase separated blends. Comparing the phase separation of SAN/PMMA blends and the phase separated blends with added LCs and lubricants, it is clear that the co-continuous structures are very similar.

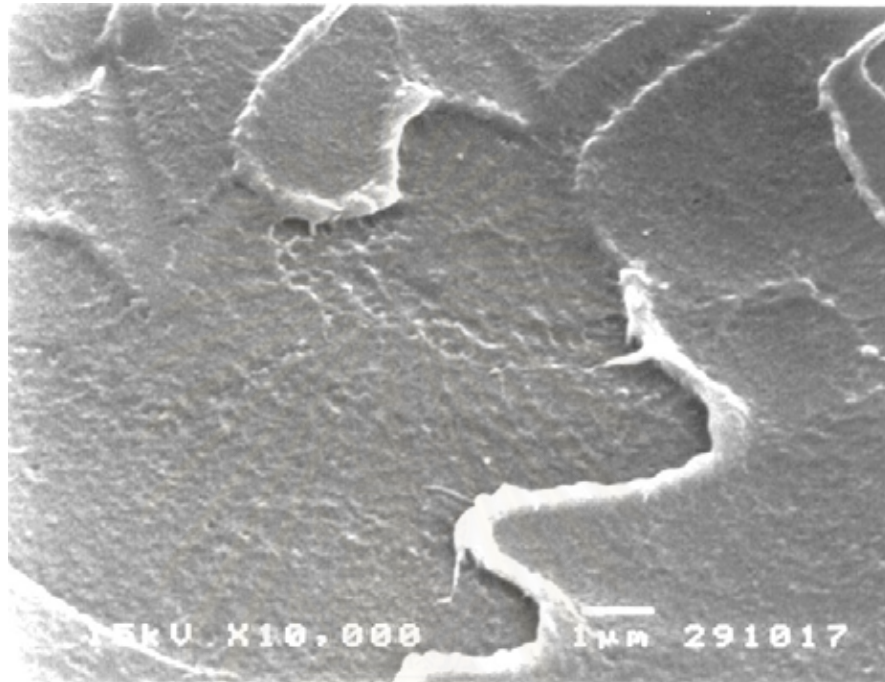


Figure 6.27 A scanning electron micrograph picture of SAN.

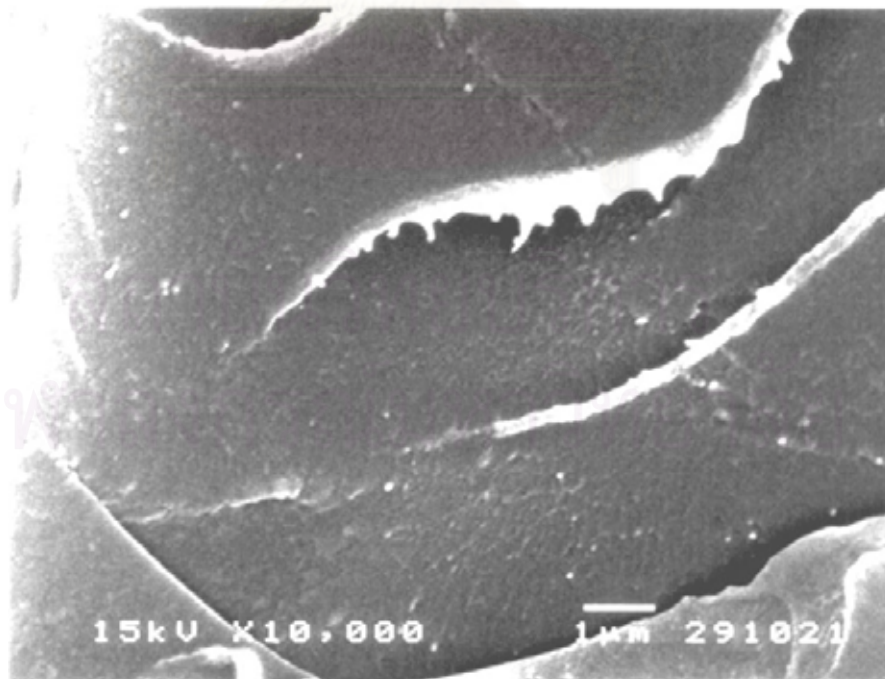


Figure 6.28 A scanning electron micrograph picture of PMMA.

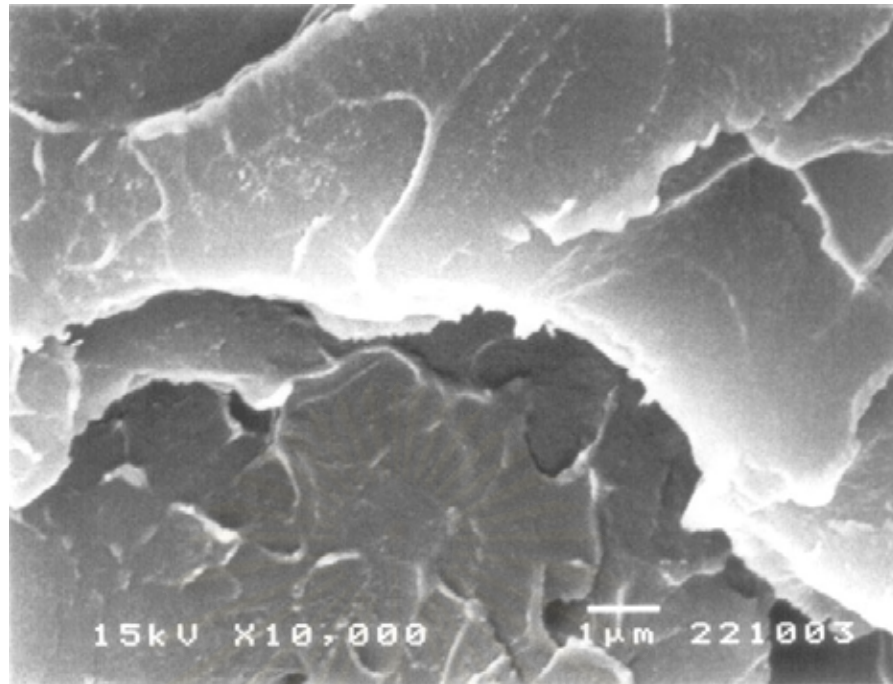


Figure 6.29 A scanning electron micrograph picture of a fractured specimen for a miscible 20/80 melt mixed SAN/PMMA blend.

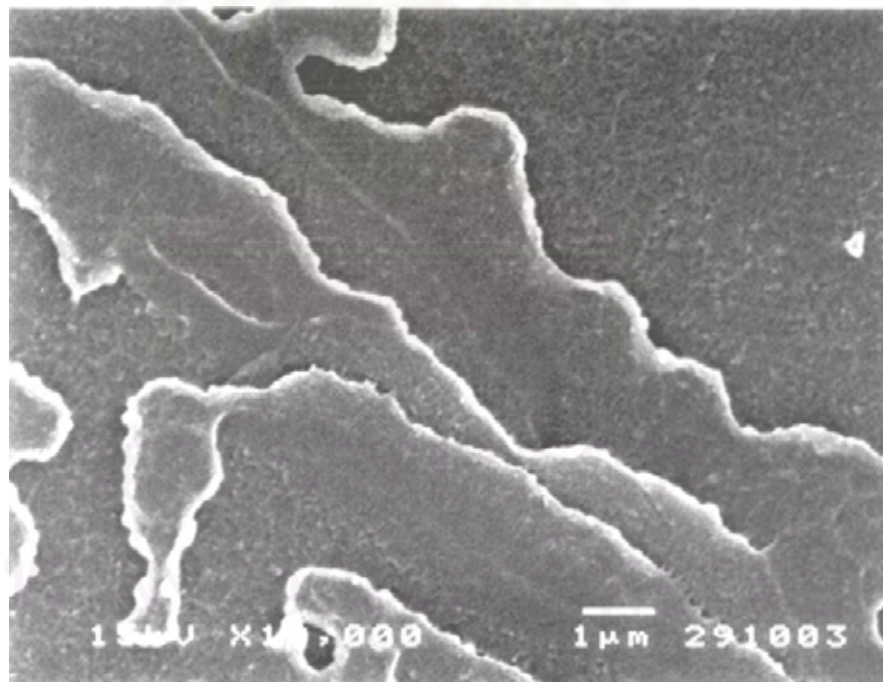


Figure 6.30 A scanning electron micrograph picture of a fractured specimen for a phased separated SAN/PMMA (20/80) at 210 °C.

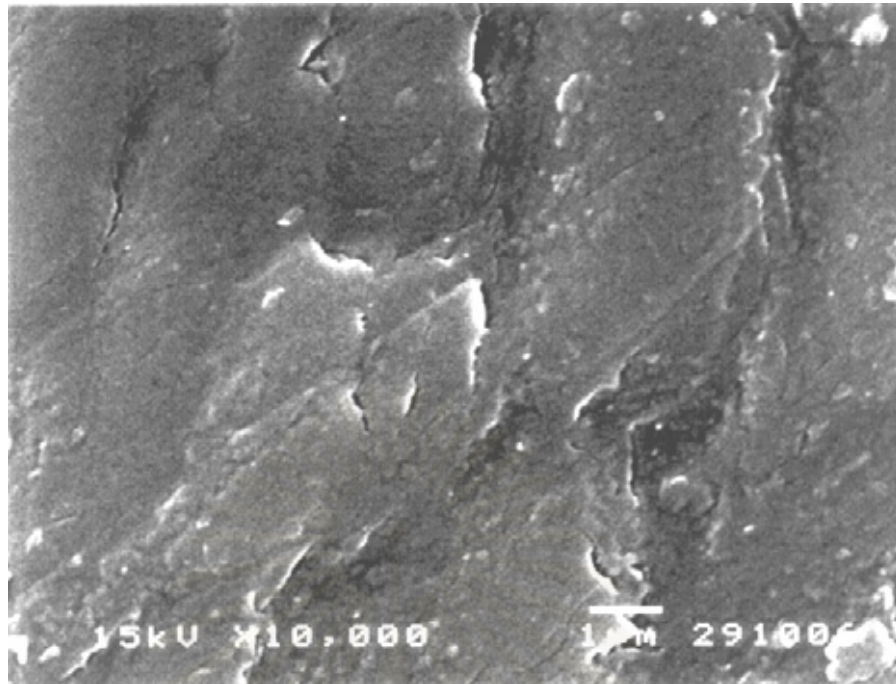


Figure 6.31 A scanning electron micrograph picture of a fractured specimen for a miscible 20/80 melt mixed SAN/PMMA blend added with 1.0 wt% of CBC33.

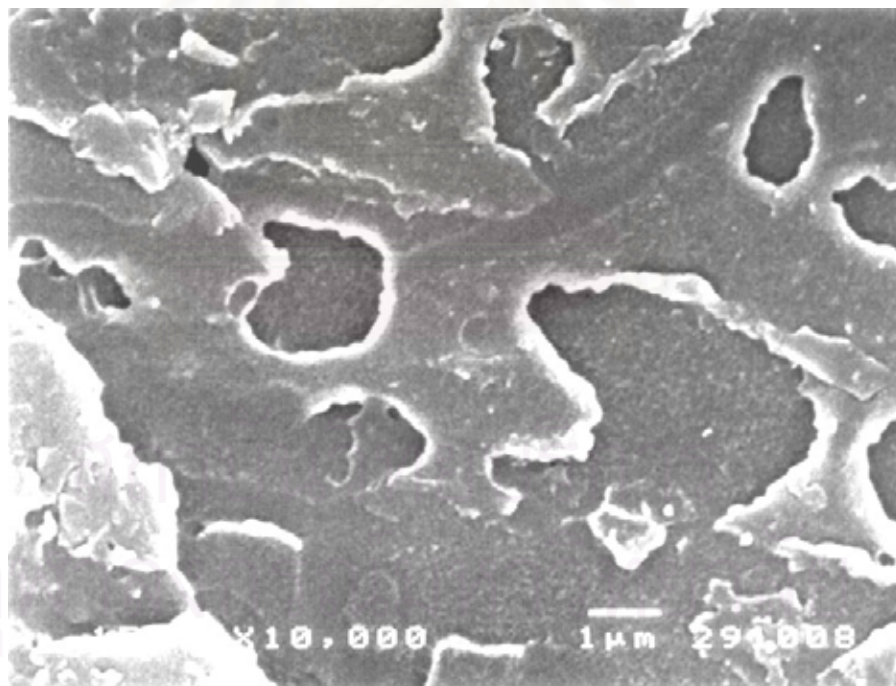


Figure 6.32 A scanning electron micrograph picture of a fractured specimen for a phase separated SAN/PMMA (20/80) at 210 °C, added with 1.0 wt% of CBC33.

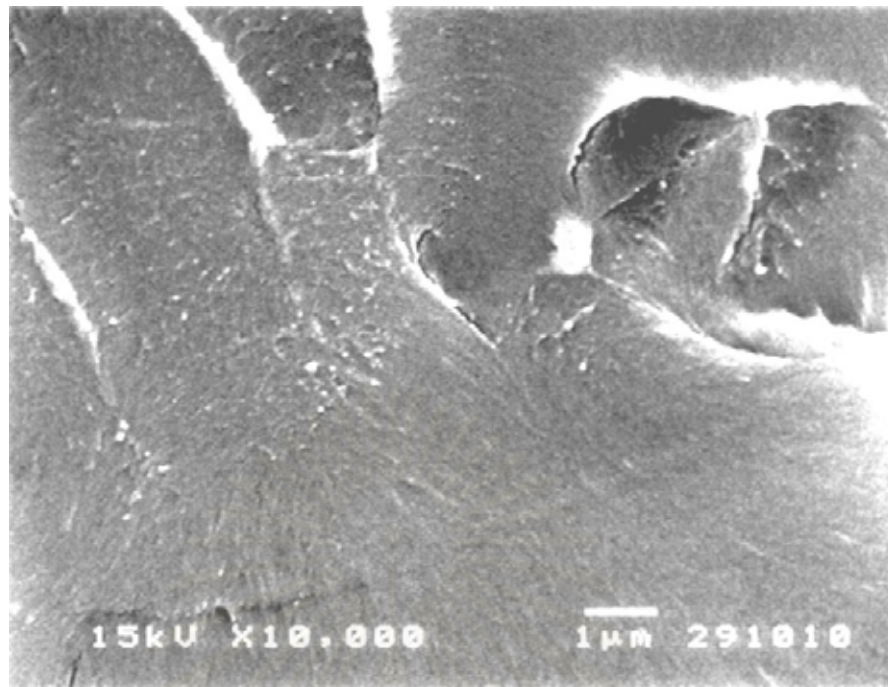


Figure 6.33 A scanning electron micrograph picture of a fractured specimen for a miscible 20/80 melt mixed SAN/PMMA blend, added with 1.0 wt% of CBC53.

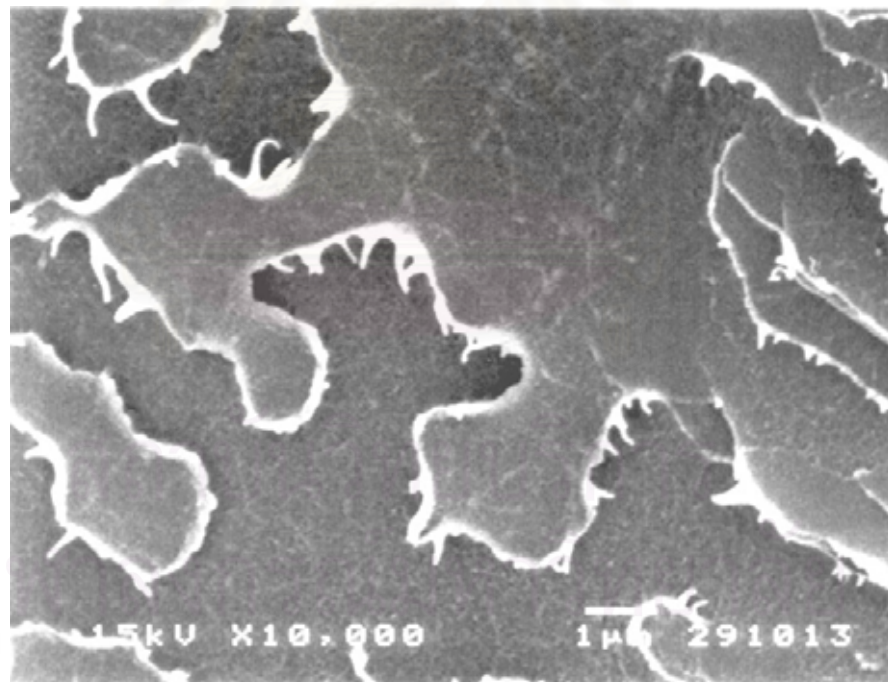


Figure 6.34 A scanning electron micrograph picture of a fractured specimen for a phased separated SAN/PMMA (20/80) at 210 °C, added with 1.0 wt% of CBC53.

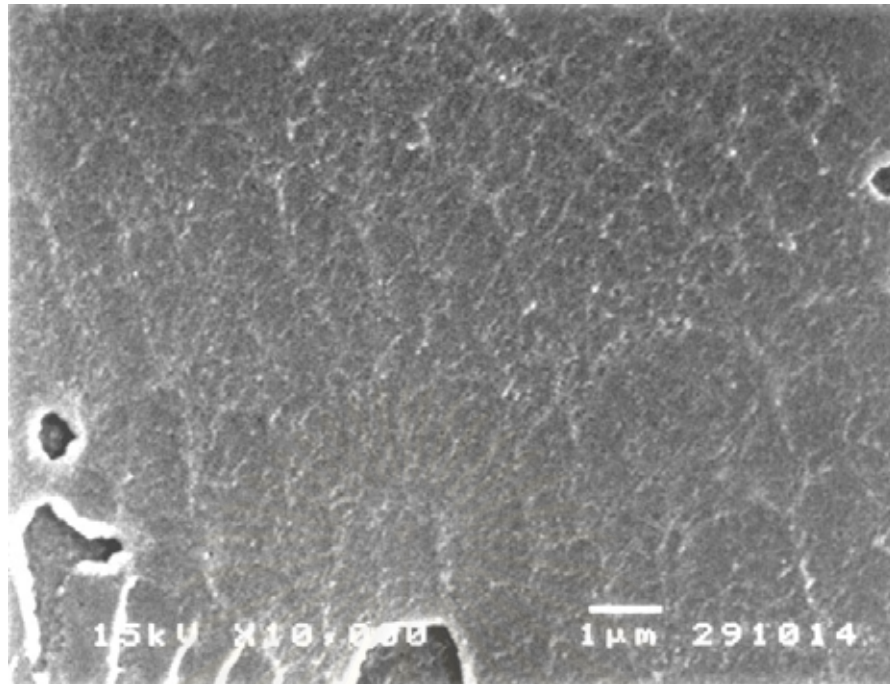


Figure 3.35 A scanning electron micrograph picture of a fractured specimen for a miscible 20/80 melt mixed SAN/PMMA blend added with 1.0 wt% of GMS.

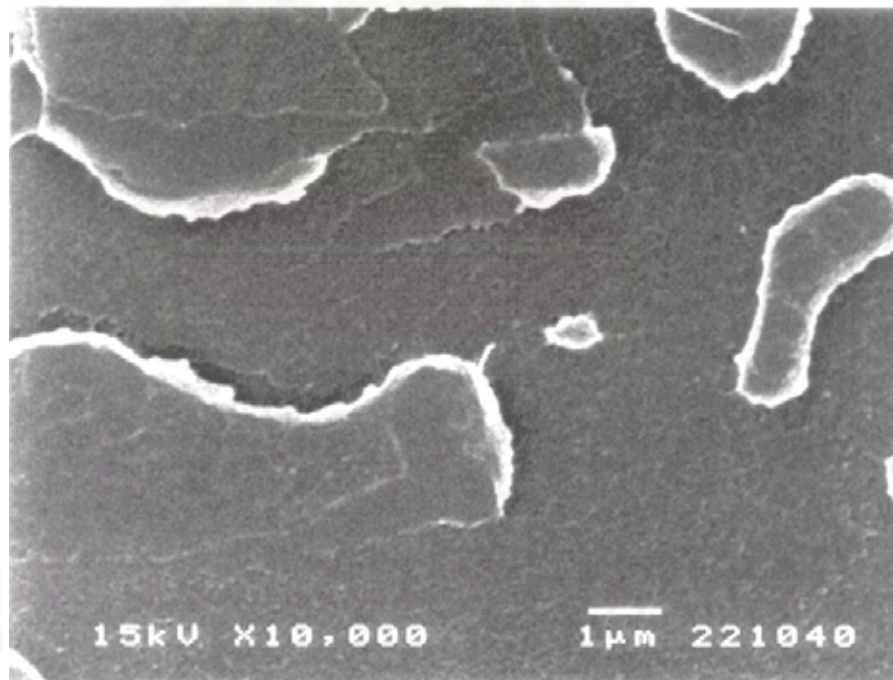


Figure 3.36 A scanning electron micrograph picture of a fractured specimen for a phased separated SAN/PMMA (20/80) at 210 °C, added with 1.0 wt% of GMS.

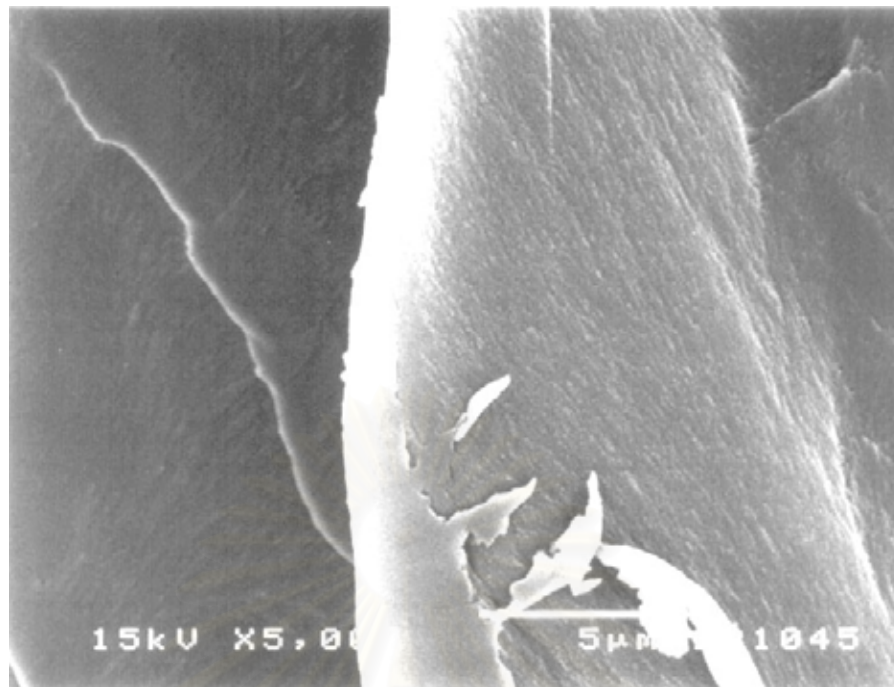


Figure 3.37 A scanning electron micrograph picture of a fractured specimen for a miscible 20/80 melt mixed SAN/PMMA blend added with 1.0 wt% of Zinc Stearate at larger scale magnification x5,000.

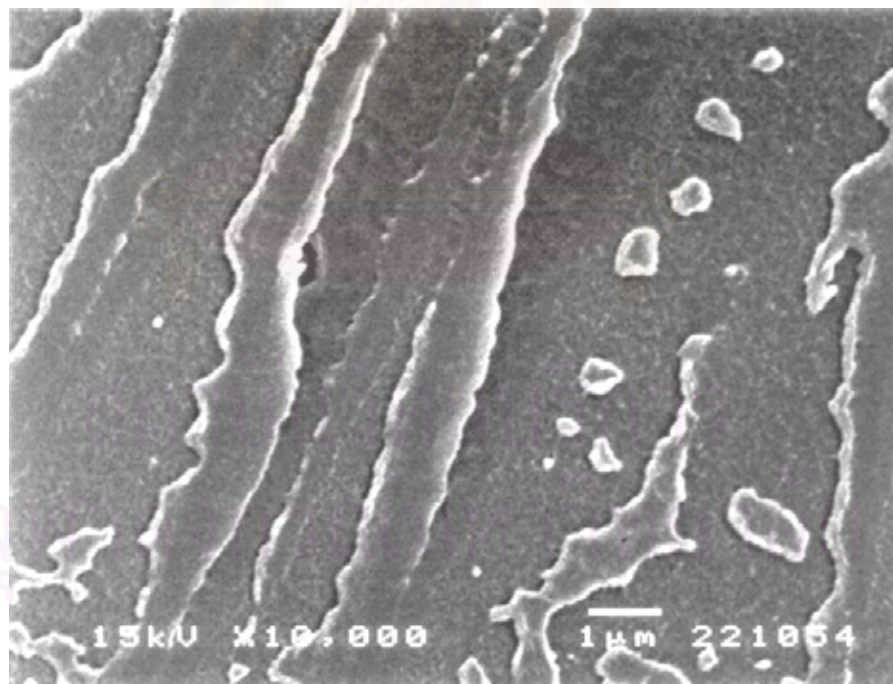


Figure 3.38 A scanning electron micrograph picture of a fractured specimen for a phase-separated SAN/PMMA (20/80) at 210 °C, added with 1.0 wt% of Zinc Stearate at larger scale magnification x10,000.

6.5 Conclusions

The results reported here show clear influences of LCs and lubricants on polymer blend. In contrast to lubricants, the addition of LCs has no effect on thermal properties of the blends as observed from DSC evidence. The T_g 's of the polymer blends after adding LCs do not change significantly. The phase boundary of SAN/PMMA blends exhibit lower critical solution temperature (LCST) behavior.

It has been shown that the early stages of spinodal structure can be observed using light scattering. The tests of the Cahn-Hilliard theory showed that such theory is still valid at the certain range of time, providing the satisfying prediction of q_m and $R(q_m)$. We can quantitatively measure the D_{app} of the polymer blend systems in the spinodal region at the same temperature and use it to estimate the lubrication activity of the small molecular additives. The Cahn-Hilliard growth rates $R(q)$ depend on LCs and lubricants concentration. The LCs could enable the molecule of the melted polymer blend to move faster than the lubricant blends. The LC addition appears to significantly increase molecular mobility while the effect of the lubricants is small.

Further experiments in molecular level may unveil the mechanism of the melted viscosity reduction of the LC blends. The SEM results in the early stage of the spinodal decomposition support the comparison done by comparing the D_{app} . It is hard to conclude from the SEM pictures of the effects of adding the small molecules alone. More complex experiments are needed to model the reduction in melt viscosity by LC.

Chapter VII

Conclusions and Recommendations

This work employed two different techniques, viz., light scattering and electron microscopy to monitor the blend of poly(methyl methacrylate) and poly(styrene-co-acrylonitrile). The miscibility and kinetics of phase separation of SAN/PMMA blends before and after adding LCs and lubricants were investigated. The effects of LCs and lubricants on the kinetics phase separation of polymer blends were clearly explored. The morphologies of SAN/PMMA blends both in miscible and phase separating regions thus have been thoroughly studied.

7.1 Conclusions

Phase diagram of SAN/PMMA blend was constructed by observing the opalescence of the blend denoted as a cloud point. The cloud point, which is defined as the first rise of scattering intensity upon heating can be obtained by performing light scattering experiments. It appears that this value depends on heating rate, the real cloud point can then be obtained from extrapolation to zero heating rate. The spinodal point on the other hand can be obtained by the projection to zero D_{app} , which is obtained from the y-axis intercept of $R(q)/q^2$ vs q^2 curve.

The rate at which structures develop in the early (or fairly early) stages of spinodal decomposition observed using light scattering allows us to measure the mobility of the molecules during the phase separation and the effect of variable amounts of additives within the blend. We can obtain indicative values of D_{app} for the polymer blend systems in the spinodal region and use it to estimate the lubrication activity of the small molecular additives at the same temperatures. There are possibly very small effects of the lubricants on the molecular mobility during phase separation, but quite great effects of addition of LC molecules can be observed, particularly for the higher temperatures. Thus the mechanism which reduces the melt viscosity in blends may not be the same for LCs and normal lubricants. Further experiments at a

molecular level, for example NMR, may unveil the mechanism of the melt viscosity reduction in the LC blends.

7.2 Recommendations for further works

Although several points regarding the behavior of the blend with LCs added or lubricants have been reported in this thesis, there are still some interesting points, which should be borne in mind and can be further studied in the future. These are some recommendations.

7.2.1 Morphology of the blends.

It is accepted that LCs have influence on miscibility and kinetics of phase separation. Measurements the fractured structures of the blends after adding LCs and lubricants using SEM were difficult to clarify the differences in their textures. More powerful technique to monitor the change of blend morphology is required.

Alternatively, spinodal structure can be investigated in three dimensions using other techniques such as AFM. The depth and size of each phase can be measured and used to construct a 3-D model. Thus it can be a useful tool to compare the morphology of the blends after adding LCs and lubricants.

7.2.2 Effects of delay time

Light scattering technique nowadays has been utilised widely; nonetheless, it should be borne in mind that such a technique can monitor the change of a system within the limitation of micro-scale. Therefore, it would be interesting to study the behavior of polymer blend below this scale limit using other powerful techniques such as SANS, SAXS or WAXS. The study of phase separation at high q might be able to explain the mystery of delay time.

We are interested to use Clarke's model to fit the experimental data in this work. Clarke *et al.* [1997] recently demonstrated that the effect of viscoelasticity due to entanglements can delay the onset of phase separation. Clarke equation (7.1) has been used to fit the experimental data in our preliminary study. The coefficients of fitting equation were found difficult to obtain and the calculated results were not in agreement with the experimental data. So, the delay time is still our interesting subject to study.

$$S_q(t) = S_q(0)[A_1 \exp\{-R_1 t\} + (1 - A_1) \exp\{-R_2 t\}] \quad (7.1)$$

where

$$A_1 = \frac{1}{2} \left[1 - \frac{2a - b}{\sqrt{b^2 - 4c}} \right] \quad (7.2)$$

$$R_1 = \frac{1}{2} \left[b + \sqrt{b^2 - 4c} \right] \quad (7.3)$$

$$R_2 = \frac{1}{2} \left[b - \sqrt{b^2 - 4c} \right] \quad (7.4)$$

with $a = R_v$, $b = R_T + R_v + R_{c0}$, and $c = R_T R_v$. The following definitions have been used for the three effective dynamic rates:

$$R_T = 2q^2 M [\chi_c - \chi + \kappa q^2] \quad (7.5)$$

$$R_{c0} = 2c_0(q) M q^2 \quad (7.6)$$

$$R_v = 1/\tau_v \quad (7.7)$$

The first of which, R_T , can be recognized as the Cahn-Hilliard relaxation, or growth rate. For simplicity we assume that the mobility, M , is independent of q .

In the limit of $R_T \ll R_{c0}, R_v$, i.e., if modes arising from the viscoelastic nature of entangled polymers are much faster than the thermodynamic mode, the solution

may be decoupled into a purely viscoelastic mode, and a modified thermodynamic (or Cahn-Hilliard) mode

$$S_q(t)/S_q(0) = A_1 \exp\{- (R_v + R_{c0})t\} + (1 - A_1) \exp\{- R_T (1 + R_{c0}/R_v)^{-1} t\} \quad (7.8)$$

The effect of adding LCs and lubricants on delay time will be investigated in the future.

7.2.3 Effects of viscoelastic of phase separation

It is clear that the values of D_{app} can use to estimate the lubrication activity of the small molecular additives at the same temperatures. The results, therefore, might become clearer if the viscoelastics effects are considered to study the effects of polymer blends after adding LCs and lubricants. A brief introduction of viscoelastics is given in the next paragraph.

Considering the motion of long linear polymer chains, it is usually different from the short ones. This has been suggested that when the concentration and molecular weight are high enough, the effect of entanglement in polymer will play an important role [Doi 1996]. The theory, which successfully describes this phenomenon, was first introduced by de Gennes [1979] called the reptation or tube model. Considering the system of a polymer melt, a single chain was assumed as the test chain was contained in a hypothetical tube trapped inside a three dimensional network formed by the other entangled chains. The model was equipped to illustrate the basic process of reptation, in which the test chain moves to leave some parts of the tube and generate new tube portion at random. The time necessary for the test chain to wind out completely from its original tube and create a new conformation was called the reptation time or relaxation, τ . The relaxation time was derived from tube diffusion, D_{tube} , over its tube length, L .

$$\tau = \frac{L^2}{D_{\text{tube}}} \quad (7.9)$$

Since D_{tube} is inversely proportional to the chain length, N , and L is linear in N .

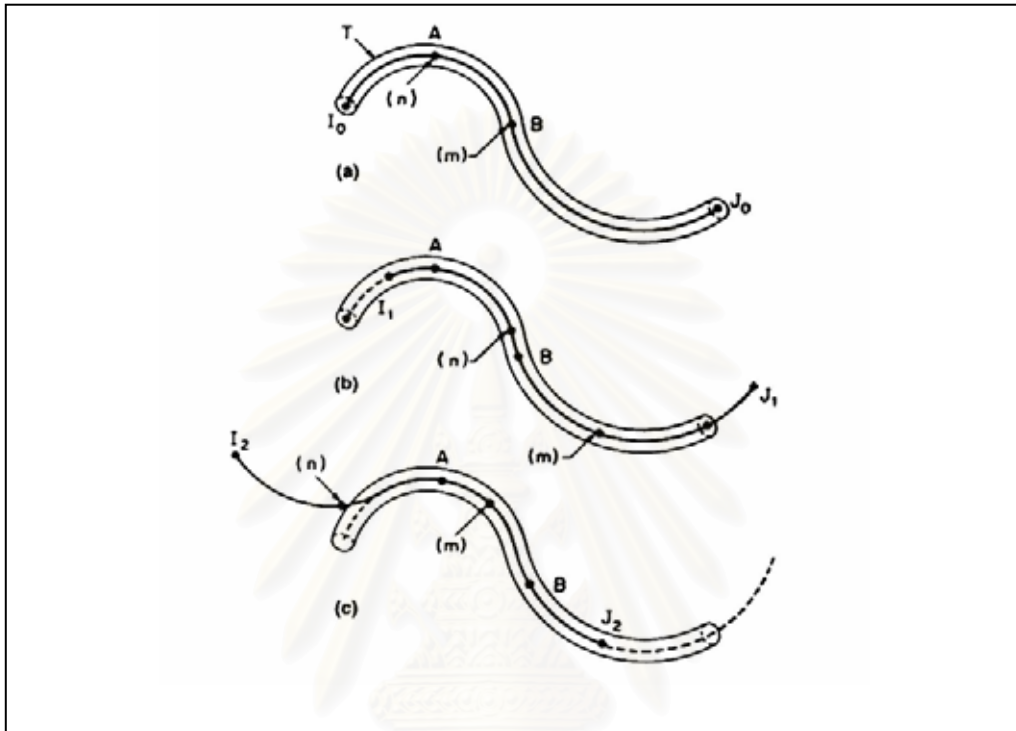


Figure 7.1 Free successive situations for a reptation chain: (a) the chain is trapped in its original tube; (b) the chain moves to the right and a certain portion (I_0I_1) of the original tube disappears; (c) the chain moves to the left and a portion (J_0J_2) of the original tube disappears [de Gennes 1979].

สถาบันวิทยบริการ
จุฬาลงกรณ์มหาวิทยาลัย

References

- Ahn, W.; Kim, C. Y.; Kim, H.; Kim, S. C., "Phase behaviour of polymer/liquid crystal blends", Macromolecules 25 (1992): 5002-5007.
- Ballauff, M., "Phase equilibria in mixtures of thermotropic liquid crystals and flexible polymers", Mol. Cryst. Liq. Cryst. 136 (1986): 175-195.
- Bernstein, R. E.; Cruz, C. A., Paul, D. R.; Barlow, J. W., "LCST behavior in polymer blends", Macromolecules 10 (1977): 681-686.
- Binder, K.; Stauffer, D., "Theory for the slowing down of the relaxation and spinodal decomposition of binary mixtures", Phys. Rev. Letts. 33, (1974) : 1006-1009.
- Binder, K., "Collective diffusion, nucleation, and spinodal decomposition in polymer mixtures", J. Chem. Phys. 79 (1983): 6387-6409.
- Binder, K.; Frisch, H. L.; Jackle, J., "Kinetics of phase separation in the presence of slowly relaxing structural variables," J. Chem. Phys. 85 (1986): 1505-1512.
- Binder, K., Spinodal decomposition. Cahn, R. W.; Haasen, P.; Kramer, E. J. (eds.), in Materials Science and Technology, 5, Weinheim : VCH, 1991.
- Binder, K., "Spinodal decomposition in confined geometry," J. Non-Equilib. Thermodyn. 23 (1998): 1-44.
- Blizard, K. C.; Baird, D. C., "The morphology and rheology of polymer blends containing a liquid crystalline copolyester", Polym. Eng. Sci. 27 (1987): 653-662.
- Buckley, A.; Conciatori, A. B.; Calundann, G. W., "Melt processable blend of a low molecular weight liquid crystalline compound and a polyolefin or polyester", U.S. Patent 4,434,262. 1984.
- Cabral, J. T.; Gerard, H.; Clarke, N.; Higgins, J. S., "Phase separation of polymer blend TMPC/PS: dependence on blending method", Physica B 408 (2000): 276-278.
- Cabral, J. T.; Higgins, J. S.; Yerina, N. A.; Magonov, S. N., "Topography of phase-separated critical and off-critical polymer mixtures" Macromolecules 35 (2002): 1941-1950.
- Cahn, J. W., "On Spinodal Decomposition". Acta Met. 9 (1961): 795 – 801.
- Cahn, J. W., "Phase separation by spinodal decomposition in isotropic systems", J. Chem. Phys. 42 (1965): 93-99.

- Cahn, J. W., "Spinodal decomposition", Trans. Metall. Soc. AIME. 242 (1968): 166-180.
- Cahn, J. W.; Hilliard, J. E., "Free energy of a nonuniform system. I. Interaction free energy", J. Chem. Phys. 28 (1958): 258-267.
- Cahn, J. W.; Hilliard, J. E., "Free energy of a nonuniform system. III. Nucleation in a two-component incompressible fluid", J. Chem. Phys. 31 (1959): 688-699.
- Cameron, N.; Cowie, J. M. G.; Ferguson, R.; Gomez Ribelles, J. L.; Mas Estelles, J., "Transition from miscibility to immiscibility in blends of poly(methyl methacrylate) and styrene-acrylonitrile copolymers with varying copolymer composition: a DSC study", Euro. Polym. J. 38 (2002): 597-605.
- Chiu, H. W.; Kyu, T., "Equilibrium phase behaviour of nematic mixtures " J. Chem. Phys. 103 (1995): 7471-7481.
- Chiu, H.-W.; Zhou, Z. L.; Kyu, T.; Cada, L. G.; Chien, L.-C., "Phase diagrams and phase separation dynamics in mixtures of side-chain liquid crystalline polymers and low molar mass liquid crystals", Macromolecules 29 (1996): 1051-1058.
- Chuenchaokit, A., "Effects of thermotropic liquid crystal on properties of polycarbonates", Master Degree Thesis, Chulalongkorn University, Bangkok, 1998.
- Clarke, N.; Mcleish, T. C. B.; Pavawongsak, S.; Higgins, J. S., "Viscoelastic effects on the early stages of phase separation in polymer blends", Macromolecules. 30 (1997): 4459-4463.
- Cook, H. E., "Bronian motion in spinodal decomposition", Acta Met. 18 (1970): 297-310.
- Cowie, J. M. G. and Lath, D., "Miscibility mapping in some blends involving poly(styrene-co-acrylonitrile)", Makromol. Chem., Macromol. Symp., 16 (1988): 103-112.
- Cummings, A.; Wilzius, P.; Bates, F. S.; Rosendale, J. H., "Light-scattering experiments on phase-separation dynamics in binary fluid mixtures", Phys. Rev. A. 45 (1992): 885-.
- de Gennes, P. G. Scaling concept in polymer physics. New York : Cornell Univ. Press, 1979.
- de Gennes, P., "Dynamics of fluctuations and spinodal decomposition in polymer blends," G. J. Chem. Phys. 72 (1980): 4756-4763.

- Demus, D.; Goodby, J.; Gray, G. W.; Spiess, H.-W.; Vill, V. Handbook of liquid crystals 2A:low molecular weight liquid crystal I. Weinheim : Wiley-VCH Press, 1998.
- Doi, M.; Edwards, S. F. The Theory of Polymer Dynamics. New York : Oxford University Press, 1986.
- Doi, M. Introduction to Polymer Physics. Oxford : Oxford University Press, 1996.
- Dorgan, J. R.; Yan, D., “Kinetics of spinodal decomposition in liquid crystalline polymers: processing effects on the phase separation morphology”, Macromolecules, 31 (1998): 193-200.
- Edel, V., “Early and late stage phase separation dynamics of polystyrene/poly(methyl methacrylate-stat-cyclohexyl methacrylate) blends”, Macromolecules, 28 (1995): 6219-6228.
- Flory, P. J., “Thermodynamics of high polymer solutions”, J. Chem. Phys. 9 (1941): 660-661.
- Flory, P. J., “Thermodynamics of high polymer solutions,” J. Chem. Phys. 10 (1942): 51-61
- Flory, P. J.; Orwoll, R. A.; Vrij, A., “Statistical mechanics of chain molecule liquids”, J. Am. Chem. Soc. 86 (1964): 3507-3520.
- Fowler, M. E.; Barlow, J. W.; Paul, D. R., “Effect of copolymer composition on the miscibility of blends of styrene-acrylonitrile copolymer with poly(methyl methacrylate)”, Polymer 28 (1987): 1177-1184.
- Guo, W.; Higgins, J. S., “Miscibility and kinetics of phase separation in polymer blends of tetramethyl-bisphenol-A polycarbonate and polystyrene”, Polymer, 31 (1990): 699-706.
- Hashimoto, T.; Kumaki, J.; Kawai, H., “Time-resolved light-scattering studies on kinetics of phase separation and phase dissolution of polymer blends. 1. Kinetics of phase separation of a binary mixture of polystyrene and poly(vinyl methyl ether)”, Macromolecules 32 (1983): 641-648.
- Hashimoto, T.; Takenaka, M.; Jinnai, H., “Studies of self-assembling processes of polymer blends in spinodal decomposition”, J. Appl. Cryst., 24 (1991): 457-466.
- Hashimoto, T. Structure and Properties of Polymer. Thomas, E. L. (ed.), in Materials Science and Technology, 12, Weinheim : VCH, 1993.

- Hashimoto T. Structure of polymer blends. In: Cahn RW, Haasen P, Kramer EJ, editors. *Materials Science and Technology*, 12, Weinheim Chichester Wiley, 1991. pp.251-300.
- Hashimoto T.; Izumitani, T., "Effects of a block copolymer on the kinetics of spinodal decomposition of polymer blends", *Macromolecules* 26 (1993): 3631-3638.
- Hashimoto T.; Izumitani, T., "Memory effects on spinodal decomposition. 1. Effects of uniaxial compression", *Macromolecules* 29 (1996): 8117-8125.
- Higashida, N.; Kressler, J.; Inoue, T., "Lower critical solution temperature and upper critical solution temperature phase behaviour in random copolymer blends: poly(styrene-co-acrylonitrile) / poly(methyl methacrylate) and poly(styrene-co-acrylonitrile) / poly(ϵ -caprolactone)", *Polymer* 36 (1995): 2761-2764.
- Higgins, J. S.; Fruitwala, H.; Tomlins, P. E., "Correlation of phase-separation behaviour in polymer blends with thermodynamic measurements in the one-phase region", *Macromolecules* 22 (1989b): 3674-3681.
- Hill, R. G.; Tomlins, P. E.; Higgins, J. S., "Preliminary study of the kinetics of phase separation in high molecular weight poly(methyl methacrylate)/solution-chlorinated polyethylene blends", *Macromolecules*. 18 (1985): 2555-2560.
- Hilliard, J. E. Phase transformations american society for metal. New York : Chapman & Hall co., Ltd., 1970.
- Hobb, S. Y.; Dekker, M. E. J.; Watkins, V. H., "Effect of interfacial forces on polymer blend morphology", *Polymer* 29 (1988): 1598-1602.
- Huggins, M. L., "Solutions of long-chain compounds.", *J. Chem. Phys.* 9 (1941): 440-450.
- Huggins, M. L., "Some properties of some solutions of long chain compounds", *J. Phys. Chem.* 46 (1942): 151-158.
- Jinnai, H.; Hasegawa, H.; Hashimoto, T.; Han, C. C., "Time-resolved small-angle neutron scattering study of spinodal decomposition in deuterated and protonated polybutadiene blends. I. Effect of initial thermal fluctuations", *J. Chem. Phys.* 99 (1993): 4845-4854.
- Kamath, S.; Colby, R. H.; Kamur, S. K., "Dynamic heterogeneity in miscible polymer blends with stiffness disparity: computer simulations using the bond fluctuation model", *Macromolecules* 36 (2003): 8567-8573.

- Kammer, H. W.; Kummerloewe, C.; Kressler, J.; Melior, J. P., "Shear-induced phase changes in polymer blends", Polymer 32 (1991): 1488-1492.
- Kim, J. Y.; Cho, C. H.; Palffy-Muhoray, P.; Mustafa, M.; Kyu, T., "Polymerization-induced phase separation in a liquid-crystal-polymer mixtures", Phys. Rev. Lett. 71 (1993): 2232-2239.
- Komura, S.; Osamura, K.; Fujii, H.; Takeda, T., "Time evolution of the structure function of quenched Al-Zn and Al-Zn-Mg alloys", Phys. Rev. B. 31 (1985): 1278-1301.
- Koningsveld, R.; Kleintjens, L. A., "Liquid-liquid phase separation in multicomponent polymer systems. x. concentration dependence of the pair-interaction parameter in the system cyclohexane-polystyrene", Macromolecules 4 (1971): 637-641.
- Kressler, J.; Kammer, H. W.; Klostermann, K., "Phase behaviour of poly(methyl methacrylate) and poly(styrene-co-acrylonitrile) blends", Polym. Bull. 15 (1986): 113-119.
- Kressler, J.; Higashida, N.; Inoue, T.; Heckmann, W.; Seitz, F., "Study of polymer-polymer interfaces: A comparison of ellipsometric and TEM data of PMMA/PS and PMMA/SAN system", Macromolecules 26 (1993): 2090-2094.
- Kyu, T.; Saldanha, J. M., "Phase separation by spinodal decomposition in polycarbonate/poly(methyl methacrylate) blends", Macromolecules 21 (1988): 1021-1026.
- Kyu, T.; Saldanha, J. M.; Kiesel, M. J. Two-phase polymer systems progress in polymer processing. Utracki, L.A. (ed.), Carl Hanser Verlag, 1991.
- Kyu, T.; Shen, C.; Chiu, H. W., "Effects of molecular weight on miscibility phase diagrams in mixtures of polymer and liquid crystals", Mol. Cryst. Liq. Cryst. 287 (1996): 27-34.
- Lee, S.; Mather, P. T.; Peason, D. S., "Phase behavior and rheology of blends containing polycarbonate and a thermotropic polyester", J. Appl. Polym. Sci. 59 (1996): 243-250.
- Lefebvre, A. A.; Lee, J. H.; Jeon, H. S.; Balsara, N. P.; Hammouda, B., "Initial stages of nucleation in phase separating polymer blends", J. Chem. Phys. 111 (1999): 6082-6099.

- Lin, Y. C.; Lee, H. W.; Winter, H. H., "Miscibility and viscoelastic properties of blends of a liquid-crystalline polymer and poly(ethylene terephthalate)", Polymer 34 (1993): 4703-4709.
- Maruta, J.; Ohnaga, T.; Inoue, T., "Demixing kinetics in a binary polymer mixture of poly(methyl methacrylate) and poly(acrylonitrile-co-styrene)," Macromolecules 26 (1993): 6386-6390.
- Mazumder, S.; Sen, D.; Batra, I. S.; Tewari, R.; Dey, G. K.; Banerjee, S.; Sequeira, A.; Amenitsch, H.; Bernstorff, S., "Phase-separation kinetics of a multicomponent alloy", Phys. Rev. B. 60 (1999): 822-830.
- Mc Crum, N.G.; Buckley, C.P.; Bucknall, C.B., Principles of polymer engineering. 2nd edition, Oxford: Oxford University Press, 1997.
- Mc Master, L. P., "Aspects of liquid-liquid phase transition phenomena in multicomponent polymeric systems", Ad. Chem. Ser., No.142 (1975): 43-65.
- Meier, G.; Fytas, G.; Momper, B.; Fleischer, G., "Interdiffusion in a homogeneous polymer blend far above its glass transition temperature", Macromolecules 26 (1993): 5310-5315
- Mendenhall, W.; Sincich, T. A Second Course in Statistics: Regression Analysis. 5th edition, New Jersey : Prentice-Hall International, 1996.
- Molau, G. E., "Heterogeneous polymer systems. III. Phase separation in styrene acrylonitrile copolymers", J. Polym. Sci. Polym. Lett. 3 (1963): 1007-.
- Motong, N., "Effects of mixing and processing on the viscosity of polycarbonate blends with low molar mass liquid crystal", Master Degree Thesis, Bangkok : Chulalongkorn University, 2002.
- Nakai, A.; Shiwaku, T.; Wang, W.; Hasegawa, H.; Hashimoto, T., "Phase separated structures formed in polymer mixtures containing a thermotropic liquid crystalline copolyester as one component", Polymer 37 (1996): 2259-2272.
- Nakai, A.; Wang, W.; Ogasawara, S.; Hasegawa, H.; Hashimoto, T., "Phase-Separated Structures in Polymer Mixtures with a Thermotropic Liquid Crystalline Copolyester as One Component: Composition Dependence", Macromolecules 31 (1998): 5391-5398.
- Newby, B. Z.; Composto, R. J., "Influence of lateral confinement on phase separation in thin film polymer blends", Macromolecules 33 (2001): 3274-3282.

- Nishi, T.; Wang, T.T.; Kwei, T. K., "Thermally Induced Phase Separation Behavior of Compatible Polymer Mixtures", Macromolecules 8 (1975): 227-.
- Nishimoto, M.; Keskkula, H.; Paul, D. R., "", Polymer 32 (1991): 272-.
- Okada, M.; Han, C. C., "Experimental study of thermal fluctuation in spinodal decomposition of a binary polymer mixture", J. Chem. Phys. 85 (1995): 5317-5327.
- Okada, M.; Kwak K. D.; Chiba, T.; Nose, T., "Phase separation morphology in the critical to off-critical crossover region", Macromolecules. 26 (1993): 6681-6683.
- Okada, M.; Sun, J.; Tao, J.; Chiba, T.; Nose, T., "Phase separation kinetics and morphology in the critical to off-critical crossover region", Macromolecules. 28 (1995): 7514-7518.
- Olabisi, O; Robeson, L. M.; Shaw, M. T., Polymer- polymer miscibility. London : Academic Press, Inc. (London) Ltd., 1979.
- Olabisi, O., Handbook of Thermoplastics : Marcel Dekker Inc. (New York) Ltd, 1997.
- Ohnaga, T.; Maruta, J.; Inoue, T., "Apparent phase dissolution at the two-phase region in polymer-polymer mixtures", Polymer 60 (1989): 1845-1850.
- Onuki, A.; Hashimoto, T., "Theory of semidilute solutions of polymer mixtures in a common solvent: blob picture and pseudobinary approximation", Macromolecules. 22 (1989): 879-890.
- Oultache, A. K.; Zhao, Y.; Jasse, B.; Monnerie, L., " Orientation and relaxation in uniaxially stretched poly(methyl methacrylate)-poly(styrene-co-acrylonitrile) compatible blends", Polymer 35 (1994): 681-686.
- Paul, D. R.; Newman, S. Polymer blend. 1&2, London : Academic Press, Inc. (London) Ltd., 1978.
- Pavawongsak, S., "Effects of molecular architecture and specific (ion-dipole) interaction on the miscibility of polymer blends", PhD. Thesis, London : Imperial College, 1996.
- Pincus, P., "Dynamics of fluctuations and spinodal decomposition in polymer blends. II", J. Chem. Phys. 75 (1981): 1996-2000.
- Powanusorn, S., "Application of low molar mass thermotropic liquid crystals as an additive for polymers", Master Degree Thesis, Bangkok : Chulalongkorn University, 2000.

- Rodrigues, J. R. S.; Kaito, A.; Soldi, V.; Pires, A. T. N., "Behaviour of the miscibility of poly(ethylene oxide)/liquid crystal blends", Polym. Int. 46 (1998): 138-142.
- Rojanapitayakorn, P., "Thermodynamics and kinetics of phase separation, morphology and tensile properties of a binary polymer blend: polymethyl methacrylate/polystyrene-co-maleic anhydride", PhD.Thesis, Bangkok : Chulalongkorn University, 2000.
- Rojanapitayakorn, P.; Thongyai, S.; Higgins, J. S.; Clarke, N., "Effects of sample preparation method on mixing and phase separation in binary polymer blends", Polymer 42 (2001): 3475-3487.
- Sasaki, K.; Hashimoto, T., "Time-resolved light scattering studies on the kinetics of phase separation and phase dissolution of polymer blends. 3. Spinodal decomposition of ternary mixtures of polymer A, polymer B and solvent", Macromolecules 17 (1984) : 2818-2825.
- Sato, T.; Han, C. C., "Dynamics of concentration fluctuation in a polymer blend on both sides of the phase boundary", J. Chem. Phys. 88 (1988): 2057-2065.
- Shen, C.; Kyu, T., "Spinodal in a polymer dispersed liquid crystal", J. Chem. Phys. 102 (1995): 556-562.
- Shimomai, K.; Higashida, N.; Ougizawa, T.; Inoue, T.; Rudolf, B.; Kressler, J., "Studies on miscibility in homopolymer/random copolymer blends by equation of state theory", Polymer 37 (1996): 5877-5882.
- Silverstein, R. M.; Bassler, G. C.; Morrill, T. C. Spectrometric Identification of Organic Compounds. New York : John Wiley & Sons, Inc., 1991.
- Snyder, H. L.; Meakin, P.; Reich, S., "Dynamical aspects of phase separation in polymer blends", Macromolecules. 16 (1983): 757-762.
- Snyder, H. L.; Meakin, P., "Details of phase separation process in polymer blends" J. Polym. Sci.: Polym. Symp. 73 (1985): 217-.
- Sompradeekul, S., "Effects of small molecular solvent on phase diagram and tensile strength of polymer blends", Master Degree Thesis, Bangkok : Chulalongkorn University, 1998.
- Soontaranun, W., "Effect of flow on the miscibility of partially miscible polymer blends", PhD. Thesis, London : Imperial College, 1997.
- Sperling, L. H. Introduction to Physical Polymer Science 3rd ed. New York : John Wiley & Son, 2001.

- Stein, D.J.; Jung, R.H.; Illers, K.H.; Hendres, H., "Phänomenologische untersuchungen zur mischbarkeit von polymeren", Angew. Makromol. Chem. 36 (1974): 89-100.
- Strobl, G. R., "Structure evolution during spinodal decomposition of polymer blends", Macromolecules. 18 (1985): 558-563.
- Strobl, G. R. The Physics of Polymers: concepts for understanding their structures and behaviour. Berlin : Springer Verlag, 1997.
- Subramanian, R.; Huang, Y. S.; Roach, J. F.; Wiff, D. R., "Factors influencing properties of SAN/PMMA blends", Mat. Res. Soc. Symp. Proc. 171 (1990): 217-224.
- Suess, M.; Kressler, J.; Kammer, H.W., "The miscibility window of poly(methyl methacrylate) / poly(styrene-co-acrylonitrile) blends", Polymer 28 (1987): 957-960.
- Takenaka, M.; Hashimoto, T., "cattering studies of self-assembling processes of polymer blends in spinodal decomposition. II. Temperature dependence", J. Chem. Phys. 96 (1992): 6177-6190.
- Thongyai, S., "Properties of miscible and phase separated polymer blends", PhD Thesis London : Imperial College, 1994.
- Tomlins, P. E.; Higgins, J. S., "Late stage spinodal decomposition in an oligomeric blend of polystyrene/polybutadiene: A test of the scaling law for the structure function" J. Chem. Phys. 90 (1989): 6691-6700.
- Tompa, H. Polymer solutions. London : Butterworth, 1956.
- Turcott, E.; Nguyen, K. T.; Garcia-Rejon, A., "Microstructure development during the injection molding of pet/lcp blends", Polym. Eng. Sci. 41 (2001): 603-617.
- Utracki, L. A., Polymer alloys and blends: thermodynamics and rheology. New York : Hanser Publishers, 1989.
- Utracki, L. A., Two-phase polymer systems. New York : Hanser Publishers, 1991.
- Wendlandt, W. W., Thermal analysis. New York : John Wiley & Sons, Inc., 1986.
- Zhang, H.; Li, F.; Yang, Y., "Statistical thermotropic theory of phase equilibria in mixtures of thermotropic liquid crystals and flexible polymers", Science in China, Ser. B 38 (1995): 412-421.

Zhang, H.; Lin, Z.; Yan, D.; Yang, Y., “Phase separation in mixtures of thermotropic liquid crystals and flexible polymers”, Science in China, Ser. B 38 (1997): 128-136.

Zheng, Q.; Du, M.; Yang, B.; Wu, G., “Relationship between dynamic rheological behaviour and phase separation of poly(methyl methacrylate) / poly(styrene-co-acrylonitrile blends”, Polymer 42 (2001): 5743-5747.



สถาบันวิทยบริการ
จุฬาลงกรณ์มหาวิทยาลัย

VITAE

Miss Sirirat Wacharawichanant was born in Nakoratchasima, Thailand in September 13, 1972. She received the Bachelor Degree of Science in Chemistry from the Department of Chemistry, Faculty of Science, Khonkean University in 1994. She graduated the Master of Engineering in Chemical Engineering from Chulalongkorn University in 1999. She entered the Doctoral of Engineering in Chemical Engineering Program from Chulalongkorn University in 1999.

PUBLICATIONS AND PRESENTATIONS

1. Rojanapitayakorn, P.; Thongyai, S.; Wacharawichanant, S., "Phase Separation Morphology in Poly(methyl methacrylate/poly(styrene-co-maleic anhydride) blends", The Polymer Processing Society Asia/Australia Regional Meeting 1999, Bangkok, Dec 1-3, 1999.
2. Wacharawichanant, S.; Thongyai, S.; Rojanapitayakorn, P., "Phase separation of poly(methyl methacrylate and styrene-acrylonitrile blends" The First Thailand Materials Science and Technology Conference, Bangkok, July 19 - 20, 2000.
3. Thongyai, S.; Wacharawichanant, S.; Mongkhonsi, T., "Comparisons of various spinodal decompositions theories to small angle light scattering experiments of tetramethyl-bisphenol-A-polycarbonate and polystyrene", J. of Metals Materials and Minerals, 11 (2),(2002): 55-64.
4. Wacharawichanant, S.; Thongyai, S.; Tanodekaew, S., "Effects of low molar mass liquid crystal on phase separation of styrene acrylonitrile and poly(methyl methacrylate) blends", The 8th Pacific Polymer Conference (PPC8), Bangkok, November 24 - 27, 2003.

5. Damrongsakkul, S.; Wacharawichanant, S.; Rimdusit, S.; Thongyai, S.; Taepaisitphongse, V.; Shiomi, T.; Sato, H.; Miya, M.; Takeshita, H.; Akenaka, K.; Takeshita, H.; Takenaka, K., “Phase separation in the blends of linear and branched poly(ethylene glycol) with methyl methacrylate-n-hexyl methacrylate random copolymer”, The 8th Pacific Polymer Conference (PPC8), Bangkok, November 24 - 27, 2003.
6. Wacharawichanant, S.; Thongyai, S.; Tanodekaew, S.; Higgins, J. S.; Clarke, N., “Spinodal decomposition as a probe to measure the effects on molecular motion in poly(styrene-co-acrylonitrile) and poly(methyl methacrylate) blends after mixing with a low molar mass liquid crystal or commercial lubricant”, Polymer 45 (2004): 2201–2209.